Thermometry based on Whispering Gallery Mode resonators

POLITECNICO DI TORINO

SCUOLA DI DOTTORATO

Dottorato in Metrologia: Scienza e Tecnica delle misure – XXIV Ciclo

Thermometry Based on Whispering Gallery Mode Resonators

Tutore:
Dott. Vito Claudio Fernicola

Cotutore:
Prof. Elio Bava

Candidato:
Lili Yu
Matricola 159344

March 2012

Acknowledgements

There are many people I would like to thank for their assistance and support during the time spent working on the PhD studies presented in this thesis.

Firstly I would like to thank all the staff of the thermodynamics division at INRIM (Istitoto Nazionale di Ricerca Metrologica). In particular my tutor Dr. Vito Fernicola provided invaluable assistance and guidance with great patience and kindness even when he had thousands of other things to do. Mauro Banfo, Roberto Dematteis, Dr. Lucia Rosso, Dr. Denis Smorgon and Luigi Lacomini also gave me plenty of help with my experiment system. Additional thanks to Dr. Roberto Gavioso and Daniele Madonna Ripa for the assistance with the Labview program and lending the network analyzer to me. Thank Pier Paolo Capra and Dr. Andrea Merlone for lending me the GPIB interface to continue my experiment. Great thanks to my co-tutor Elio Bava for spending plenty of time to correct my thesis.

During the course of my PhD study I was fortunate to spend time studying at NIST (National Institute of Standards and Technology) in USA. My sincere thanks to Dr. Michael Moldover and Dr. Gregory Strouse of Process Measurements Division for all the supports and guidance I needed during my stay. Additionally, I am grateful to Dr. Keith Gillis and Dr. James Schmidt for all the helps and hospitality with great patience. Besides, great thanks to Dr. John Wright, Dr. Weston Tew, Dr. Robert Berg, Dr. John Hurly, Karen Garrity, Dawn Cross and Wyatt Miller for the assistance during my work and usual life.

Lastly, I would like to give my sincerest thanks to my family, my boyfriend and my friends for the great support and encouragement during my stay in Italy and in USA. Thanks for being there all the time I needed!

Abstract

Whispering gallery (WG) mode resonators were studied since 1980s for precision clock oscillators and for cavity quantum electrodynamics studies. They are a kind of stable, high Q, microwave resonators where a symmetric dielectric medium, such as a cylinder or a disk, is suspended in the centre of a metal cavity. A coaxial cable or a waveguide are used to couple the EM field in the microwave region and thus to excite the system resonant frequencies. WG modes are resonant modes of higher-order azimuthal number (*m*) having most of the EM energy concentrated on the dielectric surface.

Within the temperature range of -196 °C to 500 °C the most commonly used industrial thermometer is platinum resistance thermometer (PRT) with the uncertainties of 10 mK. The PRT offers high accuracy, low drift, a wide operating range; however, it is very sensitive to mechanical shock in handing and shipping. Besides, an AC resistance bridge which is typically required as a readout device for PRT is very expensive. Accordingly, there is a great need for a stability-improved, resistant to mechanical shock, potential lower uncertainty and cost-effective industrial thermometer.

WGMR thermometer (WGMRT) is a new kind of thermometer which offers greater vibration immunity, improved stability, smaller uncertainty in temperature measurement and potential lower cost than platinum resistance thermometry.

An innovative sapphire whispering gallery thermometer (SWGT) was first explored at the National Institute of Standards and Technology (NIST) in 2007 by Strouse [1] with the uncertainty less than 10 mK. Five WGMs with nominal resonant frequencies ranging from 14.4 GHz to 19.1 GHz and with Q-factors, respectively, ranging from 20,000 to 90,000 were measured within the temperature range of 0 °C to 100 °C. The accuracies of his WGMTs were in the range of ± 0.02 °C and ice point repeatability was better than 2 mK.

The thesis reports the tests performed on several WGMR thermometers which have different shapes of crystals to evaluate their stability, resolution and repeatability in the temperature range of -40 °C to 85°C. Thermal cycle experimental results

showed a Q in excess of 100000 for the mode with the highest azimuthal number, making it possible to achieve a potential temperature resolution of 0.1 mK.

Besides, different specimens of crystals with the same nominal specification and reassemble for the same specimen were both tested to check the reproducibility of the thermometer.

The birefringence of the sapphire was also studied to make an innovative thermometer. The ratios of two doublet frequencies are sensitive to the temperature-dependent birefringence of the crystal and relatively insensitive to surface contamination and changes in the shape of the cavity. Besides, it can have an external shape that closely approximates the shape of conventional platinum resistance thermometers.

Contents

Chapter 1 Introduction

1.1 Introduction to WGM

Whispering Gallery Mode (WGM) is named after the whispering gallery at St. Paul's Cathedral in London. In this domed cathedral it was found that if the sound source and the listener were positioned appropriately, hushed voices and whispers can be heard even in great distances; interestingly, the effect does not work if one speaks normally. The reason for this is that the sound bounces along the wall of the gallery with very little loss, and so can be heard at a great distance, while if you speak normally the increased amplitude of the noise allows it to circulate the gallery multiple times so all the sounds get mixed up and can no longer be heard properly. It can be viewed that there is a narrow region near the edge of the dome where the waves propagate most efficiently, and this is known as a 'whispering gallery mode' in honour of gallery where it was discovered.

Like atomic bound states, an individual WGM is labelled by *n*, *l*, *m* which respectively represents radial component, polar component and azimuthal component. Spherical Bessel functions describe standing waves in the radial direction of spherical coordinates [2], while polar component follows spherical harmonics, and equatorial field variation is sinusoidal [3]. Specifically, *n* (= 1,2,...) gives the number of maxima in the radial field pattern of a particular WGM, while *l* (= 0,1,...) and *m* (= -*l*,...,0,...,*l*) is half the number of equatorial nodes of the field, see Figure 1.1 [4]. Azimuthal mode number m is a positive or negative integer which depends on the sense of rotation of the ray. For isotropic dielectrics, resonant frequencies are the same for + *m* and – *m* which can also be said degenerate modes. Modes with the same *l* but different *m* are degenerate for a perfect sphere but a small ellipticity removes the degeneracy and induces *m* dependent frequency shift.

The basic propagation mechanism is shown in Figure 1.2 in total reflection mechanism at the dielectric-air boundary. The smaller circle of radius a_i which is tangential to the total reflection ray is called modal caustic [5-7]. WGM has most of the energy confined between the resonator boundary and the modal caustic to within a

small region in an axial direction. From a wave-optics point of view, *m* is the number of wavelengths around the cylinder, as Figure 1.3 shows *m* is independent of radius even though the phase velocity of azimuthal mode increases in proportion with radius.

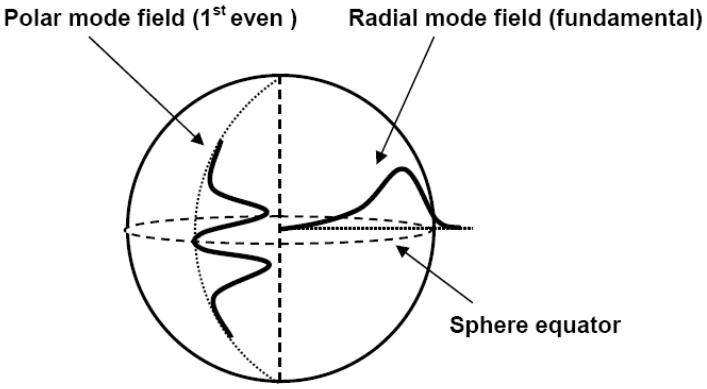

Figure 1.1 Schematic of WGM field components in a spherical resonator (not to scale)[4]

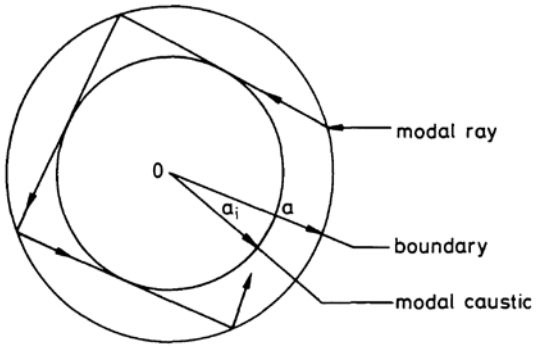

Figure 1.2 Whispering-gallery modes by ray optics[5]

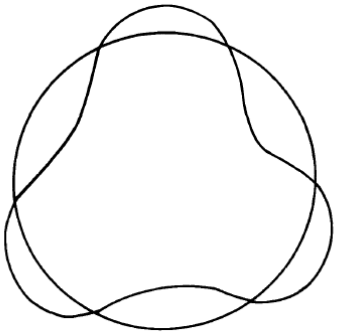

Figure 1.3 Schematic representation for field at azimuthal mode number *m*=3[6]

WGMs were studied by Lord Rayleigh since 1910 and have attracted great interests to researchers since 1980s in optical and microwave field.

It was first observed by elastic light scattering from spherical dielectric particles in liquid resonators. Since the dimension of the resonator should be comparable to the

wavelength optical WGM is too small to be used in the thermometry, however, the microwave WGM resonator (WGMR) can be few or tens millimetres which makes lots potentials in industry.

In most cases the dielectric cylinder or disk or sphere is suspended in a metal cavity and at least one microwave cable is coupled to the resonator to excite the resonant frequencies of which the resonant modes that have higher-order azimuthal number(expressed by *m*) and most of the energy is concentrated on the dielectrics are called WGM. It is a certain mode that has high Q and travels along the surface of the resonator by total reflection.

Whispering gallery mode has great advantages over other resonant modes. The WGM resonators are “oversize” for millimetre wavelength and it offers good suppression to spurious mode, very high Q factor and insensitivity to the metal cavity surface.

1.2 Research review and applications of WGM

1.2.1 Optical WGM

The studies of WGMs start almost a century ago by work of Lord Rayleigh who studied propagation of sound over a curved gallery surface [8-10]. On the other hand, in 1908 Mie published his theoretical studies on the scattering of plane electromagnetic waves by spheres in [11]. Later on, in 1909 Debye derived equations for the resonant eigenfrequencies of free dielectric and metallic spheres which can also be deduced from [11] and it naturally takes into account WGMs [12].

In optics, the first observations of WGMs can be attributed to solid state WGM lasers. Garrett *et al.* [13] observed stimulated emission into optical whispering modes of a spherical sample of CaF_2: Sm^{++} and they found that light produced by the stimulated emission is radiated tangentially form each point on the surface of the sphere which can be interpreted in terms of the electromagnetic analogue of the Rayleigh theory of the whispering gallery. Walsh *et al.* [14] observed microsecond-long transient laser operation with a several millimetres ruby ring at room temperature. WGMs were first observed by elastic light scattering from spherical dielectric particles in liquid resonators in 1970s [15, 16]. Then the WGM of dielectric

microspheres have received considerable attention. In 1980s Benner *et al.* discovered WGM has strong influence on fluorescence [17-19] and Raman scattering [20-22]. The radiative coupling of a microsphere and a beam of light is described in generalized Lorentz-Mie scattering theory by Barton *et al.* [23-25] and in modified ray theory by Serpenguzel *et al.* [26, 27].

The ideal microsphere WGM coupling device includes the following characteristics:

(1) Efficient WGM excitation performance with little potential for Q-spoiling
(2) Simple sphere-to-coupler alignment
(3) Clearly defined ports
(4) Robust and integrable structure
(5) A consistent and inexpensive fabrication process

A single prism has been used to simultaneously couple light into and out of an optical waveguide, with a guiding length of 1 cm. The method, which is simple and reproducible, utilizes two optimized gaps for the coupling regions. Coupling efficiencies in excess of 90% have been achieved.

Prism-waveguide coupling which is simple and reproducible can have a coupling efficiency of more than 90% [28, 29]. Lots of investigations were done for prism coupling to WGMs [30-35] and the best efficiency reported was 80% [31]. Prism-to-sphere coupling is among the earliest concepts and requires only relatively inexpensive hardware [30].

Besides, side-polished fiber couplers [36-38] (having limited efficiency owing to residual phase mismatch), fiber tapers [39-46] (almost ~100% coupling achieved), hollow fibers[47], “pigtailing” technique [48, 49] and special technique of coupling of the cavities and semiconductor lasers [50, 51].

Planar waveguides are used to couple to ring and disk WGRs[52, 53]. Strip-line pedestal anti-resonant reflecting waveguides are for robust coupling to microsphere resonators and for microphotonic circuits [54, 55].

The tapered fiber [39] is a very powerful and efficient coupling tool. The efficiency of tapered fiber couplers reaches 99.99% for coupling fused silica resonators [44]. Unfortunately, fiber tapers as unclad, unsupported waveguides, are very fragile and only applicable to resonators with refractive index similar to silica. They cannot be used with higher index glass and crystalline WGRs.

Take tapered fiber as an example, the light travel in the fundamental mode along the waveguide formed by the dielectric waist or taper surrounded by air. If the waist is small, the fundamental mode will have an evanescent tail extending significantly out into the free space surrounding the taper, see Figure 1.4 [56].

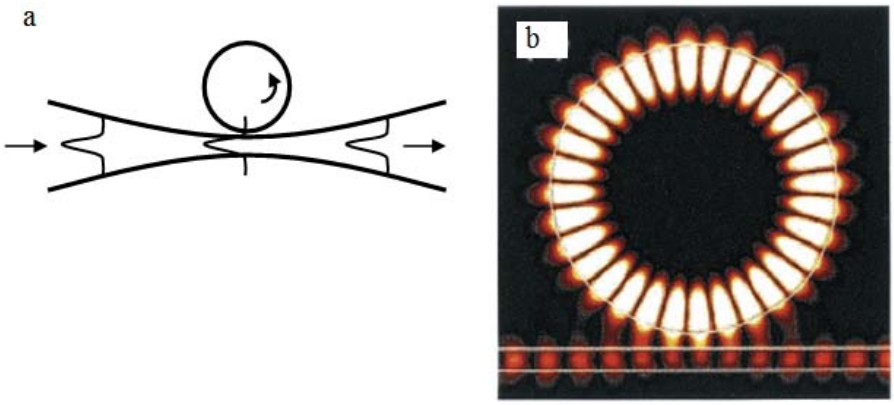

Figure 1.4 Schematic of the coupling between the fiber taper and the microsphere (not to scale)

Some examples of whispering gallery are given as follows see Figure 1.5. In the first row, they are high Q whispering gallery which have Qs of few or tens thousand while on the second row they have ultrahigh Q which can render the magnitude of 10^8 or 10^9 with the diameter less than 1 mm nonetheless.

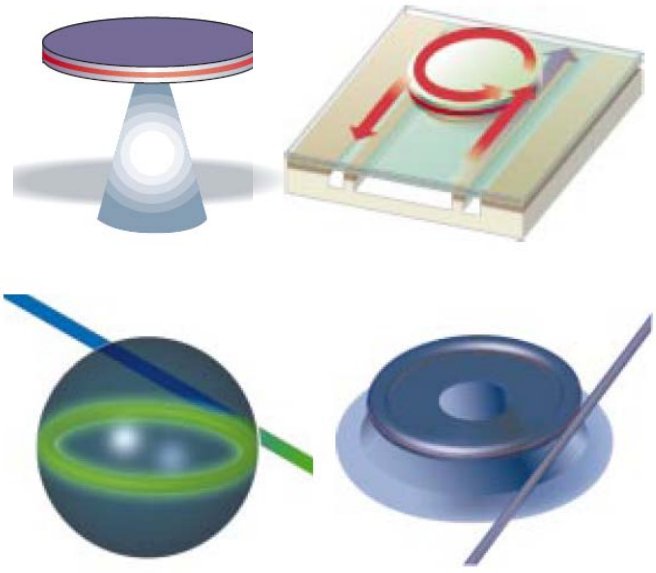

Figure 1.5 Examples of optical whispering gallery

The WGMs were found applications in measurements of spherical particle size, shape, refractive index. Chylek *et al.* [57, 58] deduced the refractive index and

diameter with relative errors of 10^{-5}~10^{-6} using the wavelength dependence of backscattering data from optically levitated particles.

WGM can also be used to determine the diameter of the optical fiber [59]. Highly accurate determination of the outer diameter of unclad glass fibers has been achieved by analysing, at fixed scattering angle, the wavelength dependence of elastically scattered radiation. The positions of resonance peaks in the scattering spectrum are strongly dependent on fiber diameter.

Besides, tunable filters [60-66] can also be realized by WGM. An all-optical tunable filter design based on a WGM resonance technique was proposed theoretically [66]. The filters are tuned by varying the refractive index or the length of the waveguide forming the ring or the cavity. Selectivity and tuning range are controlled by the coupling coefficient of the couplers, the order of resonance in the rings and the reflection coefficient of the discontinuities.

WGR-based biosensor [67-74] is one of the stages in the sensor development. An evanescent wave within the waveguide interacts with analytes on the waveguide surface in the evanescent field sensors. Surface treatments such as antibodies or oligonucleotide strands can provide specificity for the analyte; the sensor then detects only those bound to the surface. In the recent years, WGM was proved theoretically for the detection of a single virion below the mass of HIV[75] and Boyd *et al.* [76] put them into practice for the detection of biological pathogens.

High-Q WGMs result in the increase in sensitivity of various mechanical experiments. Mechanical sensors [77-79] for the measurement of strain in optical fibers [80, 81] were achieved based on WGM. A twin-ball sensor of small displacements was proposed in [81]. The predicted ultimate sensitivity in terms of displacement per unit phase shift is 8×10^{-12} cm/rad at a wavelength λ=1.55 μm (minimum of losses in fused silica), higher than in best Fabry-Pérot interferometers.

Moreover, optical WGRs can be used as efficient and compact optical switches and modulators [82-85] and so on.

1.2.2 Microwave WGM

In 1973 Braginsky, Panov *et al.* [86] discovered that sapphire resonators have extremely low electro-magnetic loss at cryogenic temperatures. Then in the middle of

1970s Dobromyslov and Vzyatyshev did theoretical analysis of WGM in dielectric disk resonators [87]. The first application of WGMR for frequency stabilisation of microwave oscillators was developed by Tsarapkin, Ivanov *et al.* in 1980 [88]. Due to its high frequency stability sapphire WGM was broadly applied for maser and oscillator [6, 89-102].

Extremely high short-term frequency stability has been realized in oscillators based on liquid helium cooled sapphire resonators with a modified mounting structure by Chang *et al.* [92]. The cryogenic sapphire oscillator has demonstrated an Allan deviation of about $5.4\times10^{-16}\,\tau^{-1/2}$ for integration time of 1 to 4s and a minimum Allan deviation of 2.4×10^{-16} at 32s. For integration times longer than 100s the oscillator frequency stability degrades approximately as $3\times10^{-17}\,\tau^{1/2}$.

The observation of above-threshold maser oscillation in a WGM resonator, whose quasi-TM is at a frequency of approximately 12.038 GHz, is supported on a cylinder of monocrystalline sapphire with a loaded Q of several hundred million. Preliminary measurements demonstrate an Allan deviation of a few times 10^{-14} for sampling intervals up to 100 s [91], until now the first whispering gallery mode maser oscillator became possible at FEMTO-ST.

The frequency stability measurement of a new kind of secondary frequency standard, the whispering gallery mode maser oscillator, is reported in [89] and a preliminary result of 10^{-14} frequency instability at 1 s integration time was accomplished.

New results on a cryogenic high power solid-state sapphire WGM maser was presented by Daniel *et al.* [90] and a new Schawlow-Townes thermally limited fundamental frequency stability on the order of $1\times10^{-17}/\sqrt{\tau}$ was estimated.

Before WGM was used, short-term fractional frequency stability was achieved only less than in the magnitude of 10^{-14} at microwave frequencies with oscillators incorporating cryogenic electromagnetic resonators [103, 104]. J.G. Hartnett *et al.* [93] presents the long-term frequency stability of the WGM oscillator 2×10^{-17} for an integration time $\tau>10^3$ s.

Furthermore, WGMs were used for very accurate permittivity and dielectric loss measurements of ultralow loss isotropic and uniaxially anisotropic single crystals [105-113]. Krupa *et al.* [105] measured several materials including sapphire, YAG,

quartz, and $SrLaAlO_4$. The total absolute uncertainty in the real part of permittivity tensor components was estimated to be ±0.1%, limited principally by the uncertainty in sample dimensions. Imaginary part of permittivity was measured with uncertainties of about 10%, limited by the accuracy of Q-factor measurements of whispering gallery modes.

Moreover, WGM technique has the highest resolution for dielectric loss tangent measurements [106, 108, 114] and a minimum variation of 6.5×10^{-5} in $tan\delta$ can be detectable[115].

In 2007 Strouse published a paper "*Sapphire Whispering Gallery Thermometer*" [1], an innovative sapphire whispering gallery thermometer (SWGT) was first explored at the National Institute of Standards and Technology (NIST) with the uncertainty less than 10 mK, see Figure 1.6. Three dimension of cavity were designed and five WGMs for the biggest cavity with nominal resonant frequencies ranging from 14.4 GHz to 19.1 GHz and with *Q*-factors, respectively, ranging from 20,000 to 90,000 were measured within the temperature rang from 0 °C to 100 °C. The accuracies of his WGMTs were in the range of ± 0.02 °C and ice point repeatability was better than 2 mK.

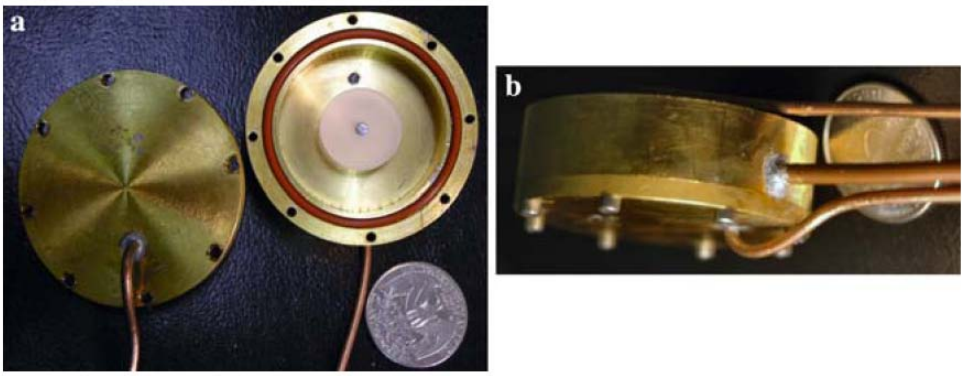

Figure 1.6 (a) Open SWGT with the mounted α-Al_2O_3 disk, microwave cables, and the 0mm length antenna, and (b) sealed SWGT with the added vacuum line

Surely, the stability of the thermometry system depends on the following factors:

(1) Stable support of the dielectric crystal inside the cavity

(2) Minimization of the effect of thermal expansion on the positioning of crystal

(3) Short length of the antennas communicating with crystal

(4) Weak coupling between the antennas and the crystals

(5) Tight seal or vacuum created in the chamber and

(6) Thermal conductivity of each of the elements in the resonator

Of course these factors needn't all be present in each thermometer. It is known to everyone that calibrating an industrial thermometer is extremely expensive so the WGMRT is much more cost efficient than the conventional platinum resistance thermometer.

During the experiments Moldover *et al.* [116] also found the possibility of using WGMR to measure other environmental factors, such as humidity. Because the dielectric permittivity is also affected by humidity then the resonant frequency of the dielectric resonator will change with the humidity.

1.3 Microwave WGM theoretical framework

At least one microwave guide is coupled to the dielectric to provide signals for propagation at a resonant frequency around the annular area around the equator and receives the signal from the dielectric. WGMs are selected such that microwave energy is concentrated on the periphery of the crystal so it provides a low energy density at the sidewall of the metal cavity and at the centre of the crystal along axial direction, as illustrated in Figure 1.7 [117].

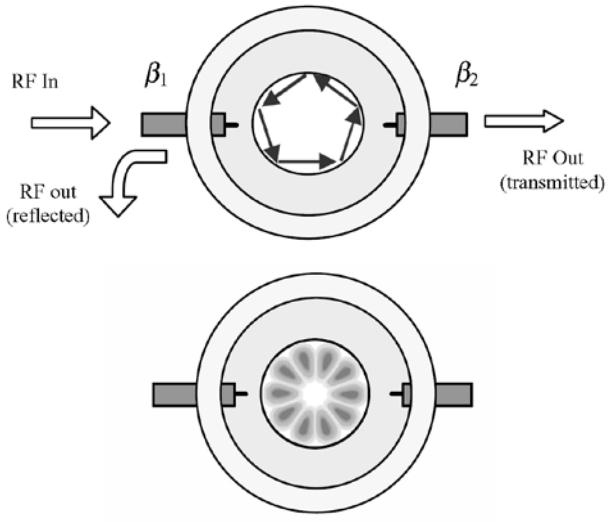

Figure 1.7 Basic principles of WGMR

A temperature determination unit is needed for receiving the signal from the output microwave guide, measuring the centre frequency of the resonance to

determine the temperature of the dielectrics based on a predetermined relationship between resonance frequency and temperature of the dielectrics which may be determined by calibrating the WGMRT against a suitable thermometer. Pumping the WGMRT to vacuum can give a better signal and at the same time get rid of the disturbance of the frequency pressure dependence. So far, a network analyser is used to get the resonant modes between 10 MHz and 20 GHz. Lorentzian fitting programme written by Labview or VB can get the centre frequency and Q of the resonances. The approximate schematic drawing for experiment system is given in Figure 1.8. Of course, knowing the nominal WGM values, it is possible to build an SWGT measurement system at a fraction of the cost of a network analyser.

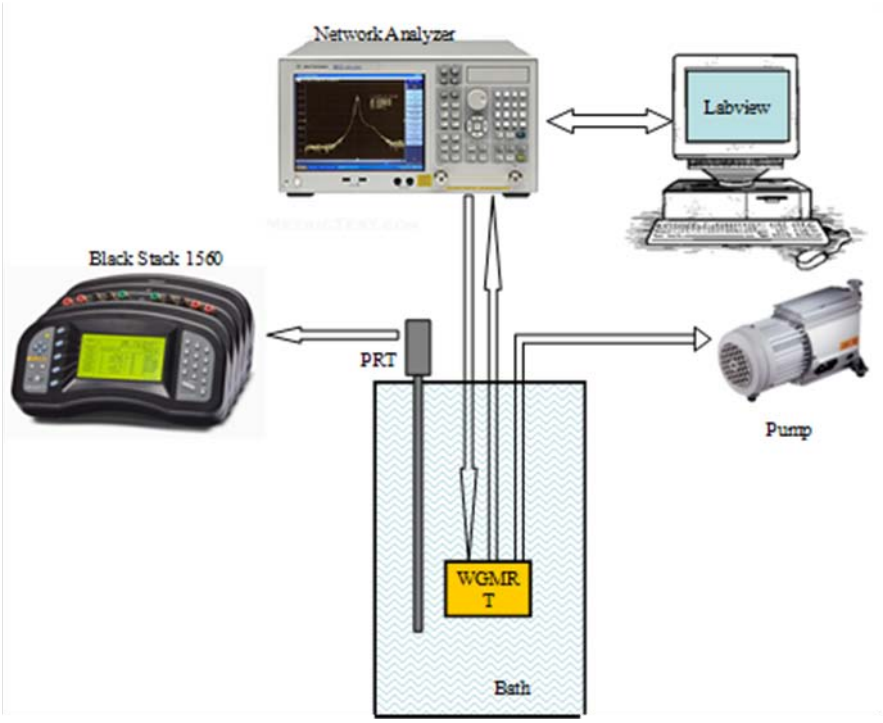

Figure 1.8 Schematic diagram of the measurement system

WG electromagnetic modes can be divided into families depending on their field configuration and further characterized by the number (m) of full waves around the perimeter of the sapphire ring or disk. It is characterized by two polarizations, transverse electric modes (TM-modes) and transversal magnetic modes (TE-modes) [118]. For TM modes, E is radial so it can be excited by a straight antenna directed along the radial direction. While for TE modes, E is axial so the mode is most conveniently excited by a loop antenna whose axis is oriented along the azimuthal direction [107]. In other words, if straight probes are used, only electric modes can be

excited while loop probes could excite more modes: both electric and magnetic modes. However, loop probes produce stronger perturbation to be taken into account and the reproducibility of the thermometer becomes worse. Besides, the strength of the cavity coupling could be changed by altering the vertical distance between the probe and the resonator.

For transmitting electromagnetic energy with low loss waveguide and coaxial lines can be relied. Waveguide has the advantage of high power-handling capability and low loss but is bulky and expensive [119]. Coaxial line has very high bandwidth and is convenient for test application. So in the microwave WGM resonators coaxial lines are used broadly.

As seen in Figure 1.9, it is an electrical cable with an inner conductor surrounded by a flexible, tubular insulating layer, surrounded by a tubular conducting shield. The advantage of coaxial design is that the electric and magnetic fields are confined to the dielectric with little leakage outside the shield. On the contrary, electric and magnetic fields outside the cable are largely kept from causing interference to signals inside the cable.

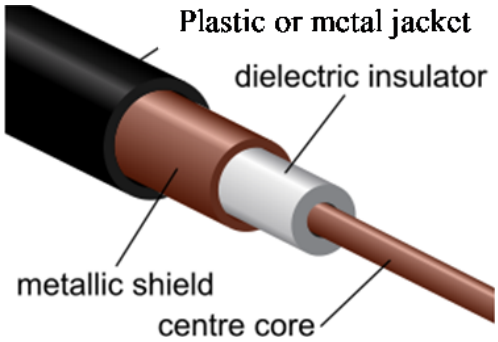

Figure 1.9 Coaxial cable cutaway

There are different kinds of coaxial lines depending on the flexibility, flexible coaxial lines, semi-rigid coaxial lines and rigid coaxial lines. Actually, for the thermometer semi-rigid or rigid coaxial lines are used because of the temperature resistance of the jacket materials.

The characteristic impedance of the cable (Z_0) is a very important parameter for coaxial line because the source and load impedance should be matched to ensure maximum power transfer and 50 ohm is mostly used.

Assuming there are no paramagnetic impurities in the crystal, frequency–temperature dependence due to changes in permittivity of the sapphire crystal can be expressed as[120, 121][113]:

$$\frac{1}{f_0}\frac{\partial f}{\partial T} = \underbrace{-\frac{1}{2}p_{\varepsilon_\perp}\alpha^*_{\varepsilon_\perp} - \frac{1}{2}p_{\varepsilon_{//}}\alpha^*_{\varepsilon_{//}}}_{dielectric\ contribution} \underbrace{-p_D\alpha^*_D - p_h\alpha^*_h}_{dimensional\ contribution} \qquad (1\text{-}1)$$

Where $p_{\varepsilon_\perp}$ and $p_{\varepsilon_{//}}$ are the electric energy filling factor perpendicular and parallel to the crystal axis, p_D and p_h are the radial and axial energy filling factor, α^*_ε is the temperature coefficient of permittivity, α^*_D and α^*_h are radial and axial thermal expansion coefficient respectively.

The frequency-temperature dependence is about 40~70 ppm/K as a result of the permittivity-temperature change of 80~140 ppm/K at room temperature [122], while the frequency change due to the thermal expansion of the sapphire is only 5~6 ppm/K, see Figure 1.10 [121, 123].

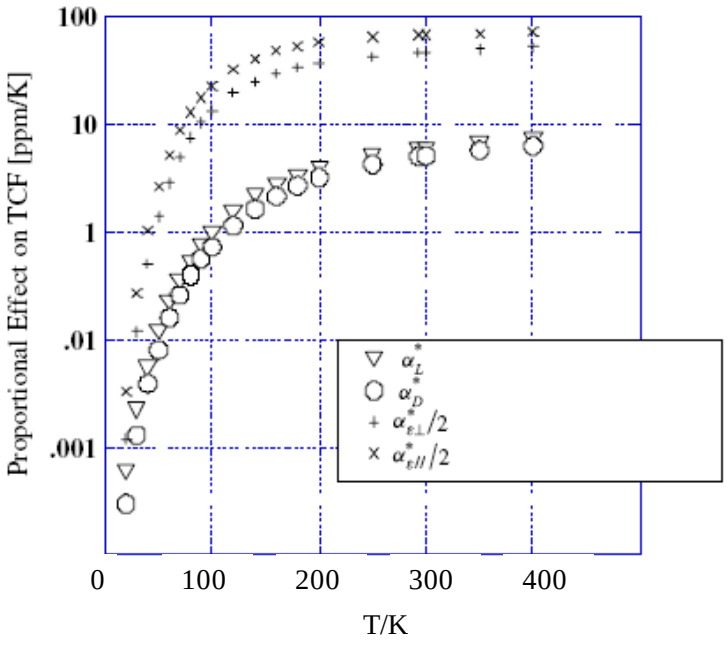

Figure 1.10 Sapphire expansion coefficients and temperature coefficient of permittivity from 4 K to 400 K

Besides, thermal expansion of the copper cavity is a significant factor. Because microwave energy density at the walls is greatly reduced, typically 100 to 10000

times, to enable a high Q, the frequency sensitivity to copper expansion is reduced by the same factor. Thus the 15 PPM/Kelvin copper expansion is reduced to 0.15 PPM/Kelvin or smaller [123], as given in Figure 1.11.

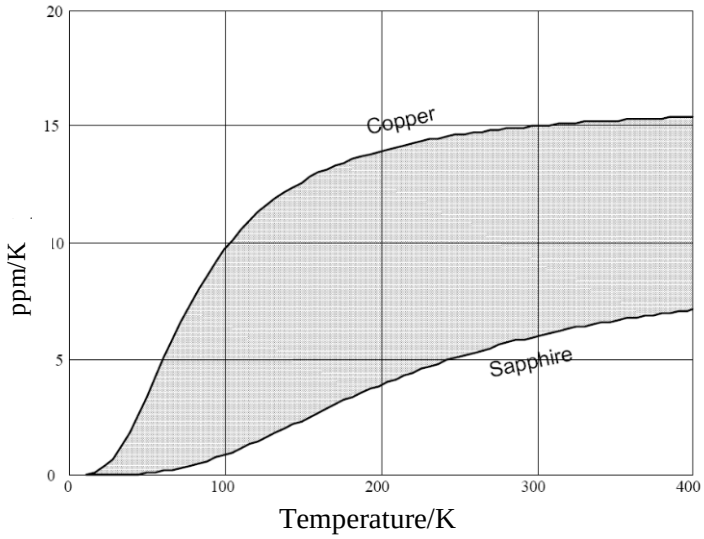

Figure 1.11 Thermal expansion coefficients for copper and sapphire [123]

1.3.1 Q factor

The Q factor (quality factor) of a resonance frequency can be defined via energy storage and resonance bandwidth. According to the energy storage Q can be defined as:

$$Q = 2\pi \frac{Stored\ Energy}{Energy\ Lost\ Per\ Optical\ Cycle} \qquad (1\text{-}2)$$

What is most commonly used is the definition of Q via resonance bandwidth:

$$Q = \frac{f_0}{2g} \qquad (1\text{-}3)$$

Where g is the half-width defined as the width of f for which the energy is half the peak of centre resonance frequency f_0. As seen in Figure 1.12, Q factor is partially dependent on the frequency. The high Q modes reduce sensitivity to changes in cable properties and external electronics. The higher the Q factor the greater the energy in the signal output from the dielectric and the greater the signal to noise ratio (SNR) of the output signal. The greater SNR of the output signal allows the resonant frequency to be detected easily and more precisely [116].

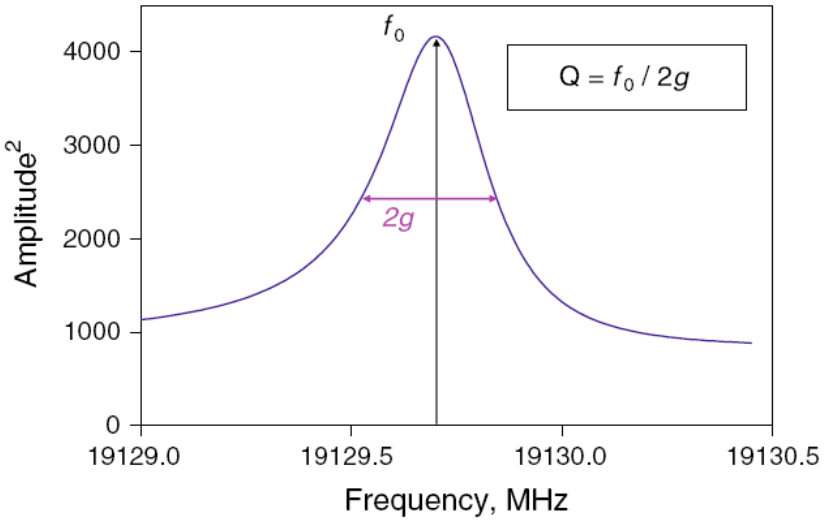

Figure 1.12 Q-factor determination for a resonance

Associated with different kinds of losses of the resonator, the total Q factor can be expressed as [111]:

$$Q^{-1} = Q_d^{-1} + Q_c^{-1} + Q_r^{-1} + Q_{coupling}^{-1} \tag{1-4}$$

Here Q_d, Q_c, Q_r and $Q_{coupling}$ represent the Q factor due to dielectric losses, conduction losses, radiation losses and coupling losses respectively, of which for a loaded resonator the dielectric losses and conduction losses are the main sources which are related as [108, 111, 113, 124, 125]:

$$Q_d^{-1} = \sum_{i=1}^{I} p_{ei} \tan \delta_i \tag{1-5}$$

$$Q_c^{-1} = R_S / G \tag{1-6}$$

Where p_{ei} is the electric energy filling factor for the ith dielectric region (the ratio of the electric energy stored in the DR to the total electric energy stored in the resonant system); tanδ is the loss tangent of the dielectrics; R_s is the surface resistance of the metal shield at a given resonant frequency; G is the geometric factor of the shield. Permittivity is actually a complex number, so “epsilon” is made up of two parts:

$$\varepsilon = \varepsilon' - j\varepsilon'' \tag{1-7}$$

Then the loss tangent can be given by:

$$\tan\delta = \frac{\varepsilon''}{\varepsilon'} \qquad (1\text{-}8)$$

In a WGMR the resonant frequency is smaller than that for the empty cavity and the frequency shift depends on the real permittivity and thickness of the sample while the Q factor due to dielectric losses exhibits very characteristic behaviour as a function of the imaginary part of the permittivity.

1.3.2 Resonator losses and dielectric materials

For a dielectric unloaded cavity, the electromagnetic (EM) energy is stored both within the volume of the cavity itself and the evanescent field surrounding the cavity. The radiation loss and dielectric loss are the main factor limiting the Q factor of the resonator. While for a dielectric loaded cavity, the metallic cavity shields and confines the EM inside the cavity, radiation loss becomes negligible but conduction loss becomes a new factor to think about [95, 125-127]. However, WGMR has most of the energy concentrated on the dielectrics so the conductor loss is also insignificant. Then, finding a kind of dielectric which has very low dielectric loss is in great need. Besides, the coupling loss may reduce the Q unless it is made very low.

In order to minimize the conduction loss and maximize the thermal conductivity as a thermometer, cavity materials are very important. The electric current flows mainly at the "skin" of the conductor, at an average depth called the skin depth. The skin effect causes the effective resistance of the conductor to increase at higher frequencies where the skin depth is smaller, thus reducing the effective cross-section of the conductor. The skin depth is thus defined as the depth below the surface of the conductor at which the current density has fallen to 1/e (about 0.37) of surface current density [118]:

$$\delta = \sqrt{\frac{2}{\mu\sigma\omega}} \qquad (1\text{-}9)$$

Where σ is the conductivity of the conductor; ω is angular frequency of current; μ is absolute magnetic permeability of the conductor.

For microwave, silver, copper and gold are three best conductors whose skin depth at 10 GHz are respectively 0.64 μm, 0.65 μm and 0.79 μm. Therefore, most of

the current flows in an extremely thin region near the surface. The resonant cavity can be made of copper with gold plated in which way the thermal conductivity of copper is very high and at the same time the gold plating can prevent the oxidation. In microwave band a layer of 3 μm gold is thick enough.

In order to make a good thermometer, dielectric constant, quality (Q) factor ($Q \propto 1/\tan\delta$), and temperature coefficient of the dielectrics must be carefully controlled. Plenty kinds of ceramics were studied by researches by using the WGM method. R Ratheesh *et al.* [127] found that BMT can obtain the highest Q factor of 25000 at 13.2 GHz and the temperature coefficient of BMT ceramics is only 10 ppm/K. Quartz [95, 105, 110]and YAG [95] whose loss tangent are in the magnitude of 10^{-5} for RF at room temperature drew lots of attention too. Zychowica *et al.*[95] discovered that for most ceramic materials like single crystal YAG the product of frequency and Q factor is almost constant due to dielectric losses while for single crystal quartz and some low loss plastics like polyethylene or Teflon dielectric loss tangent increases much slower than linearly. Pure quartz ($Si0_2$) single crystal was known as a good microwave dielectric which presents low dielectric losses and slight permittivity anisotropy. Moreover, due to the extensive use of quartz in piezoelectric transducers and resonators, high purity, well orientated and low cost single crystals are easily available. In 1999 V. Giordano *et al.* developed quartz WGMRs with the Q factor in the order of 50000 at l6GHz at 300K [107]. Moreover, Strout *et al.* showed in his paper "*The temperature coefficient of quartz crystal oscillators*" the temperature coefficient of frequency of quartz is about 20 ppm/K at room temperature. For higher permittivity materials such as YAG and sapphire, in an unloaded resonator the radiation losses drastically decrease with increasing the azimuthal number *m*. Rutile is a mineral composed primarily of titanium dioxide TiO_2 which renders high permittivity and low loss were studied by Tobar *et al.* [128, 129].

Afterwards, sapphire attracts people's attention because of its low loss (in the magnitude of 10^{-6} or even lower), higher dielectric constant and higher temperature sensitivity (about 40 ppm/K-70 ppm/K) since 1970s [117]. Moreover, because rutile has an opposite temperature coefficient of permittivity (TCP) it is often used to design a zero TCF resonator. A comparison of frequency sensitivity of quartz and sapphire was given by Lajoic *et al.*[96] in Table 1.1. Material properties comparison between sapphire and rutile are also given in Table 1.2.

Table 1.1 Frequency sensitivity of quartz and sapphire

		$\frac{1}{\varepsilon_z}\cdot\frac{\Delta\varepsilon_z}{\Delta T}$	$\frac{1}{\varepsilon_t}\cdot\frac{\Delta\varepsilon_t}{\Delta T}$	α_T	$\frac{1}{f}\cdot\frac{\Delta f}{\Delta T}$ *for WGH*	$\frac{1}{f}\cdot\frac{\Delta f}{\Delta T}$ *for WGE*
Quartz	300 K	22	14	13.6	25	-21
	77K	< 1	< 1	5.6	-6	-6
Sapphire	300 K	125	107	5	-70	-55
	77K	20	22	0.1	-10	-10

Table 1.2 Material properties of sapphire and rutile at 270 K

Material	$\varepsilon_{//}$	$\varepsilon_{\perp}$	$\tan\delta_{//}$	$\tan\delta_{\perp}$
Sapphire	11.5458	9.3733	4.18×10^{-6}	6.69×10^{-6}
Rutile	169.041	87.6482	9.05×10^{-5}	7.20×10^{-5}

Due to excellent chemical stability, good thermal conductivity, high heat resistance and light transmission sapphire plays an ever-increasingly important role as a material for high reliability Opto-Electrics today. Sapphire is a single crystal aluminium oxide (Al_2O_3) whose softening point is around 1800 °C. Because of its hexagonal crystalline sapphire exhibits anisotropy in many optical and physical properties, see Figure 1.13. Sapphire has the same atomic composition as pure alumina (Al_2O_3) but alumina is amorphous while sapphire is crystalline. The exact characteristics of an optical component made from sapphire depend on the orientation of the optic axis or c-axis relative to the element surface. Moreover, sapphire exhibits birefringence, a difference in index of refraction in orthogonal directions.

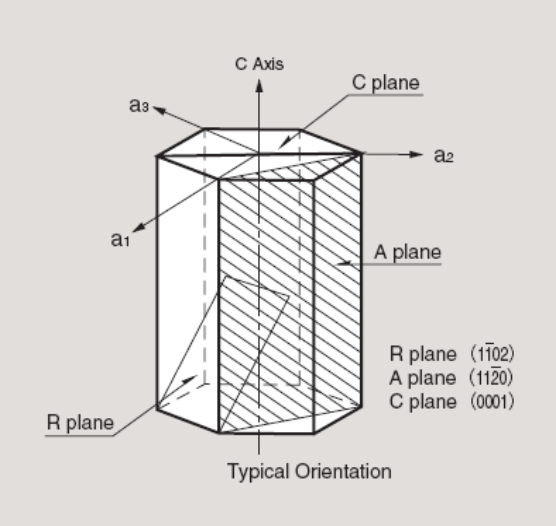

Figure 1.13 Sapphire unit cell

Figure 1.14 shows two sets of measurements of the dielectric constants of sapphire from Krupka *et al.* [105]. The smooth curves fit to the data of Shelby *et al.* [122]. As seen in two figures, the permittivity of the sapphire doesn't change linearly with the temperature but in polynomial function. Mehl [130] did fitting to these two sets of data and the corresponding equations are given as follows (the unit of the temperature in the following equations are given in Kelvin).

$$\varepsilon_{\perp} = 9.2676 + T(-0.000238995 + T(0.0000029 + T(-2.4\times10^{-9}))) \quad (1\text{-}10)$$

$$\varepsilon_{//} = 11.347 + T(-0.00046 + T(0.00000591 + T(-5.6\times10^{-9}))) \quad (1\text{-}11)$$

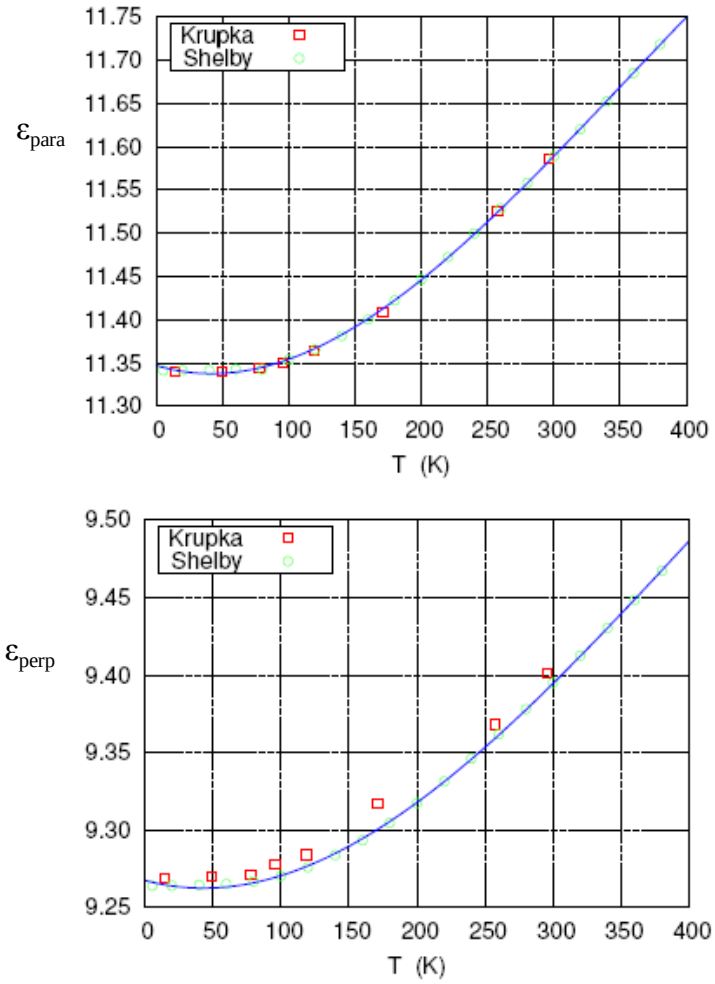

Figure 1.14 Dielectric parameters of sapphire, from Krupa *et al.* [105] and Shelby *et al.* [122]

Figure 1.15 illustrates three sets of measurements of the loss tangent of sapphire from Krupka *et al.* so the Q of the resonator will become lower and lower when the temperature goes higher.

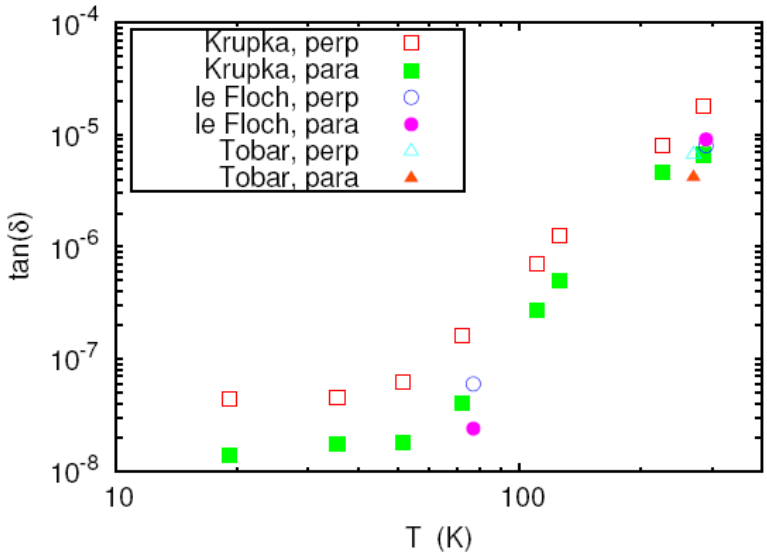

Figure 1.15 Loss factor for sapphire from Krupka *et al.* [105], Le Floch *et al.* [131], and Tobar *et al.* [128]

The sapphires used in this thesis have two kinds of orientations; one has c-axis aligned with z-axis of the sapphire (0° orientation sapphire) and the other one has the c-axis perpendicular to the a-axis (90° orientation sapphire). The modes for 0° orientation sapphire are doubly degenerate with azimuthal phase of the two submodes differing by 90°, while for 90° orientation sapphire azimuthal mode degeneracy is lifted greatly.

1.4 Research motivation

Among various types of industrial thermometers exist today Platinum Resistance Thermometer (PRT) is the most commonly used within the temperature range of -196 °C to 500 °C with the uncertainties of less than 10 mK. PRT offers not only great accuracy, stability and repeatability but also benefits from low drift, wide operating range and its suitability for precision applications.

However, platinum resistance thermometers are very delicate instruments. Shock, vibration, or any other form of acceleration may change the physical state of the annealed, loosely supported platinum resistance element. It is empirically well known that even a little mechanical shock causes easily the resistance change equivalent to more than some tenth of millikelvins in temperature and that strong shock causes the change of some millikelvins. Careless day-to-day handing of a thermometer over one year can increase its resistance at the triple point of water by an

amount equivalent to 0.1 K [132]. Depending on the reason for this change in R_{tp}, unless calibrated it could lead to temperature errors as high as 10 mK. Similar changes may be caused by an apparatus that transmits vibrations to the thermometer or by shipping the thermometer in an unsuitable container.

Furthermore, an AC resistance bridge is typically required as a readout device for standard platinum resistance thermometers which is very expensive ($50 000~$75 000).

Under these circumstances a new industrial thermometer WGMRT which offers greater vibration immunity, improved stability, potential lower uncertainty and lower cost than PRT emerges.

1.5 The possible development tendency

In order to be used broadly in industrial, the dimensions of the sapphire WGMRT should be at least comparable to PRT. However, the WGM gets higher and higher when the diameter of the sapphire becomes smaller and smaller. Besides, the dielectric loss tangent limits the intrinsic performance of the resonator and the network analyzer presently works only at frequency lower than 20 GHz. Very high Q factor at relatively low frequency can be achieved by Bragg reflection technique in a small compact resonator [133-135].

Strouse and Moldover [116] proposed the future tendency of the resonator thermometer will be like Brag Reflector as shown in Figure 1.16. In this thermometer there is less cross talk between spurious modes and whispering gallery modes and great possibility to be made smaller. But because of the complexity of the dielectrics the machining and mode calculation will be big problems.

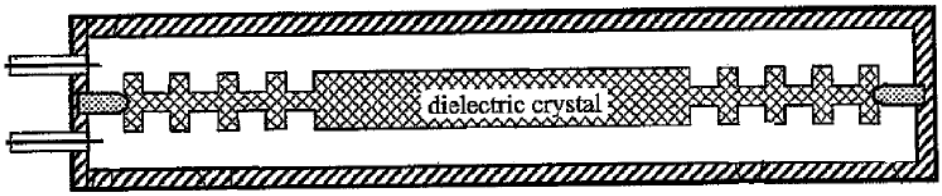

Figure 1.16 Brag reflection mode thermometer

1.6 Conclusion and main contents of thesis

The Ph.D. thesis aims to develop a new kind of industrial thermometer that can render both shock resistance and high performance at the same time. This thesis consists of most of the researches about WGMT done during my Phd since 2009 at INRIM and NIST.

Chapter 1 described some basic knowledge about WGM and talked about the theory feasibility of the research. The state of the art of the WGMRT and the applications were also reported. Besides, the motivation of the research and the possible development dependency was presented too.

Chapter 2 introduces cylindrical sapphire WGMRT which has similar dimensions to one of the NIST SWGTs [1]. Three series of experiments were done at INRIM within the temperature range of -40 °C to 85 °C based on two sapphires. Ice melting point repeatability and stability will also be specified in this chapter. The frequency response with temperature between 15 °C and 25 °C was logged to compare with PRT. After three sets of experiments, reproducibility of the WGMRT will be analyzed. Comparisons between the calculation and experiments will be carried on too.

A new shape of sapphire, spherical sapphire which is new to now, was illustrated in Chapter 3. Series of experiments were done at INRIM within the temperature range of -40 °C to 85 °C. Ice melting point repeatability and stability will also be specified in this chapter for WGMRT based on spherical sapphire. The frequency response with temperature between 15 °C and 25 °C was logged to compare PRT with cylindrical sapphire WGMRT. All the specifications of this new thermometer will be compared with cylindrical one referred in last chapter. Four different samples with the same nominal specification and reassemble for one of the specimen were all tested to check the reproducibility of the thermometer.

In Chapter 4, my research done at NIST which were focused on the sapphire rods will be described. At the same time Mehl did the calculation by finite element method to match with my experiments. Moreover, dimensions optimizations were done to decrease the size of the thermometer with highest Q factor based on handy sapphires. Furthermore, two kinds of orientations of sapphire rods were tested and

birefringence of the 90° orientation sapphire was used to make a new kind of thermometer. After the agreements of the experimental results and calculations in certain accuracy a newly sapphire resonator capsule thermometer was designed. This part contributes a lot for making the WGMT smaller and compact.

Two appendixes were enclosed at the end of the thesis. They listed all my experiments results corresponding to the figures shown in the former chapters and the schematic drawing of my WGMRTs.

Chapter 2 Cylindrical Sapphire WGMRT

2.1 Introduction

As a result of the easy machining and assembling of the cylindrical sapphire, a cylindrical sapphire WGMRT was first developed by Strouse [1]. Three kinds of dimensions were fabricated and only one of the dimensions was reported. The overall accuracy of the system was in the range of ± 0.02 °C and its ice melting point stability was less than 1 mK with a frequency resolution equivalent to 0.05mK.

Based on Strouse's work in paper "Sapphire Whispering Gallery Thermometer" [1], cylindrical sapphires which have the same nominal dimensions as one of them referred in his paper were machined. Cavity sizes are also the optimized dimensions but with two antennas soldered on one side. All the experiments in this chapter were carried out in INRIM.

The sapphire was used in this experiment was purchased from Crystal Systems Inc. and it is HEMEX sapphire disk with 12 mm ∅ by 12 mm thickness and a 2 mm ∅ center hole goes through. The C-axis of the sapphire is aligned with z axis within ±6', see Figure 2.1, the drawing and the picture of the sapphire are given.

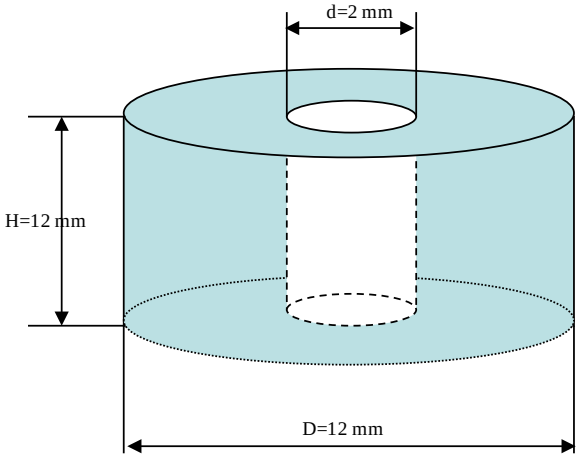

Figure 2.1 Drawing and picture of 0° orientation sapphire used in the experiment

A brass screw through the hole holds the sapphire inside a gold-plated copper cavity. Spacers between the sapphire and the cavity cap keep it in the preferred position where the EM field coupling is maximum with respect to the relevant WGMs

but minimum to the neighbor modes. Since the WGMs have the advantage that most of the EM energies are concentrated to the equatorial circle of the spherical crystal, the central hole, the screw and the small spacers do not affect the performance of the WGM resonator thermometer. Viton o-rings were used to seal the cavity which was continuously vacuumed in order to prevent humidity condensation into the cavity through a vacuum line. Two microwave coaxial cables were tin-brazed to the top cap of the cavity where the sapphire sphere was located. The central conductors of the coaxial cables were trimmed so the lengths of the probes penetrate into the cavity are 0 mm. In this way the Q factor of the resonance modes are greatly enhanced and the spurious modes are greatly reduces; in addition, it improved the reproducibility, stability and shock resistance of the thermometer.

Pictures of the cylindrical sapphire WGMRT are given as follows. Figure 2.2a shows the top cap of the cavity where the mounted cylindrical sapphire, the microwave cables, and the antennas are fixed. Figure 2.2b represents the polished gold plated bottom cap, the cavity body with o-ring seals and the vacuum line. The schematic drawing for the cavity are given in Figure B 1, Figure B 2 and Figure B 3.

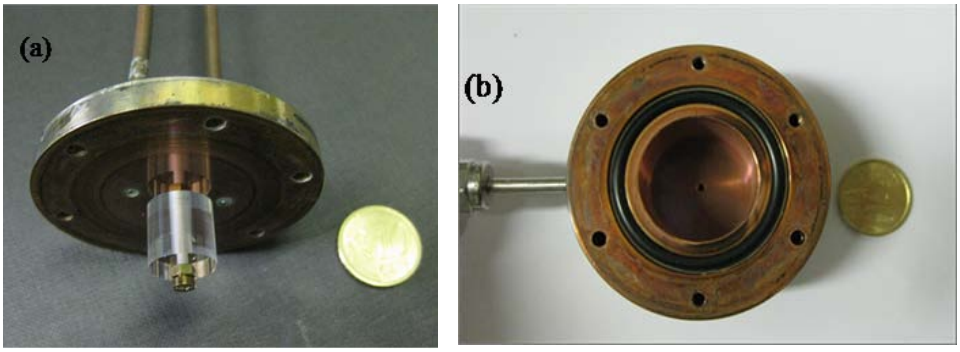

Figure 2.2 (a) Top cap of the cavity with the cylindrical sapphire and antennas; (b) polished gold plated bottom cap, cavity body with o-rings seals and the vacuum line.

2.2 Cylindrical Sapphire WGMRT Calculation

Before starting the experiments, Finite Element Method (FEM) analysis was carried out to locate the WGMs. There are three WGMs near 12.4070 GHz (WGM3), 15.1471 GHz (WGM4) and 17.8404 GHz (WGM5) respectively with azimuthal number m equal to 3, 4 and 5. Table 2.1 presents the calculation result of three WGMs. The Q improves with the increase of the azimuthal number. In the analysis all the metal surfaces were treated as perfect electric conductor and the sapphire was treated

as lossless too. Thereby, the practical Q will be much lower than the calculated one. In the calculation, the permittivity of the sapphire is used as: $\varepsilon_x = \varepsilon_y = \varepsilon_{\perp} = 9.391$, $\varepsilon_z = \varepsilon_{//} = 11.5869$ which come from Mehl's [130] fits to two sets of measurements of Krupka et al. [105] and Shelby *et al.* [122].

Table 2.1 The calculated WGMs and Qs for cylindrical sapphire WGMRT

Mode	m	f_{cal}/GHz	Q_{cal}
1	3	12.4046	298420
2	4	15.1471	1513100
3	5	17.8411	4717600

Figure 2.3 shows the patterns of the electric energy density for three WGMs. As expected, the WGM has most of the energy concentrated near the edge of the sapphire so the central hole and screws have negligible perturbation to the energy distribution.

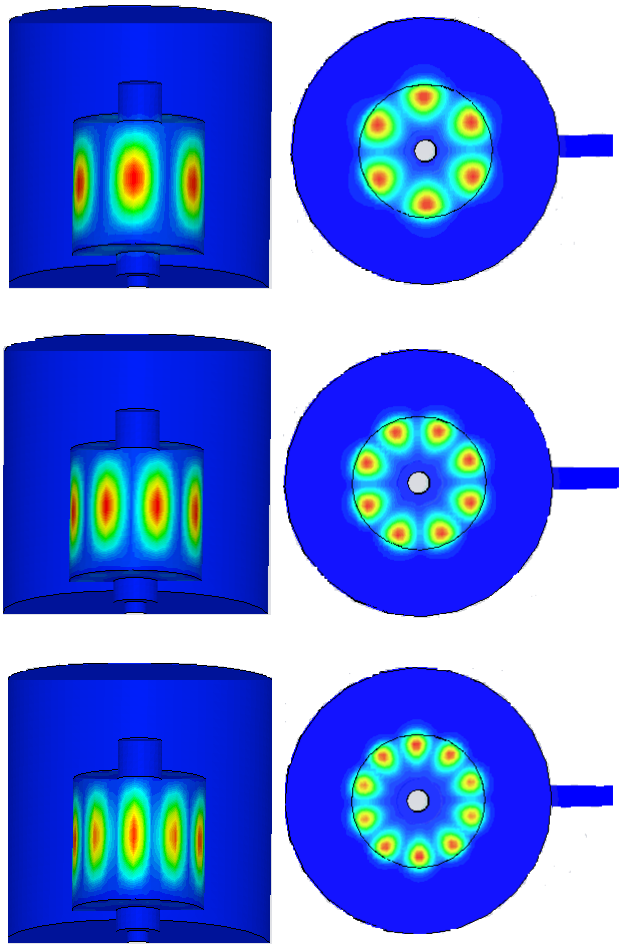

Figure 2.3 3D and 2D electric energy densities for WGMs

2.3 Experiments on Cylindrical Sapphire WGMRT

Experiments in this chapter were carried out at INRIM. Series of experiments were performed within the temperature range of -40 °C to 85 °C with a standard deviation of better than 3 mK based on two cylindrical sapphires which have the same nominal specifications. The corresponding characteristics of the WGMRT will be reported based on two sapphires. The uncertainty, repeatability, stability, hysteresis error, frequency temperature sensitivity and frequency response with temperature of the cylindrical sapphire WGMRT will be reported. Moreover, two sapphires which have the same nominal specification and the reassemble for one of them (sapphire 2') will be tested respectively to explore the reproducibility of the thermometer.

Experiments were performed in a Hart Scientific 7381 bath with an INRIM calibrated PRT read by 1560 Black Stack bridge. The center frequencies and Qs at each temperature were logged by an Agilent E5071C Network Analyzer and corresponding Labview programme. A picture of measurement system is given in Figure 2.4 (computer is not included).

Experimental measurements showed a Q in excess of 170000 for the mode with the highest azimuthal number, making it possible to achieve a potential temperature resolution of 0.05 mK.

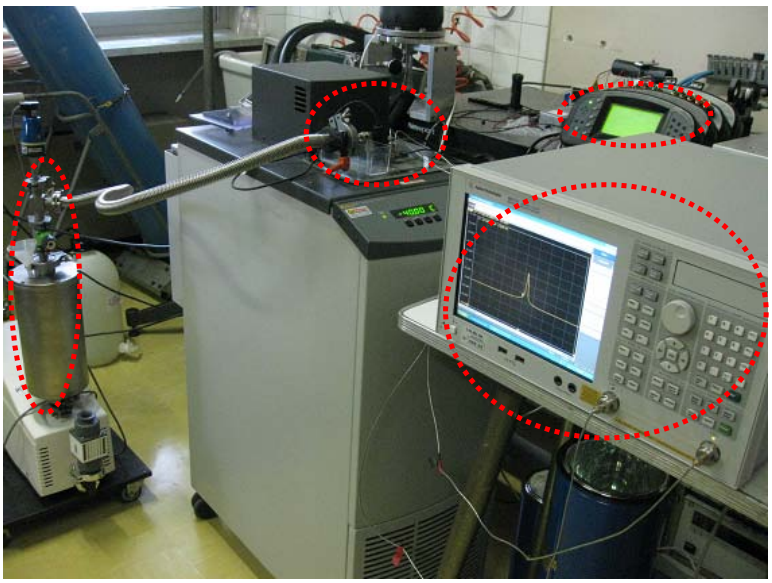

Figure 2.4 Picture of measurement system

2.3.1 Thermal Cycling Experiments

Thermal cycling experiments were carried out in the temperature range of -40 °C to 85 °C. Two sapphires were tested respectively and then repeated for one of the sapphires. Three sets of experiment results based on two sapphires are enclosed respectively in appendix in Table A 1, Table A 2 and Table A 3. The frequency and Q factor decrease with the ascending of the temperature see Figure 2.5 and Figure 2.6, take WGM5 as an example.

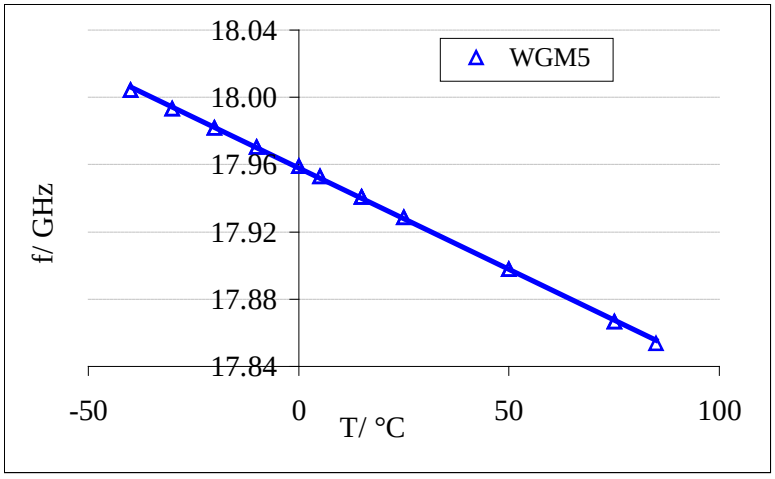

Figure 2.5 Frequency change with the temperature of the cylindrical sapphire WGMRT

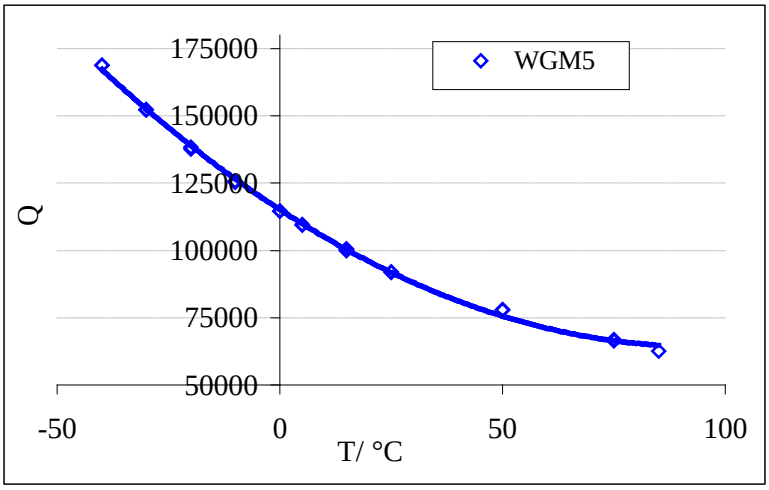

Figure 2.6 Q factor change with the temperature of the cylindrical sapphire WGMRT

In order to know how the WGMs change as a function of temperature, cubic fit was first employed to the thermal cycle experiments data, see Figure 2.7 and Figure 2.8 and they both show the suggestions of using quartic fit.

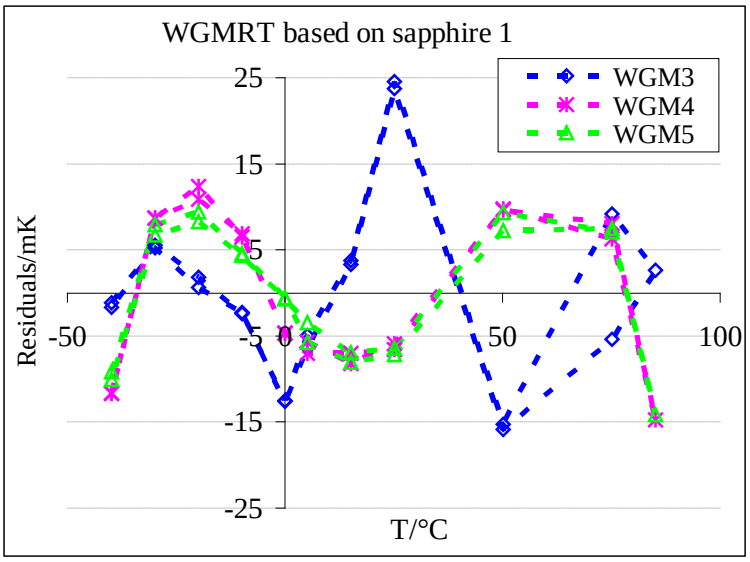

Figure 2.7 Cubic fit residuals for three WGMs(sapphire 1)

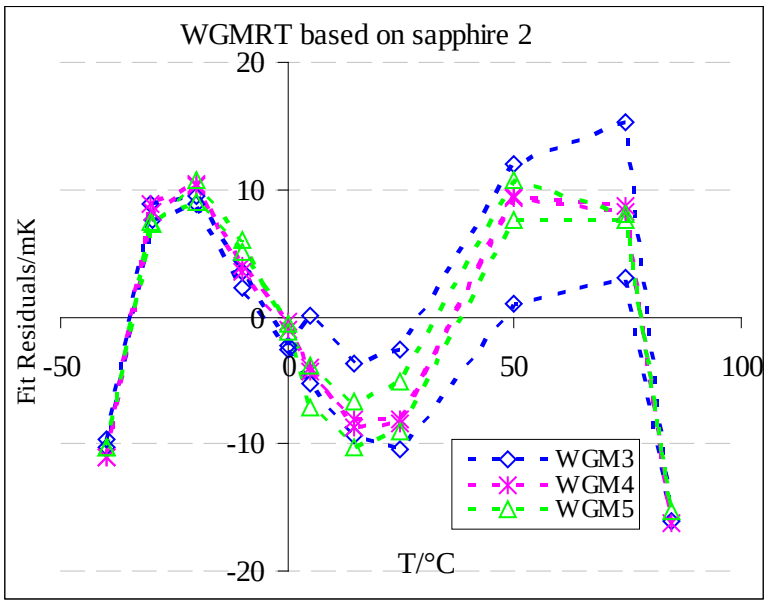

Figure 2.8 Cubic fit residuals for three WGMs(sapphire 2)

Figure 2.9 illustrates the quartic fit residuals of three WGMs based on sapphire 1 and significant improvements are expected from around ± 25 mK, 15 mK and 15 mK to ± 25 mK, ± 4 mK and ± 2 mK respectively for WGM3, WGM4 and WGM5 and they are not totally correlated as a function of the increasing azimuthal mode. The standard deviation of the residuals also decreases from 10.6 mK, 9.0 K and 7.7 by cubic fit to 10.1 mK, 1.8 mK and 0.8 mK by quartic fit. Besides, there is not significant hysterisis error can be seen from sapphire1-based WGMRT for three

WGMs except that WGM5 shows a hysterisis error of 2.3 mK around 5 °C and 50 °C, see Figure 2.10.

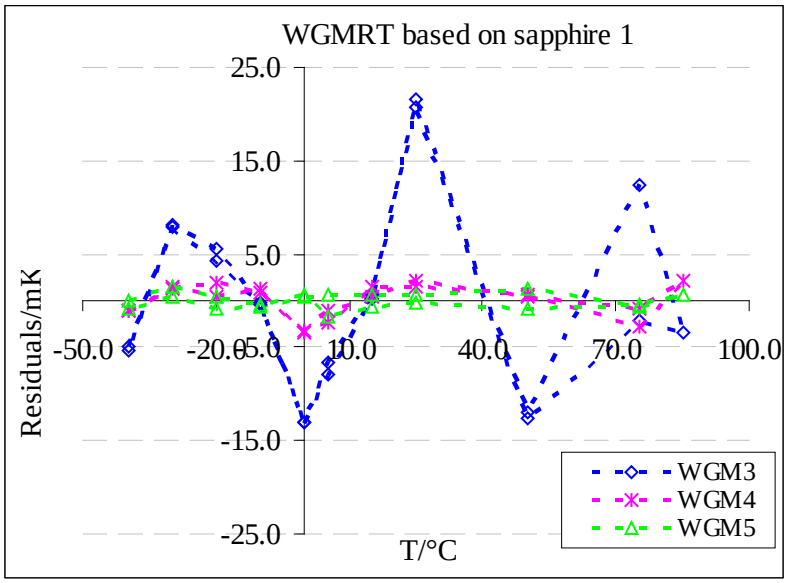

Figure 2.9 Quartic fit residuals for three WGMs (sapphire 1)

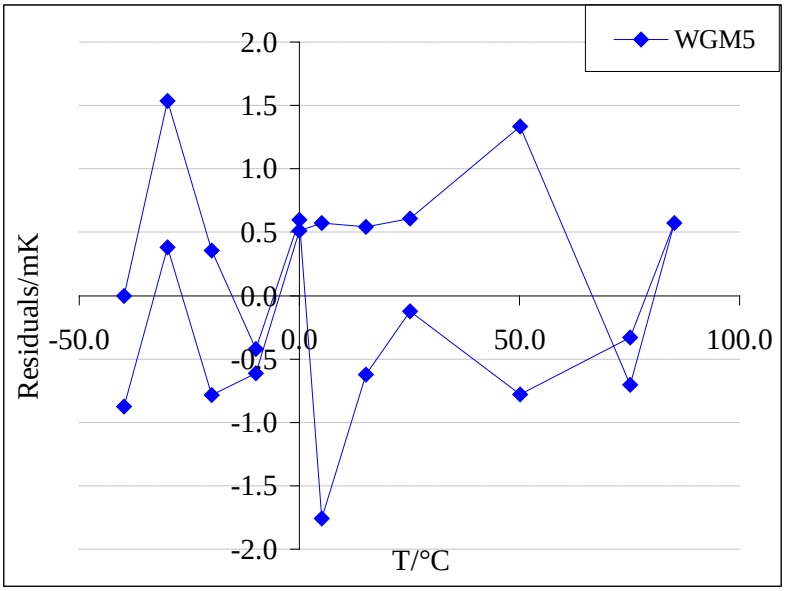

Figure 2.10 Quartic fit residuals for WGM5 (sapphire 1)

Figure 2.11 illustrates the quartic fit residuals of three WGMs based on sapphire 2 and significant improvements are also expected from around ± 15 mK to ± 8 mK, ± 3 mK and ± 3 mK respectively for WGM3, WGM4 and WGM5. The standard deviation of the residuals decreases from 8 mK, 9 mK and 8 mK by cubic fit to 3 mK, 1 mK and 1 mK by quartic fit. Furthermore, a maximum of 16 mK hysteresis error for WGM3 was also shown which should mainly come from the property of the bath.

WGM4 doesn't have significant hysterisis error like sapphire 1 based WGMRT and WGM5 shows a maximum hysterisis error of 3.2 mK, see Figure 2.12 and Figure 2.13.

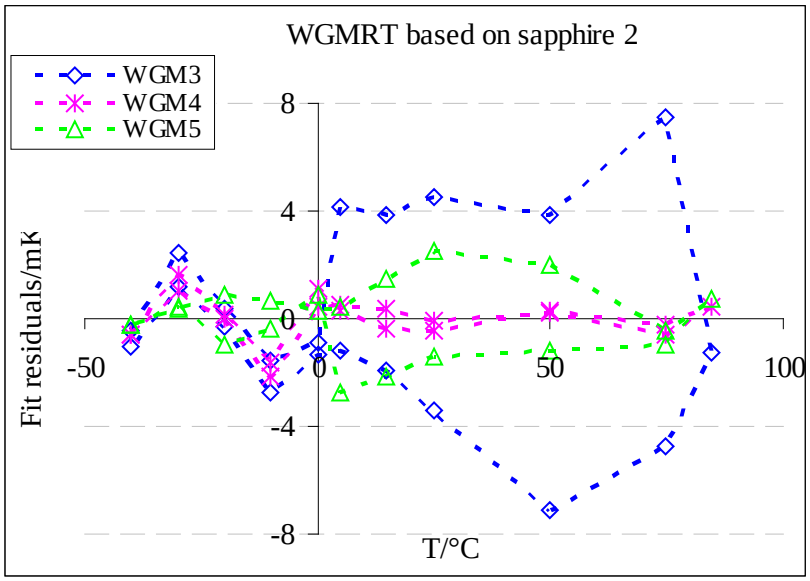

Figure 2.11 Quartic fit residuals for three WGMs (sapphire 2)

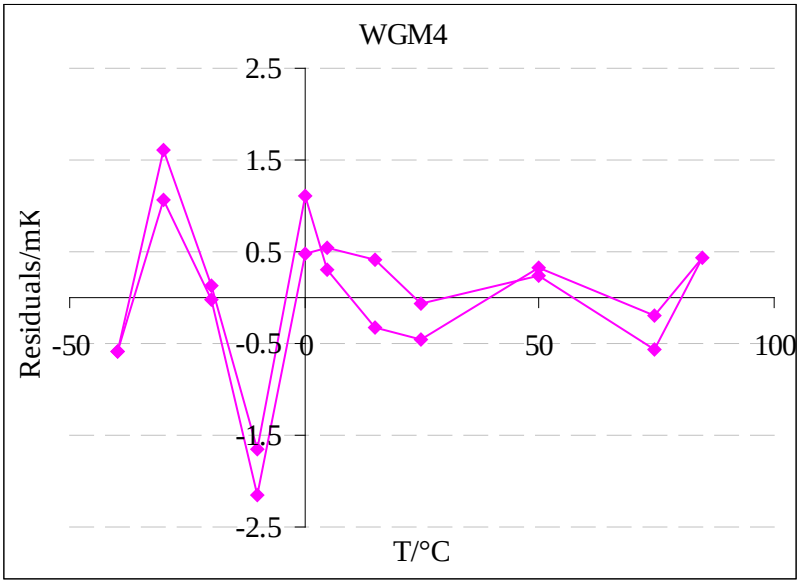

Figure 2.12 Quartic fit residuals for WGM4 (sapphire 2)

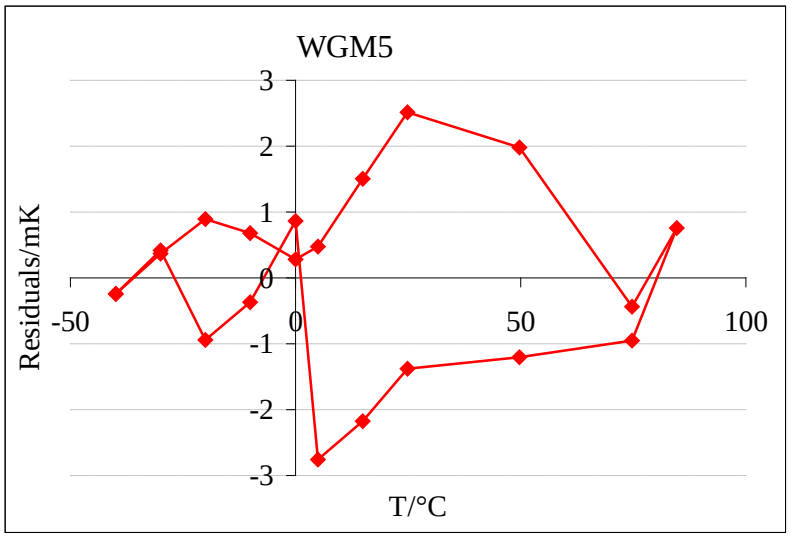

Figure 2.13 Quartic fit residuals for WGM5 (sapphire 2)

As illustrated in Figure 2.14 the WGM resonator temperature sensor has a fractional frequency temperature sensitivity ($\Delta f/f/\Delta T$) ranging from -59 ppm/K at -40 °C to -72 ppm/K at 85 °C. Besides, it is also obvious that the fractional frequency temperature sensitivity changes as a function of the increasing azimuthal mode i.e. the higher the azimuthal number the more sensitive the frequency to the temperature.

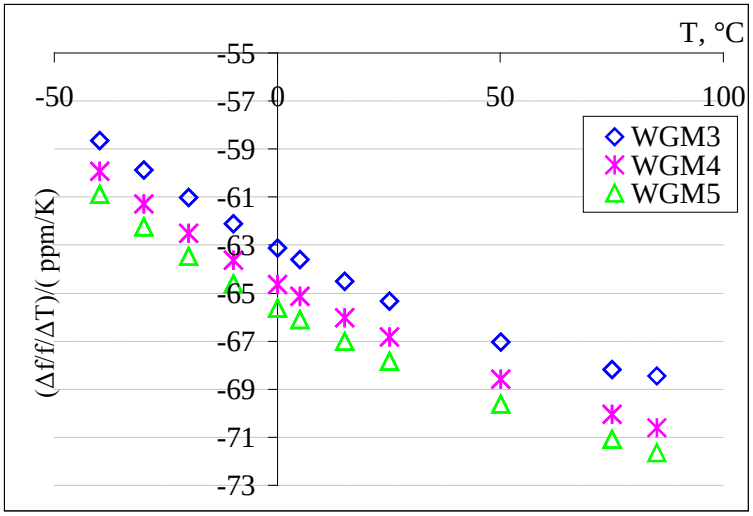

Figure 2.14 Fractional frequency temperature sensitivity for three WGMs

2.3.2 Ice Melting Point Repeatability and Stability

The cylindrical sapphire WGMRT was immersed into the ice melting point dewar at a depth of 30 cm for three days. The picture of the measurement systems are given in Figure 2.15.

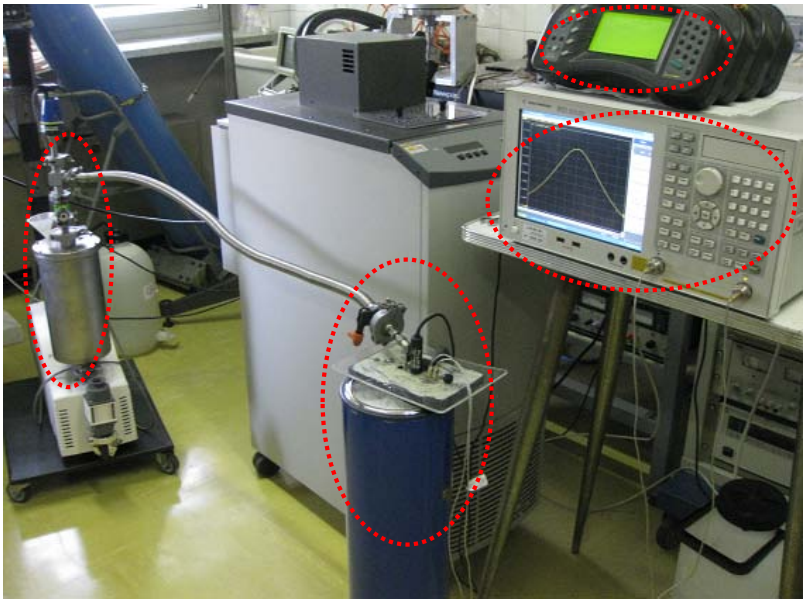

Figure 2.15 Ice melting point repeatability and stability measurement systems

The ice melting point repeatability for WGMRT based on sapphire 1 is shown in Figure 2.16 and it shows a repeatability of better than ± 0.5 mK. There isn't significant drift can be seen from Figure 2. 16. While the WGMRT based on sapphire 2 has a repeatability of ± 5 mK which is mainly limited by the ice temperatures, see Figure 2.17. The ice melting point temperature for WGMRT based on sapphire 2 has a standard deviation of more than 3 mK, see the enclosed in Table A 4 and Table A 5.

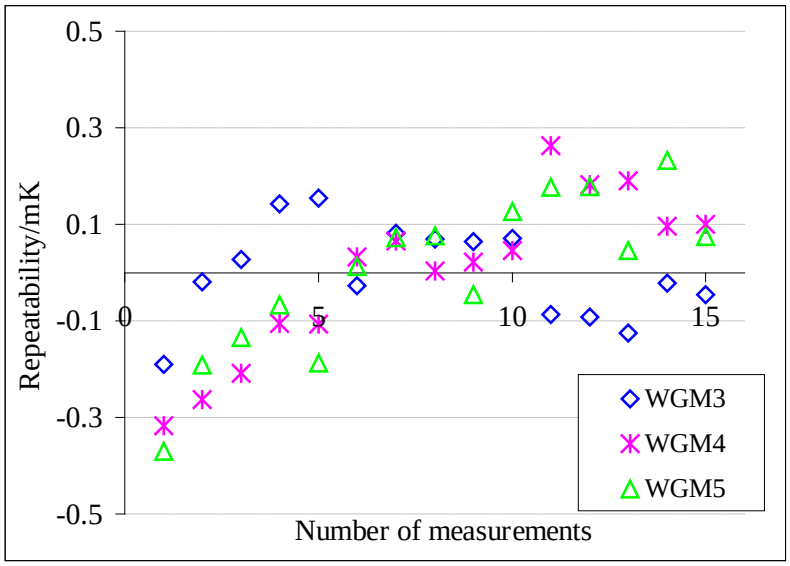

Figure 2.16 Ice melting point repeatability for three WGMs (based on sapphire 1)

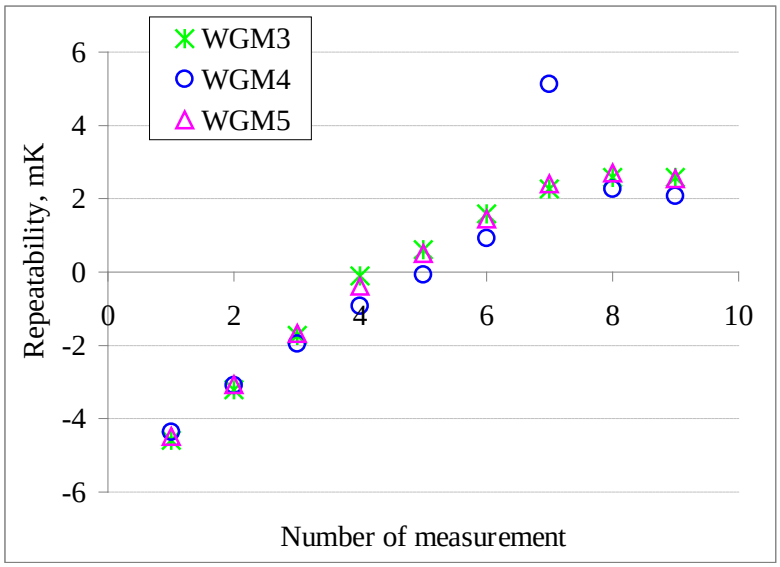

Figure 2.17 Ice melting point repeatability for three WGMs (based on sapphire 2)

The ice melting point stability of the temperature sensor was also explored in more than one hour. The calibrated PRT and the WGM resonator temperature sensor values were both logged during the same time period and the comparisons are given respectively in Figure 2.18, Figure 2.19 and Figure 2.20 for three WGMs.

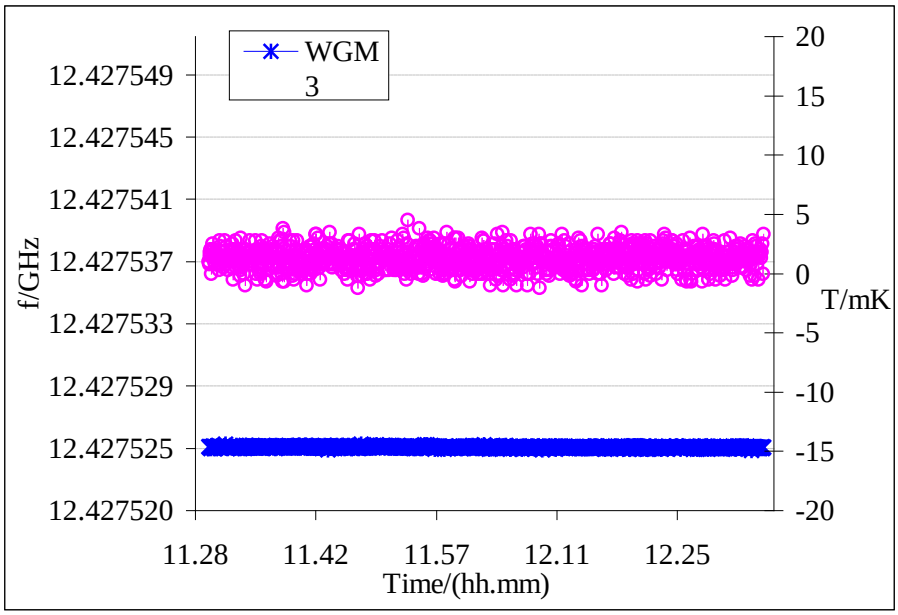

Figure 2.18 Ice melting point stability for WGM3

Figure 2.18 illustrates WGMRT based on WGM3 has an ice melting point stability of about 0.54 mK with comparison to 5.7 mK of PRT. WGM3 shows a temperature range from 14.4 mK to 14.9 mK during the experiment time period while

PRT displays a temperature range from -1.20 mK to 4.50 mK. There is a shift of 15 mK from 0 °C which is mainly due to the measurement accuracy of the sapphire1-based WGMRT is around ± 25 mK based on WGM3.

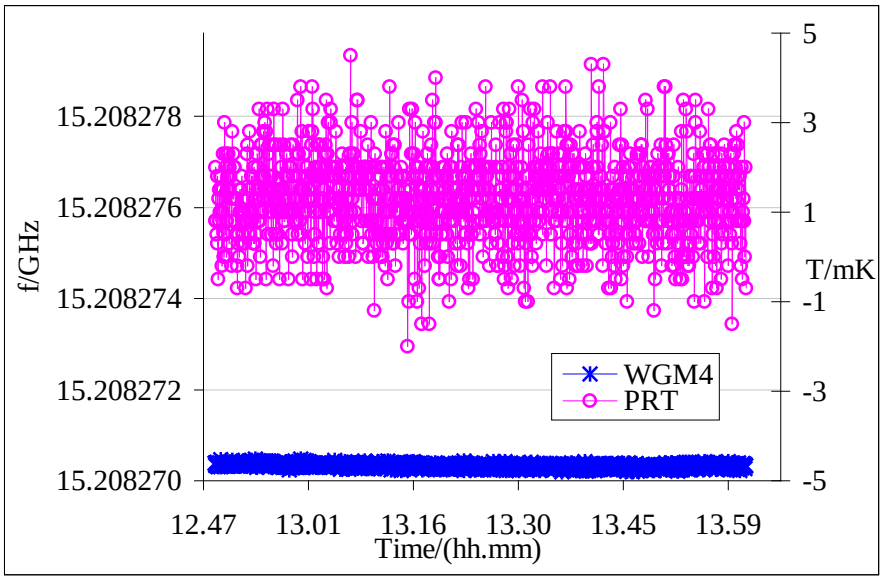

Figure 2.19 Ice melting point stability for WGM4

Figure 2.19 describes WGMRT based on WGM4 has an ice melting point stability of about 0.3 mK with comparison to 6.5 mK of PRT. WGM4 shows a temperature range from 4.51 mK to 4.79 mK during the experiment time period while PRT reads a temperature range from -2.0 mK to 4.5 mK. There is still a shift of around 4.5 mK from the ice melting point temperature.

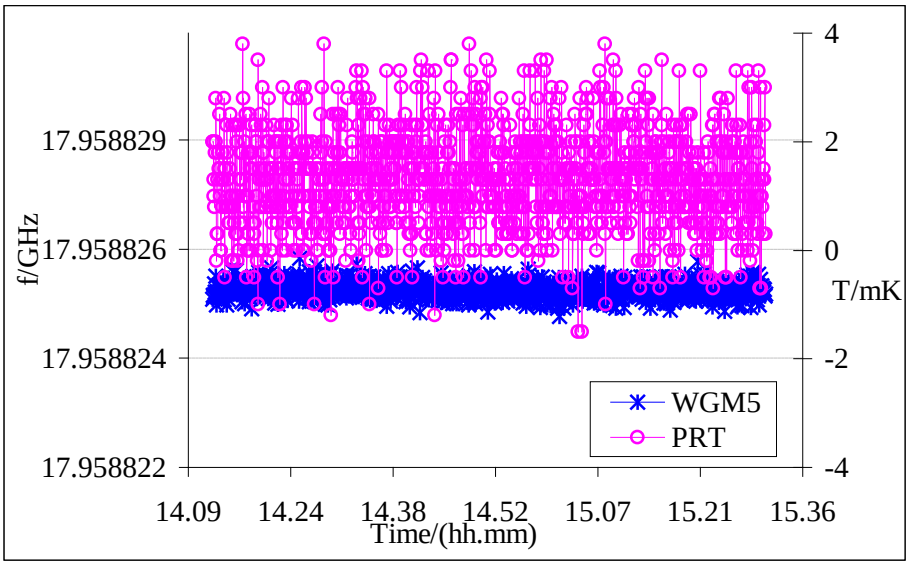

Figure 2.20 Ice melting point stability for WGM5

Figure 2.20 illustrates WGMRT based on WGM5 has an ice melting point stability of about 1.1 mK with comparison to 5.3 mK of PRT. WGM5 shows a temperature range from 0.15 mK to 1.22 mK during the experiment time period while PRT reads a temperature range from -1.5 mK to 3.8 mK. A shift of about less than 1 mK can be seen from the reading.

2.3.3 Frequency Temperature Response Time

Several thermal cycles between 15 °C and 25 °C were tested to explore the frequency temperature response of the cylindrical sapphire WGMRT with temperature change, see Figure 2.21. The WGM increases with the descending of the temperature and for clarity, a zoom in of part of the response was shown in Figure 2.22. As illustrated in Figure 2.22 the WGM resonator temperature sensor responses very quickly with the temperature change with only several minutes delay due to the big mass and vacuum state of the cavity compared to PRT. Nevertheless, the bath power is not high enough to change the temperature quickly may limit the response time of the PRT.

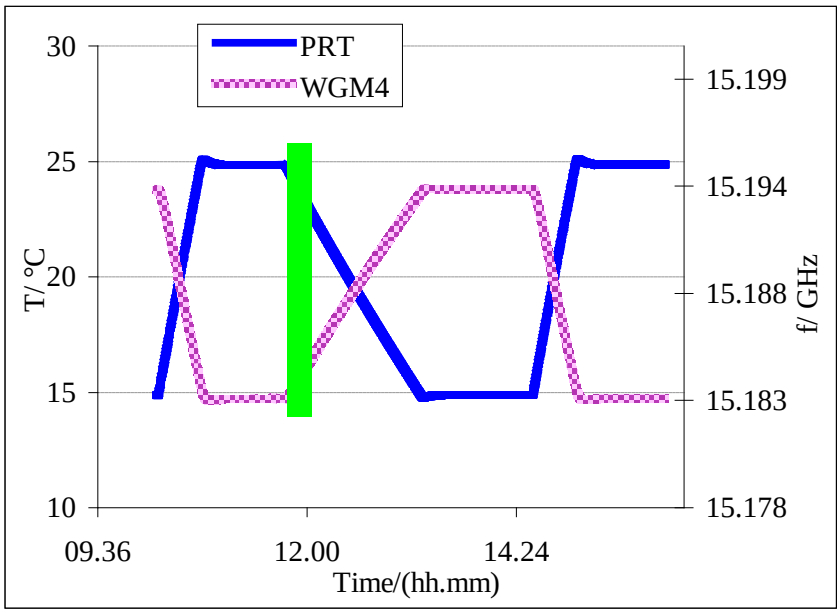

Figure 2.21 Frequency response of the WGM resonator temperature sensor with the temperature change

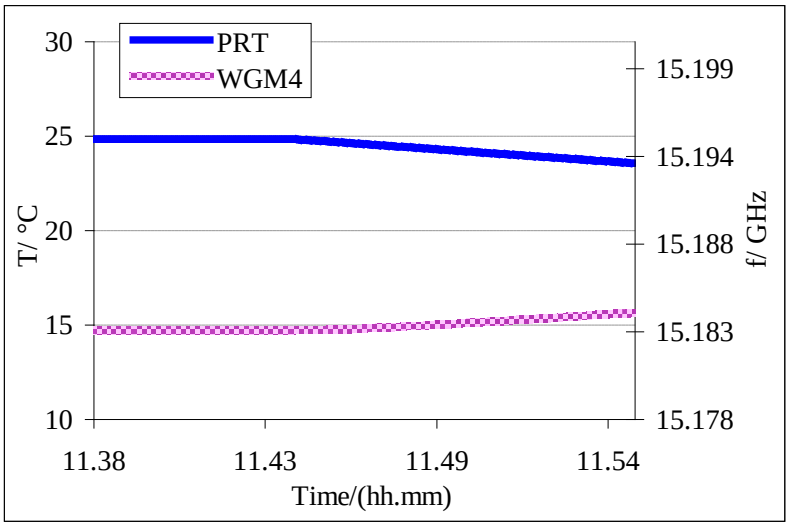

Figure 2.22 Response time of the WGM resonator temperature sensor

2.3.4 Reproducibility Experiments

Two cylindrical sapphires that have the same nominal specifications were explored to investigate the reproducibility of the WGMRT. Besides, the reassemble for one of the sapphire (sapphire 2') was tested too.

The quartic fit functions for WGMRT are given in the format of:

$$f = a_{4i} \cdot T^4 + a_{3i} \cdot T^3 + a_{2i} \cdot T^2 + a_{1i} \cdot T + a_{0i} \qquad (2\text{-}1)$$

Table 2.2 shows the quartic fitting coefficients for three sets experiments of which a_0 is the one that should be calibrated for every specific WGMRT. Take the coefficients for sapphire 1 as the basic one, the calibrated fit residuals for the experiments data based on sapphire 2 (and 2') are shown respectively in Figure 2.23, Figure 2.24 and Figure 2.25.

Table 2.2 Quartic fit coefficient for three sets of experiments for all WGMs

WGM	Sapphire	$a_4 \times e^{12}$	$a_3 \times e^{9}$	$a_2 \times e^{7}$	$a_1 \times e^{4}$	a_0
3	1	1.82464	1.55201	-5.85634	-7.84381	12.42753617
	2	-4.56204	1.88662	-5.70431	-7.84705	12.42973833
	2'	-5.38857	2.02139	-5.71849	-7.84739	12.42728680
4	1	-6.43598	2.38884	-7.07795	-9.38200	15.20827530
	2	-6.43631	2.39286	-7.10113	-9.83201	15.21018041
	2'	-6.01304	2.36334	-7.11649	-9.82862	15.20950557
5	1	-6.72068	2.77616	-8.46959	-1.17857	17.95882628
	2	-7.43343	2.83470	-8.46514	-1.17870	17.96084597
	2'	-4.70421	2.51608	-8.41938	-1.17831	17.96061369

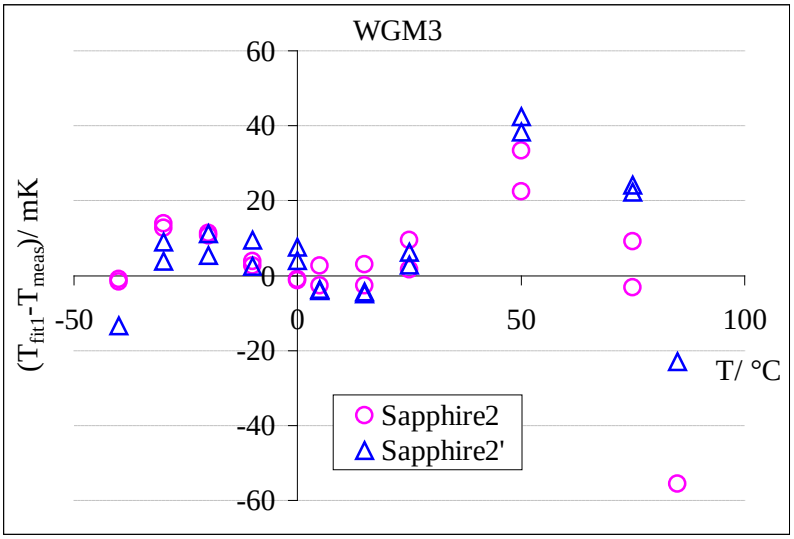

Figure 2.23 Reproducibility of the cylindrical sapphire WGMRT based on WGM3 of sapphire 2 (and 2')

As illustrated in Figure 2.23, the reproducibility of the WGMRT based on WGM3 is about ± 50 mK. It is also noticed that at 50 °C the reproducibility is the worst temperature which should relate to the bath because during the experiments, 50 °C always has the worst stability.

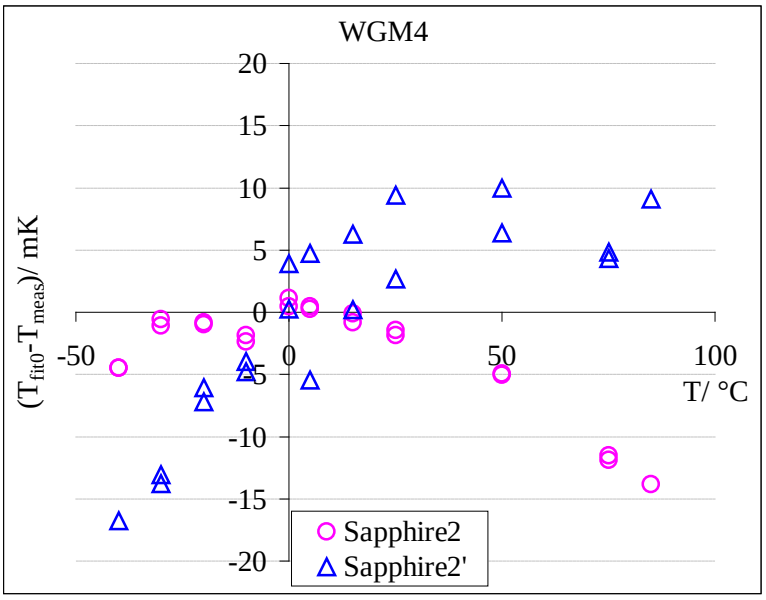

Figure 2.24 Reproducibility of the cylindrical sapphire WGMRT based on WGM4 of sapphire 2 (and 2')

Figure 2.24 also shows that the WGMRT renders a reproducibility of about ± 15 mK based on WGM4 in the temperature range of -40 °C to 85 °C.

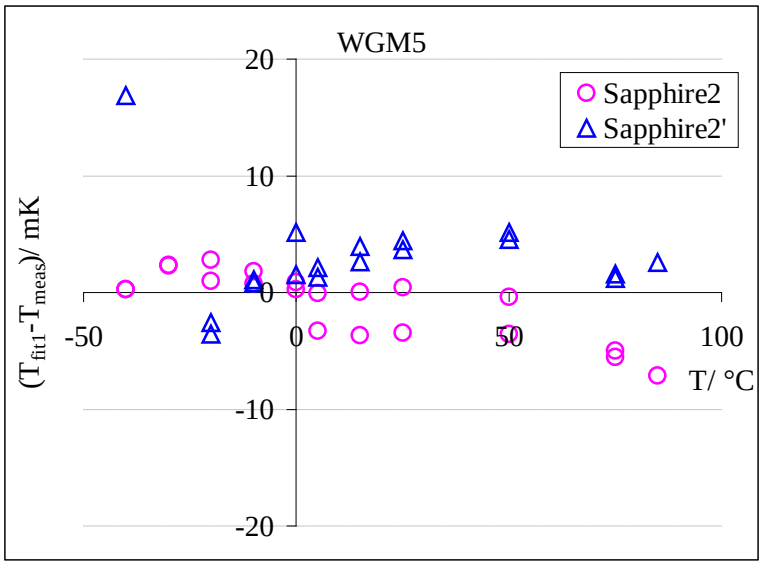

Figure 2.25 Reproducibility of the cylindrical sapphire WGMRT based on WGM5 of sapphire 2 (and 2')

WGMRT can offer a reproducibility of about ± 20 mK (mostly better than ± 10 mK) based on WGM5 as described in Figure 2.25.

In fact the residuals given in three aforementioned figures are from not only different sapphire samples but also their assemble status, like the force put on sapphire and the real distances between antenna and sapphire and so on.

Comparisons between sapphire 2 and 2' (reassembled sapphire 2) were also carried on to study about the reproducibility of the WGMRT based on the same sapphire limited by underlying assemble conditions of different people each time.

By fitting the experiment data based on sapphire 2' with the equation of sapphire 2, the WGMRT reproducibility is shown in Figure 2.26, Figure 2.27 and Figure 2.28. Figure 2.26 describes a reproducibility of better than ± 40 mK for the calibrated WGMRT based on WGM3 while Figure 2.27 illustrates a reproducibility of about ± 20 mK (except one temperature) based on WGM4. Furthermore, a reproducibility of better than ± 20 mK (mostly better than 10 mK) based on WGM5 is obtained as shown in Figure 2.28.

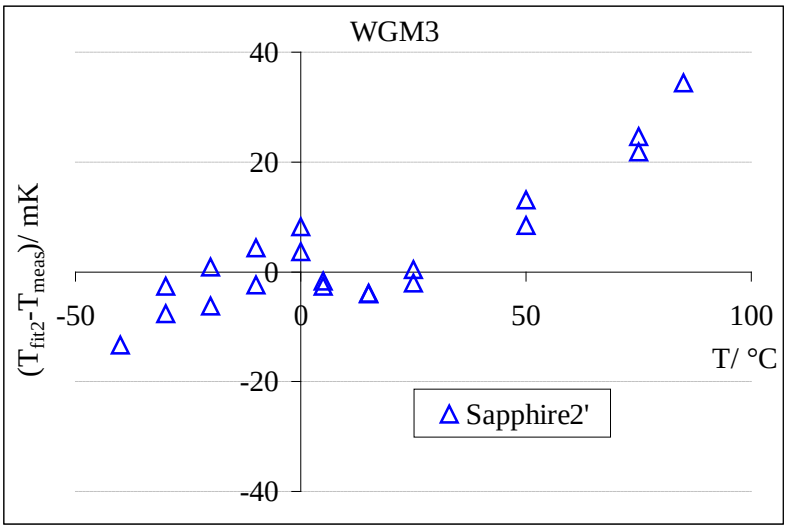

Figure 2.26 Fit residuals for WGM3 of sapphire 2' based on fitting equation of sapphire 2

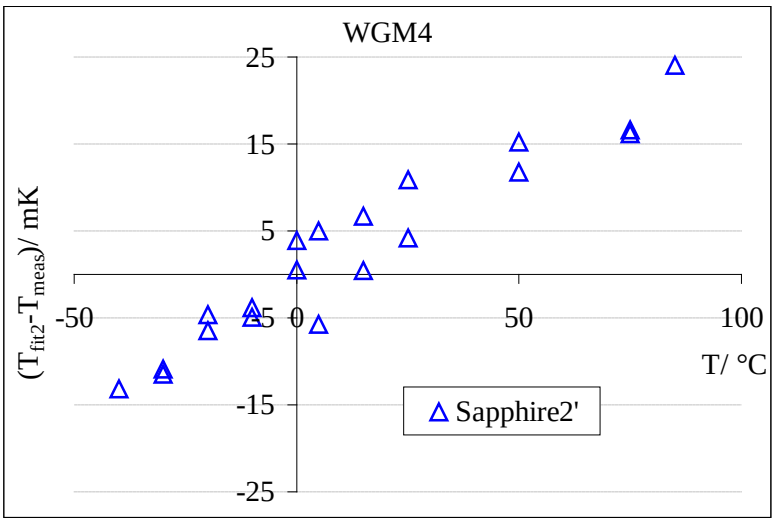

Figure 2.27 Fit residuals for WGM4 of sapphire 2' based on fitting equation of sapphire 2

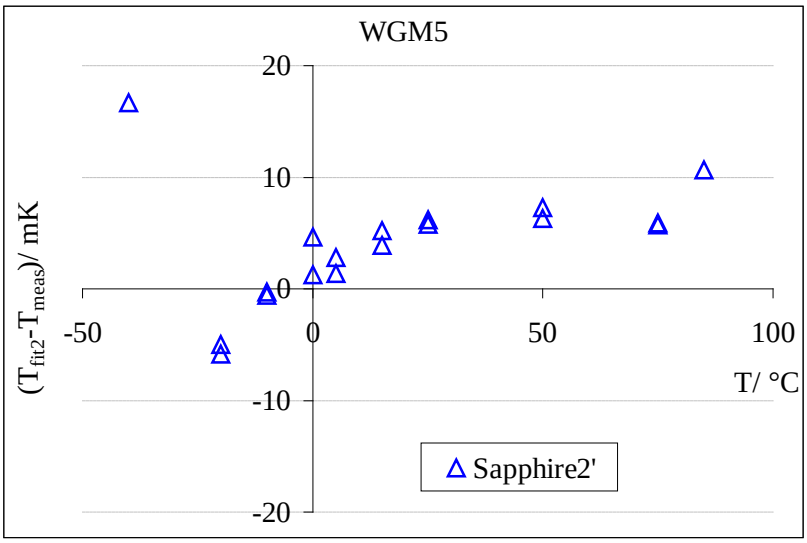

Figure 2.28 Fit residuals for WGM5 of sapphire 2' based on fitting equation of sapphire 2

Combing two series of experiments forementioned, the reproducibility of the WGMRT is mainly limited by the assemble status each time for the sapphires which have the same nominal specifications. Moreover, during the second reassemble test, for some reason the inside surface of the cavity was remachined therefore there is another factor that may bring about reproducibility problem. However, as shown in the analysis results, WGMs are not sensitive to the cavity size and polishing status in certain range.

2.4 Calculation and Experiments Comparisons

As shown in equation (1-1), the resonant frequency of the thermometer changes with the temperature is mainly due to the permittivity changes. The corresponding permittivity at each temperature can be calculated according to equation (1-10) and (1-11) based on Figure 1.14. The corresponding WGMs at each temperature are calculated in Table 2.3.

Table 2.3 Permittivity calculation results at corresponding temperatures

T/ °C	$\varepsilon_{\perp}$	$\varepsilon_{//}$
-40	9.3391	11.4900
-30	9.3464	11.5041
-20	9.3540	11.5184
-10	9.3618	11.5332
0	9.3698	11.5482
5	9.3738	11.5558
15	9.3821	11.5712
25	9.3905	11.5868
50	9.4122	11.6265
75	9.4346	11.6669
85	9.4437	11.6831

Based on the permittivity calculation results shown in Table 2.3, three WGMs were calculated at each temperature by FEM analysis. Comparisons between the calculation and the experiments frequencies are carried on, see Table 2.4.

Table 2.4 Comparisons between the calculated and the experimental frequencies

T / °C	f_{3exp} /GHz	f_{3cal} /GHz	$\Delta f_3/f_3$ /%	f_{4exp} /GHz	f_{4cal} /GHz	$\Delta f_4/f_4$ /%	f_{5exp} /GHz	f_{5cal} /GHz	$\Delta f_5/f_5$ /%
85	12.3601	12.3606	0.00	15.1230	15.0979	0.17	17.8563	17.7703	0.48
75	12.3686	12.3684	0.00	15.1336	15.1077	0.17	17.8690	17.7820	0.49
50	12.3895	12.3879	0.01	15.1597	15.1322	0.18	17.9004	17.8105	0.50
25	12.4099	12.4071	0.02	15.1853	15.1563	0.19	17.9311	17.8405	0.51
15	12.4179	12.4146	0.03	15.1954	15.1658	0.20	17.9431	17.8519	0.51
5	12.4259	12.4221	0.03	15.2053	15.1752	0.20	17.9550	17.8631	0.51
0	12.4297	12.4258	0.03	15.2102	15.1799	0.20	17.9608	17.8687	0.52
-10	12.4376	12.4331	0.04	15.2200	15.1890	0.20	17.9726	17.8797	0.52
-20	12.4452	12.4403	0.04	15.2296	15.1890	0.27	17.9841	17.8906	0.52
-30	12.4527	12.4473	0.04	15.2390	15.2069	0.21	17.9953	17.9011	0.53
-40	12.4600	12.4541	0.05	15.2482	15.2155	0.21	18.0064	17.9115	0.53

As illustrated in Table 2.4, the experimental frequencies are very close to the calculated ones with accuracies better than 1% and the frequency differences are in the same magnitude for the modes that have the same azimuthal mode number.

2.5 Uncertainty Budget

The uncertainty budget of the cylindrical sapphire WGMRT was calculated based on the former experiments and documents at hand. There are two uncertainty source components; one is from the measurement sensor and the other one is from the calibration components used during the experiments. The analysis results are given in Table 2.5.

As seen in Table 2.5, the sensors render only a standard uncertainty of 0.9 mk while the calibration components which is necessary for the experiments give a standard uncertainty of 4.6 mk. Combining these two components, the expanded uncertainty (95%) for the each measurement can be less than 10 mK.

Table 2.5 Uncertainty budget of the cylindrical sapphire WGMRT

Uncertainty source	Estimate	Unit	Unc. type	Distribution	Divisor	Std. Unc.	Unit
Sensor components							
Network analyzer resolution	0.05	mK	B	Rectangular	3.46	0.0	mK
Lorentzian fit of f_peak	0.03	mK	B	Rectangular	3.46	0.0	mK
Repeatability of f_peak	0.5	mK	A	Normal	1.96	0.3	mK
Fitting curve residuals	3	mK	B	Rectangular	3.46	0.9	mK
						0.9	**mK**
Calibration components							
Bath stability	5	mK	A	Normal	1.96	2.6	mK
Temperature gradient	7	mK	B	Rectangular	3.46	2.0	mK
Bridge calibration	4	mK	B	Normal	1.96	2.0	mK
PRT calibration	5	mK	B	Normal	1.96	2.6	mK
						4.6	**mK**
Combined standard deviation						4.7	mK
Expanded uncertainty (95%)						**9.2**	**mK**

2.6 Conclusions

This chapter describes the details of the cylindrical sapphire WGMRT made in INRIM which is designed based on Strouse's paper "*Sapphire Whispering Gallery Thermometer*" [1].

Before starting the experiments, calculations were firstly done to check the feasibility of the design and locate the WGMs. Three WGMs exist in the range of 3GHz to 20 GHz theoretically which lie near to 12.4046 GHz, 15.1471 GHz and 17.8411 GHz with azimuthal mode number equals to 3, 4 and 5 respectively.

Thermal cycle experiments in the temperature range of -40 °C to 85 °C were performed based on two pieces of sapphires which have the same nominal specifications with Q in excess of 170000 at -40 °C. Quartic fit was carried on and an accuracy of ± 8 mK, ± 3 mK and ± 3 mK respectively for WGM3, WGM4 and WGM5 with corresponding standard deviation of 3 mK, 1 mK and 1 mK. Besides, WGM3 shows a maximum hysteresis error of 16 mK while WGM4 and WGM5 have a much smaller hysteresis for both sapphires.

The fractional frequency temperature sensitivity ($(\Delta f_0/\Delta T)/f_0$) increases from -56 ppm/K at -40 °C to -67 ppm/K at 85 °C as a function of the increasing azimuthal mode.

Sapphire 1 can has an ice melting point repeatability of better than 0.4 mK while sapphire 2 renders a repeatability of 5 mK which is mainly limited by the ice temperatures and an ice melting point stability in one hour better than 1.1 mK was achieved based on two sapphires for three WGMs

Frequency response to the temperature change was also checked. A temperature step from 15 °C to 25 °C was conducted to compare with PRT and it turns out that the cylindrical sapphire WGMRT can response fast enough even though it has big mass.

The reproducibility of the WGMRT is ± 50 mK, ± 15 mK and ± 20 mK (mostly better than ± 10 mK) based on three WGMs in the temperature range of -40 °C to 85 °C which are from not only different sapphire samples but also distinct assemble status, like the force put on sapphire and the real distances between antenna and sapphire and so on. However, by reassembling the same sapphire it shows a reproducibility of ± 40 mK, ± 20 mK and ± 20 mK (mostly better than 10 mK) respectively which is similar as before. Therefore, the reproducibility of the WGMRT is mainly limited by the assemble status each time based on the sapphires with the same nominal specifications but insensitive to the cavity size and polishing status in certain range.

Comparisons between calculation and experiments were done and with accuracies of better than 1%. Furthermore, the frequency differences are in the same magnitude for the modes that have the same azimuthal mode number.

Uncertainty budget analysis results show that the measurement uncertainty mainly comes from the calibration components used for the experiments measurement. The combined uncertainty (95%) can be less than 10 mK.

In conclusion, the cylindrical sapphire WGMRT is accessible for the industrial thermometer based on the previous experiment results. However, for extensive application a much compact WGM resonator thermometer capsule whose size is similar to PRT is one of the major research directions.

Chapter 3 Spherical-sapphire-based WGM resonator thermometer

3.1 Introduction

A novel microwave WGM resonator based on a spherical sapphire crystal was developed at INRIM and the feasibility of a WGM thermometer was proved. One of the WGM near to 13.6 GHz was investigated over the temperature -40 °C to 85 °C with Q-factor as large as 100000. This paper reports the stability, repeatability, resolution, frequency temperature sensitivity and frequency response with temperature change for spherical-sapphire-based WGM resonator thermometer prototype and comparisons with NIST SWGT made with cylindrical sapphire are implemented too. Four sapphires with the same specifications were experimented separately and one of them was also repeated to explore the repeatability and reproducibility of the thermometer.

Nowadays, most of the work on the microwave WGM resonator and their application as a thermometer are focused on the cylindrical sapphire because of the easy mounting and machining. The authors in this paper developed a WGM resonator thermometer with spherical sapphire. Spherical-sapphire-based WGM resonator are mostly studied in the optical wavelength range for tunable filters, optical biosensors, mechanical sensors, switches and modulators *et al.* as referred in Chapter 1, nevertheless this is new in the field of microwave resonator thermometer applications. The stability, resolution, repeatability and frequency temperature sensitivity for this INRIM WGM resonator thermometer will be reported in the paper. Moreover, comparisons with conventional whispering gallery mode thermometer with cylindrical sapphire are carried out.

The spherical-sapphire-based WGM resonator thermometer is designed based on the NIST SWGT [1] with nominal sapphire diameter of 12 mm and the cylindrical cavity sizes are similar to the optimized dimension for cylindrical sapphire with cavity radius and height twice the sapphire radius values.

The sapphire sphere, purity of material 99.996%, is a single crystal synthetic sapphire (α-Al2O3) with its c-axis aligned with the geometric z-axis within ± 1°, a hole of 2 mm in diameter was drilled along z-axis. A brass screw goes through the hole to fix the sapphire sphere inside the gold plated copper cavity. Species keep it in the preferred position where the EM field coupling is maximum with respect to to the concerned WGMs but maximum to the neighbor modes. Since the WGMs have the advantage that most of the EM energies are concentrated to the equatorial circle of the crystal, the central hole, the screw and the small species do not affect the performance of the WGM resonator thermometer. Viton o-rings are used to seal the cavity which was continuously pumped to eliminate the humidity in the cavity through one soldered vacuum line. Besides, two microwave coaxial cables were both soldered to the top cap of the cavity where the sapphire sphere was located. The central conductors of the coaxial cables were trimmed so the lengths of the probes penetrate into the cavity are 0 mm. In this way the Q of the resonance modes are greatly advanced and spurious modes are greatly reduces; what's more, it improves the reproducibility, stability and shock resistance of the thermometer.

Figure 3.1a shows top cap of the cavity with mounted spherical sapphire, microwave cables, and two flush antennas. Figure 3.1b represents polished gold plated bottom cap, cavity body with o-rings and the vacuum line.

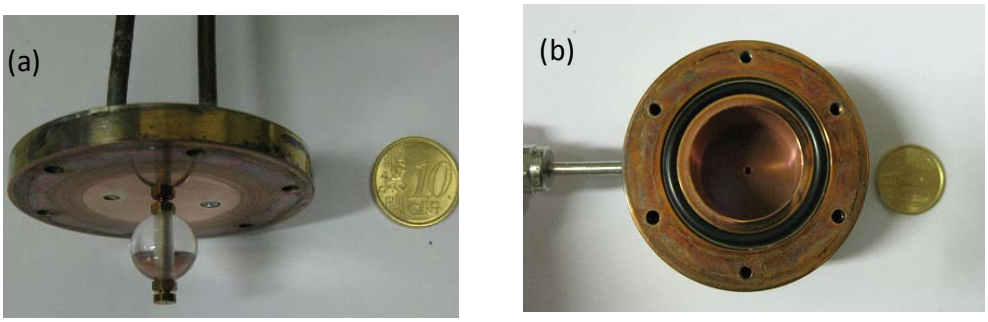

Figure 3.1 (a) Top cap of the cavity with mounted spherical sapphire and (b) polished gold plated bottom cap, cavity body with o-rings and the vacuum line

3.2 Theoretical analysis results

FEM analyses were carried out based on the INRIM WGM resonator thermometer in last part. The permittivity at room temperature used in the calculation

is as follows: $\varepsilon_x = \varepsilon_y = 9.391, \varepsilon_z = 11.5869$ which come from Mehl's fits to two sets of measurements of Krupka *et al.* [105] and Shelby *et al.* [122]

In the frequency range from 300 MHz to 20 GHz, three WGMs exist near 13.5362 GHz (WGM1), 16.3446 GHz (WGM2) and 19.0684 GHz (WGM3) respectively with corresponding azimuthal mode numbers m equal to 3, 4 and 5. The patterns of the electric energy densities for WGMs are given in Figure 3.2.

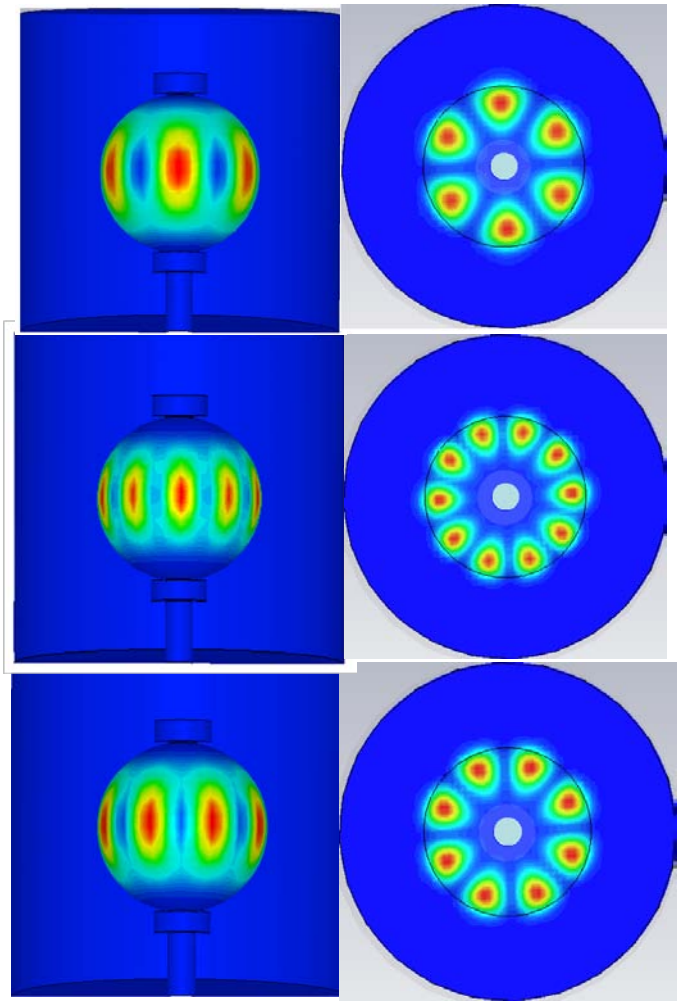

Figure 3.2 The patterns of the electric energy densities for WGMs

As discussed before, the WGMs concentrate most of the energy in the crystal in a region that is close to the surface, so the central hole, the supporting screw that goes through and the bolts have negligible perturbations to the WGMs.

All the metal materials are treated as perfect electric conductors (PECs) which means lossless; the dielectric is also taken as lossless. So the ideal calculated Qs are much higher than the value actually reached in practical resonators. The calculated

WGMs and the corresponding Qs are given in Table 3.1, where m is the azimuthal mode number; Q factors improve with the increasing of the azimuthal number *m*.

Table 3.1 WGMs and Qs calculation results for INRIM WGM resonator thermometer

Mode	*m*	f/GHz	Q
24	3	13.5362	309610
46	4	16.3446	2057200
71	5	19.0684	6148800

3.3 Experimental measurements

In order to fix the spherical sapphire inside the cavity, a long brass screw with two bolts is employed. Since the coupling strength of WGMs changes with the temperatures[136], different distances from the antennae are tried to get lower coupling to the neighour modes and high enough coupling strength to WGMs. In this paper only one of the WGMs around 13.5362 GHz (named WGM1) is experimented and reported because at this fixed position antennas have strong enough coupling to this mode and low coupling to the neighbours at the same time. The other two WGMs should have better performance than WGM1 theoretically.

The INRIM WGM resonator thermometer measurement systems are mainly composed of five parts, Agilent E5071C network analyser, pumping systems, an INRIM ITS-90 calibrated PRT with a readout device 1560 Black Stack bridge for measuring the bath temperature of an ethanol bath whose experimental stability turns out to be better than 3 mK above -40 °C up to 85 °C. Besides, a Labview program was used for logging and analyzing center frequencies and Qs for f_0 determination of better than 0.2 mK from the network analyzer whose resolution can be smaller than 0.2 mK for the mode with Q higher than 50000. The measurement systems are the same as shown in Figure 2.4.

All the resonant frequencies f_0 and half-width g is determined by fitting with the resonant line shape function and one example of the fitting residuals are given in Figure 3.3. On the basis of average of a fit to WGM1 the uncertainty in determining f_0 is less than 0.03 mK.

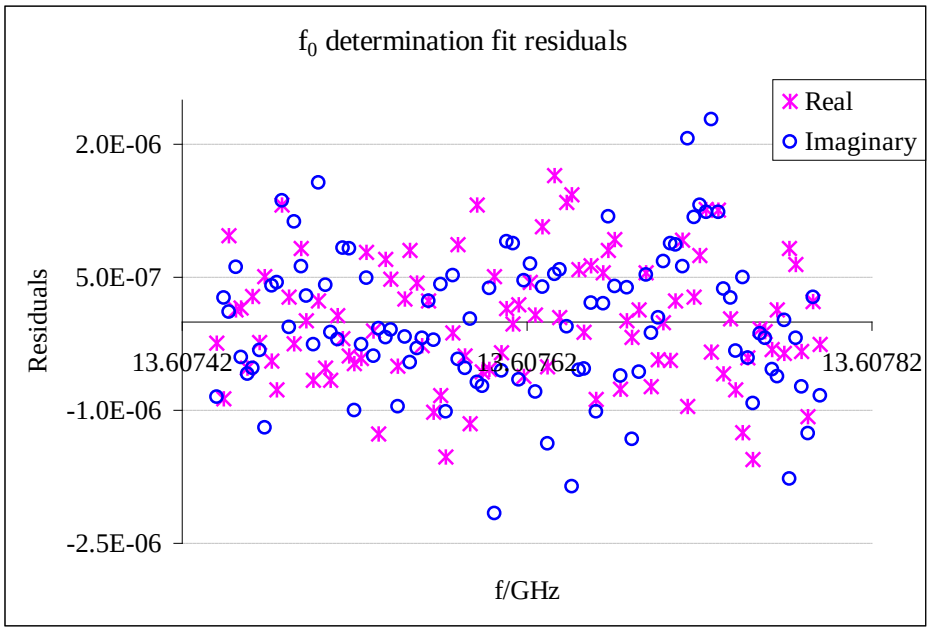

Figure 3.3 Fit residuals of the determination of f_0 for one mode

3.3.1 Thermal cycling measurement

Thermal cycling experiments are performed between -40 °C and 85 °C at -40 °C, -30 °C, -20 °C, -10 °C, 0 °C, 5 °C, 15 °C, 25 °C, 50 °C, 75 °C and 85 °C respectively. Four sapphires are named as sapphire 1, sapphire 2, sapphire 3 and sapphire 4 respectively and the one that was repeated is named as sapphire 1'. The center frequency and Q factor at each temperature based on sapphire 1 are provided in Table 3.2.

As seen in Table 3.2 the temperature uncertainty of the bath is smaller than 1.5 mK (k=1) from -40 °C to 85 °C. The Q factor of the WGM increases with the temperature decreases. Figures for resonant frequency and Q changes with temperatures are presented in Figure 3.4 and Figure 3.5.

Table 3.2 Thermal cycling experiment results (sapphire 1)

Nominal T/ °C	Real T/°C	Std Dev/°C	WGM_1/GHz	Q_1
-40	-39.88386	0.00103	13.643696	107620
-30	-29.88818	0.00099	13.635947	100224
-20	-19.89965	0.00076	13.628037	93756
-10	-9.90244	0.00119	13.619971	87409
0	0.00154	0.00091	13.611845	82481
5	5.09074	0.00100	13.607616	81152
15	15.09538	0.00120	13.599225	77315
25	25.09465	0.00130	13.590732	74169
50	50.10045	0.00111	13.569082	65213
75	75.11768	0.00115	13.546928	58607
85	85.12865	0.00114	13.537945	56030
75	75.11186	0.00119	13.546934	58615
50	50.08646	0.00111	13.569097	66443
25	25.08480	0.00143	13.590741	73486
15	15.08684	0.00117	13.599234	76748
5	5.08554	0.00112	13.607623	80183
0	0.00190	0.00098	13.611845	82073
-10	-9.91082	0.00132	13.619979	85626
-20	-19.90646	0.00119	13.628044	92283
-30	-29.89110	0.00080	13.635950	99127
-40	-39.88496	0.00136	13.643700	107775

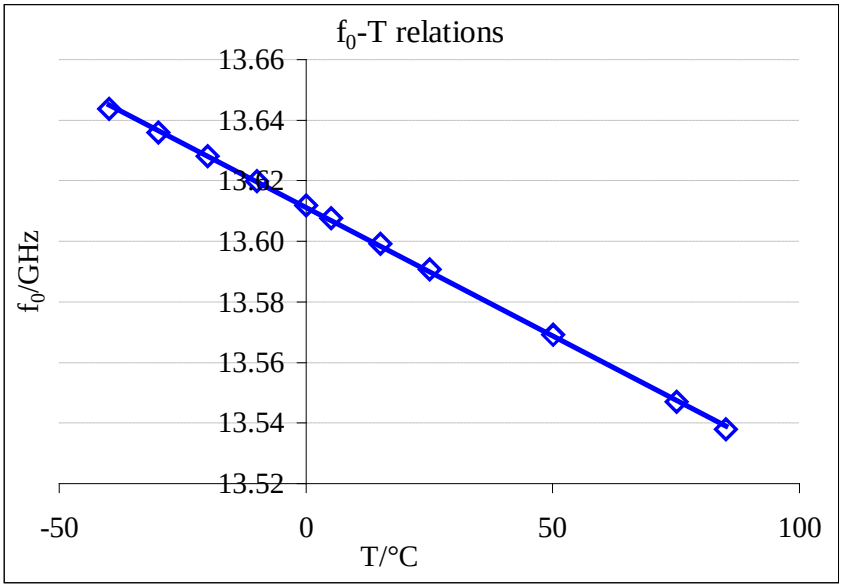

Figure 3.4 Resonant frequency f_0 change with temperatures

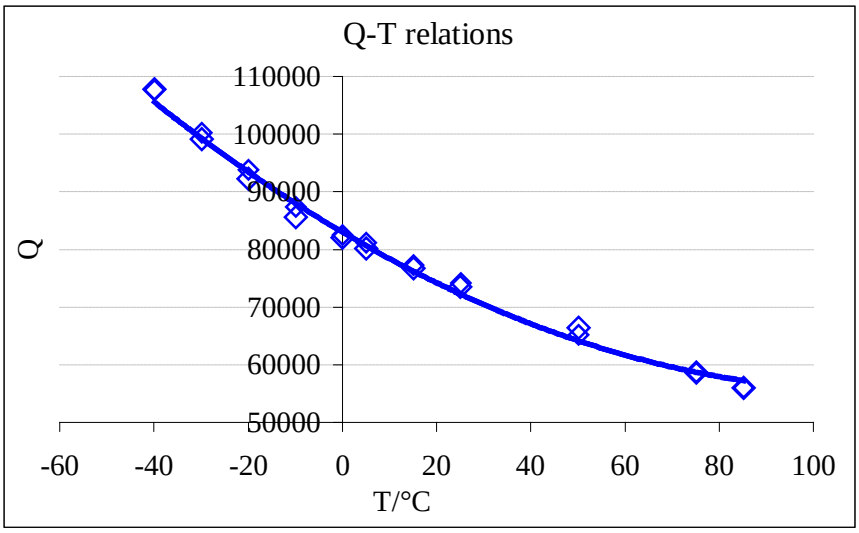

Figure 3.5 Q change with temperatures

Based on the experimental data in Table 3.2 cubic and quartic fit for f_0 and T were implemented and the corresponding fitting residuals are given as follows, see Figure 3.6 and Figure 3.7.

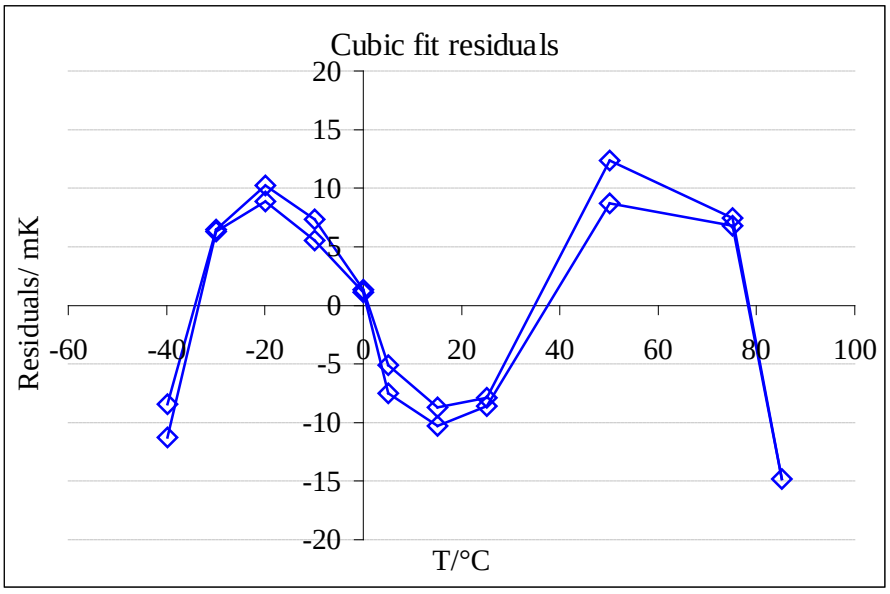

Figure 3.6 Cubic fit residuals of WGM resonator thermometer based on spherical sapphire

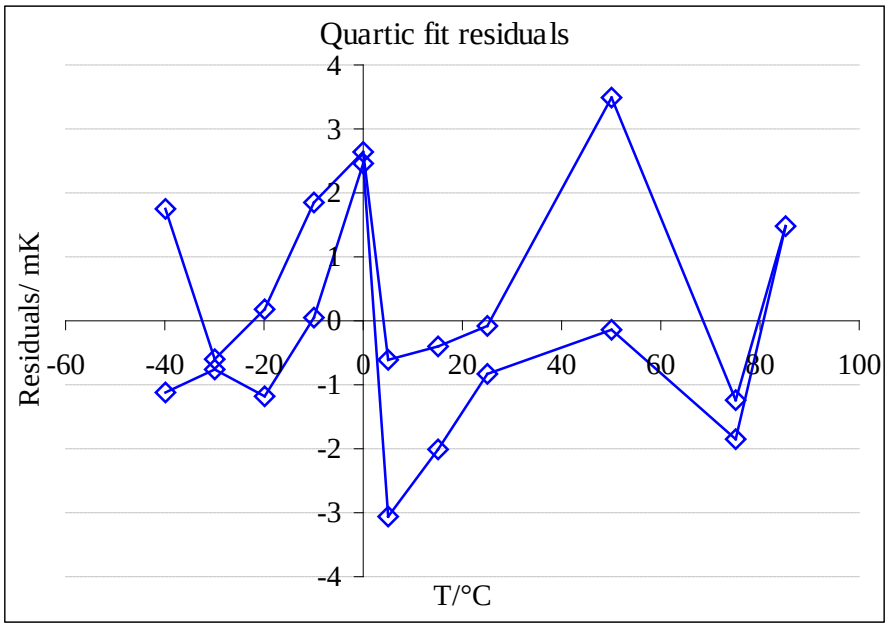

Figure 3.7 Quartic fit residuals of WGM resonator thermometer based on spherical sapphire

Figure 3.6 shows a structure that suggests the use of a quartic fit function and as illustrated in Figure 3.7 quartic fit residuals are improved significantly from ± 20 mK to ± 4 mK. Compared to cylindrical-sapphire-based SWGT in NIST [1] this spherical-sapphire-based WGM resonator thermometer is much more accurate. Besides, the standard deviation of the quartic fitting residuals is only 1.7 mK and shows great improvement with comparison to 8.7 mK by cubic fitting for sapphire 1.

For the other four sapphires (sapphire 1', 2, 3, 4), the measurement uncertainties are different from one to another. Sapphire 1' shows a cubic fit residual of ± 20 mK and with no significant improvements after the quartic fit while the standard deviations were improved from 10.5 mK to 8.5 mK. Sapphire 2 offers a cubic fit residual of ± 20 mK and no improvements can be seen from the quartic fit and the standard deviation are improved insignificantly from 8.9 mK to 8.4 mK. A cubic fit residual of ± 20 mK was significantly improved to ± 8 mK based on quartic fit for sapphire 3 and the standard deviation of 8.0 mK to 4.2 mK was gained. Lastly, sapphire 4 demonstrates a cubic fit residual of ± 25 mK and a quartic fit residual of ± 15 mK with standard deviation improves from 10.8 mK to 6.7 mK. Overall, the spherical-sapphire-based WGM resonator thermometer can have an accuracy of better than ± 20 after appropriate fit.

Moreover, as seen in Figure 3.7 hysterisis error based on sapphire 1 was also discovered in the thermal cycle with a maximum of 4 mK at 50 °C. For the other four sapphires, hysterisis error can also be seen of which sapphire 1' has the maximum value of 25 mK at 5 °C. All the experiments data based on the other four sapphires are enclosed in Table A 6~Table A 9.

As described in Figure 3.8, for the spherical-sapphire-based WGM resonator thermometer the fractional frequency temperature sensitivity ($(\Delta f_0/dT)/f_0$) cubically change from -56 ppm/K at -40 °C to -67 ppm/K at 85 °C. The relevant calculations results are enclosed in Table A 10.

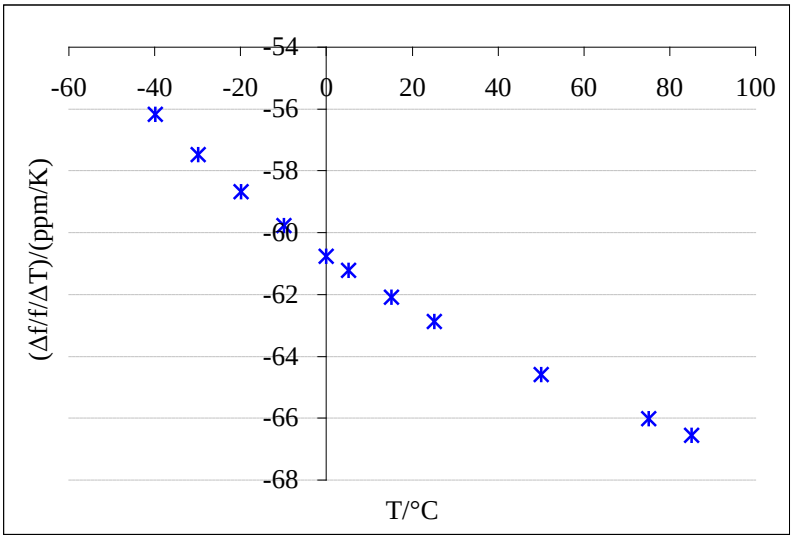

Figure 3.8 f_0 versus T sensitivity for WGM1 at each temperature (sapphire 1)

3.3.2 Ice melting point repeatability and stability

The spherical-sapphire-based WGM resonator thermometer was immersed into the ice melting point dewar at a depth of around 30 cm for three days. The measurement systems are the same as shown in Figure 2.15. Two series of experiments were repeated based on sapphire 1 and sapphire 4. The results based on sapphire 1 and sapphire 4 are given respectively in Figure 3.9 and Figure 3.10 , and Table A 11 and Table A 12.

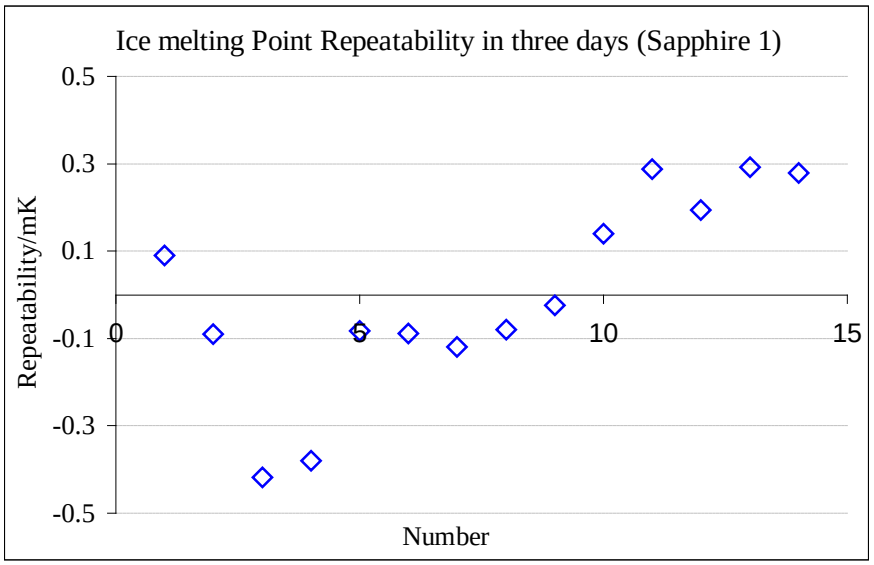

Figure 3.9 Ice melting point repeatability in three days (sapphire 1)

As illustrated in Figure 3.9, the spherical-sapphire-based WGM resonator thermometer that is based on sapphire 1 has repeatability of better than ± 0.5 mK in those three days which is much better than the cylindrical-sapphire-based WGM resonator thermometer published by Strouse [1].

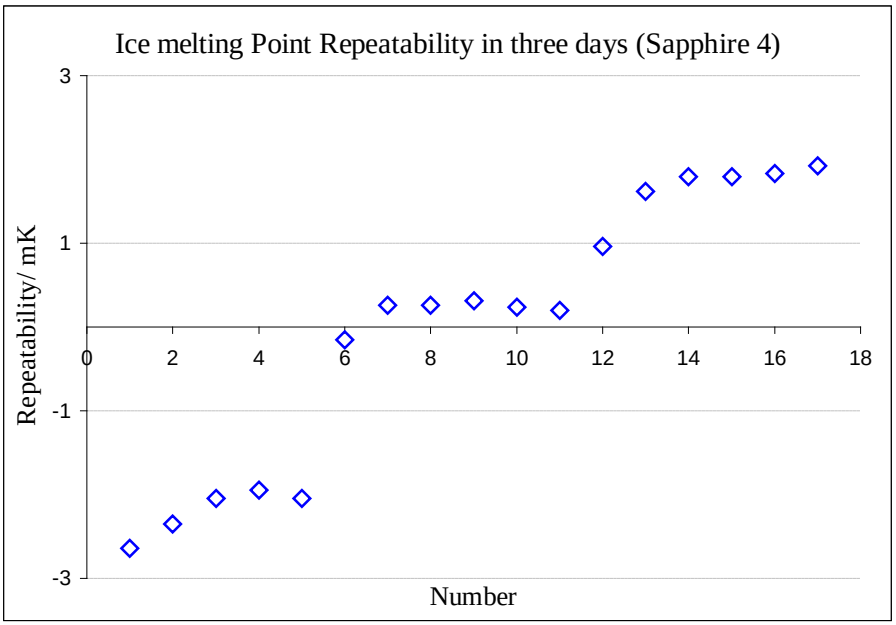

Figure 3.10 Ice melting point repeatability in three days (sapphire 4)

Figure 3.10 shows an ice melting point repeatability of ± 3 mK in three days based on sapphire 4 and it also shows different drift rate every day.

Furthermore, the ice melting point stability test was also carried out based on sapphire 1 in about one hour. As described in Figure 3.11, the spherical-based-sapphire WGM resonator thermometer shows a stability of better than 0.2 mK with comparison to the stability of about 7 mK of PRT after the equilibrium. The spherical-based-sapphire WGM resonator thermometer reads ice melting point temperature in the range of -1.13mK to -0.98 mK with comparison the PRT reading of -1.20 mK to 4.30 mK. The shift is not as significant as cylindrical sapphire WGMRT referred in Chapter 2.

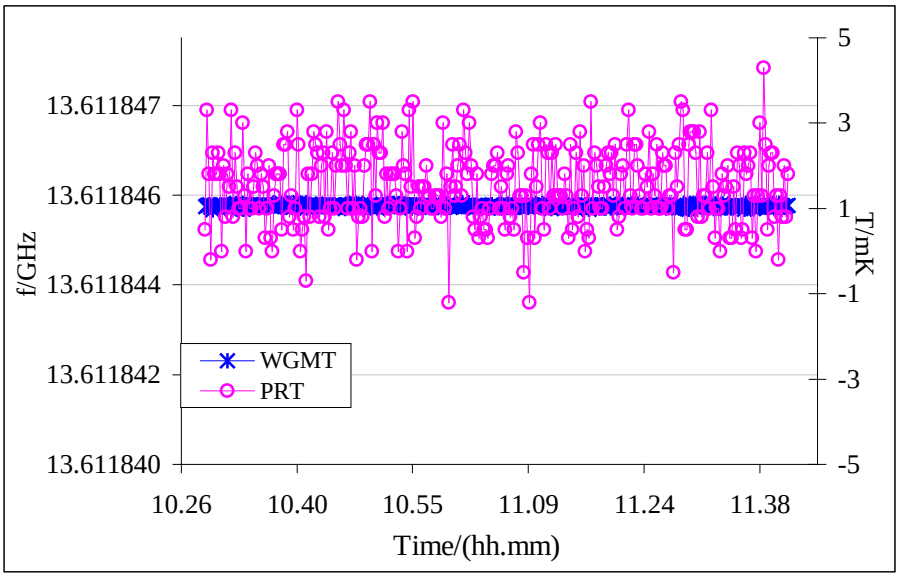

Figure 3.11 Ice melting point stability

3.3.3 Frequency response to the temperature change

Experiments based on temperature step from 15 °C to 25 °C are implemented to compare the response to the temperature change of PRT and spherical-sapphire-based WGM resonator thermometer based on sapphire 1. The experiments results for more than one cycle are as follows and Figure 3.12 shows that the frequency increases with the decrease of the temperature and vice versa.

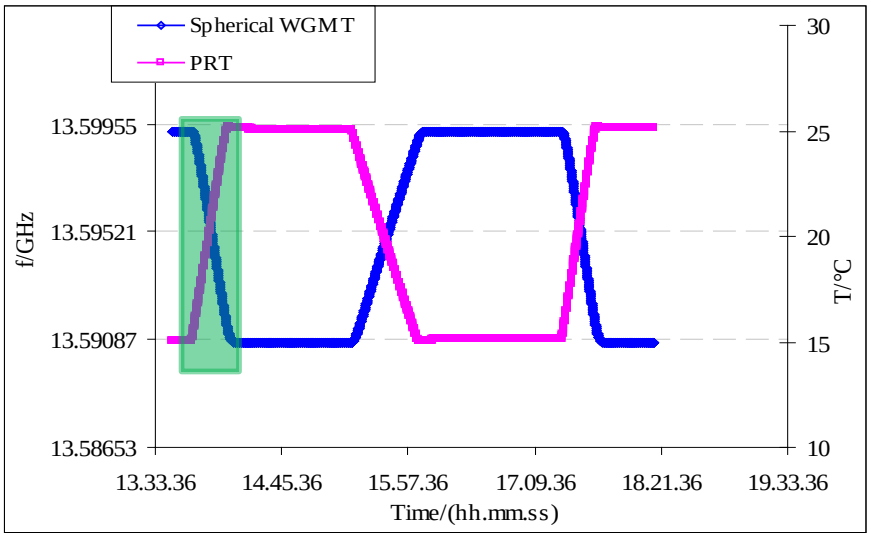

Figure 3.12 Comparisons of the response time between WGMT and PRT

A zoom-in picture for the green part in Figure 3.12 is offered in Figure 3.13 to see clearly the delay time of the frequency response to the temperature change. Even though the current WGM resonator thermometer has bigger mass than PRT, its response of frequency to temperature is still very quickly and in about less than 2 minutes as in Figure 3.13 and this works for both ascending and descending of the temperature. Obviously, the main limit of the response time is due to the power of the bath. If the bath power is bigger in order to have much faster temperature change the PRT will show great superiority over this WGM resonator thermometer. As a result, trying to make much smaller WGM resonator thermometer whose size is similar to PRT is one of the main developing guides.

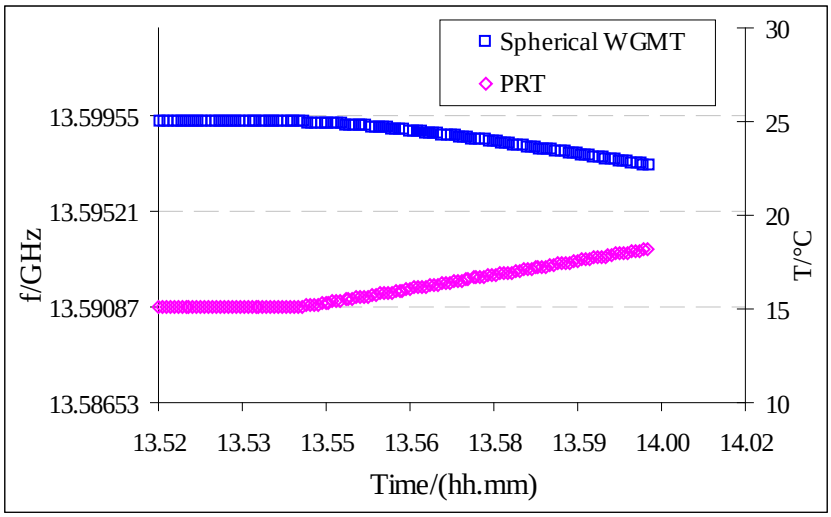

Figure 3.13 Zoom in of one part of the response comparison from Figure 3.12

3.4 Reproducibility

Four spherical sapphires that have the same nominal specifications were explored to investigate the reproducibility of the thermometer. Besides, the reassemble for one of the sapphire (sapphire 1') was tested too.

The quartic fit functions for WGMRT are given in the format of

$$f = a_4 \cdot T^4 + a_3 \cdot T^3 + a_2 \cdot T^2 + a_1 \cdot T + a_0 \qquad (3\text{-}1)$$

Table 3.3 shows the quartic fitting coefficients for five sets of experiments of which a_0 is the one that should be calibrated for every specific thermometer. Take the coefficients for sapphire 1 as the basic one, the calibrated fit residuals for the experiments data based on the other four sapphires are shown in Figure 3.14.

Table 3.3 Quartic fit coefficient for five sets of experiments for all WGMs

Sapphire	$a_4 \times e^{12}$	$a_3 \times e^{9}$	$a_2 \times e^{7}$	$a_1 \times e^{4}$	a_0
1	-5.23136	2.04984	-6.19969	-8.26958	13.61184451
2	-1.91924	1.79443	-6.27622	-8.25822	13.61079552
3	-4.20064	1.93850	-6.19846	-8.26134	13.61133191
4	-5.66429	2.04151	-6.16573	-8.26646	13.61189817
1'	-3.88041	1.88829	-6.18800	-8.26330	13.61082860

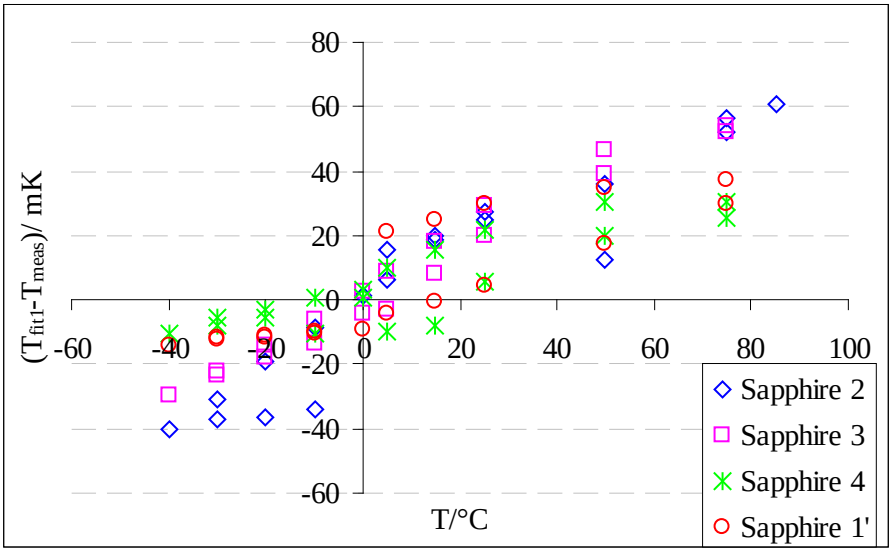

Figure 3.14 Reproducibility of the spherical-sapphire-based WGM resonator thermometer

As illustrated in Figure 3.14, the reproducibility of the spherical-sapphire-based WGM resonator thermometer is about ± 70 mK in the temperature range of -40 °C to

85 °C. A reproducibility of better than ± 40 mK can be gotten based on sapphire 4 and 1'. In fact the residuals are from not only different sapphire samples but also their assemble status, like the force put on sapphire and the real distances between antenna and sapphire and so on.

Comparisons between sapphire 1 and 1' (reassembled sapphire 1) were also carried on to study about the reproducibility of the thermometer based on the same sapphire limited by underlying assemble conditions of different people each time.

By fitting the experiment data based on sapphire 1' with the equation of sapphire 1, the spherical-sapphire-based WGM resonator thermometer reproducibility is shown in Figure 3.15. It describes a reproducibility of better than ± 40 mK for the calibrated thermometer.

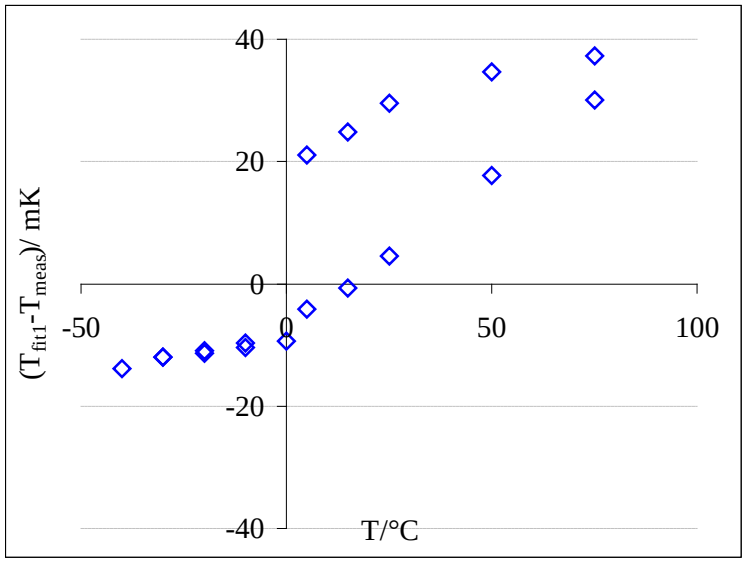

Figure 3.15 Reproducibility of the spherical-sapphire-based WGM resonator thermometer based on the same sapphire

Compared to Figure 3.14, there aren't significant differences between the thermometers that are based on the same sapphire or not. In other word, the reproducibility of the spherical-sapphire-based WGM resonator thermometer is mainly limited by the assemble status each time for the sapphires which have the same nominal specifications. Moreover, other differences based on the experiments based on sapphire 1 and the other four sapphires are the cavity status. Due to the pumping cable was broken after the experiments of sapphire 1, the cavity was machined and polished and re-soldered. Therefore, there are other factors that may bring about reproducibility problem, like the dimension of the cavity and the surface

smoothness *et al.* However, as shown in the analysis results, spherical-sapphire-based WGM resonator thermometer is not sensitive to these factors like cylindrical sapphire WGM resonator thermometer.

3.5 Uncertainty Budget

The uncertainty budget of the spherical-sapphire-based WGMRT was calculated based on the former experiments and documents at hand. There are two uncertainty source components like the cylindrical one in Chapter 2, one is from the measurement sensor and the other one is from the calibration components. The analysis results are given in Table 3.4.

Table 3.4 Uncertainty budget of the spherical-sapphire-based WGMRT

Uncertainty source	**Estimate**	**Unit**	**Unc. type**	**Distribution**	**Divisor**	**Std. Unc.**	**Unit**
Sensor components							
Network analyzer resolution	0.05	mK	B	Rectangular	3.46	0.0	mK
Lorentzian fit of f_peak	0.03	mK	B	Rectangular	3.46	0.0	mK
Repeatability of f_peak	0.5	mK	A	Normal	1.96	0.3	mK
Fitting curve residuals	3.5	mK	B	Rectangular	3.46	1.0	mK
						1.0	**mK**
Calibration components							
Bath stability	5	mK	A	Normal	1.96	2.6	mK
Temperature gradient	7	mK	B	Rectangular	3.46	2.0	mK
Bridge calibration	4	mK	B	Normal	1.96	2.0	mK
PRT calibration	5	mK	B	Normal	1.96	2.6	mK
						4.6	**mK**
Combined standard deviation						4.7	mK
Expanded uncertainty (95%)						**9.3**	**mK**

As seen in Table 3.4, the sensors render a standard uncertainty of 1.0 mk while the calibration components give a standard uncertainty of 4.6 mk. Combining these two components, the expanded uncertainty (95%) for the each measurement can be less than 10 mK.

3.6 Conclusion

This chapter introduces the details of the novel spherical-sapphire-based WGM resonator thermometer made in INRIM.

Before starting the experiments, calculations were firstly done to check the feasibility of the design and locate the WGMs. Three WGMs exist in the range of 3 GHz to 20 GHz which lies near to 13.5362 GHz, 16.3446 GHz and 19.0684 GHz with very high Q.

Thermal cycle experiments from -40 °C to 85 °C were performed with Q of more than 100000. Cubic fit and quartic fit were both carried out and an accuracy of ± 4 mK was obtained by quartic fit with standard deviation smaller than 1.7 mK for sapphire 1 based thermometer. Combing the other four sapphires, the spherical-sapphire-based WGM resonator thermometer can have an accuracy of better than ± 20 after appropriate fit.

Hysterisis error was also discovered in the thermal cycle with a maximum value of 25 mK at 5 °C for sapphire 1'-based thermometer.

The fractional frequency temperature sensitivity ($(\Delta f_0/\Delta T)/f_0$) for WGM1 increases from -56 ppm/K at -40 °C to -67 ppm/K at 85 °C based on the thermal cycle experiments in this temperature range.

Ice melting point repeatability and stability were both implemented. The ice melting point repeatability in three days is better than ± 0.5 mK for sapphire 1 and of ± 3 mK based on sapphire 4.

The stability of the spherical-sapphire-based WGM resonator thermometer based on sapphire 1 is 0.5 mK which is much better than the PRT whose stability in the same time range is about 7 mK.

Frequency response to the temperature change was also checked. A temperature step from 15 °C to 25 °C was conducted to compare with PRT and it turns out that the spherical-sapphire-based WGM resonator thermometer can response very fast even though it has big mass.

The reproducibility of the spherical-sapphire-based WGM resonator thermometer is about ± 60 mK in the temperature range of -40 °C to 85 °C based on

different sapphires while a reproducibility of better than ± 40 mK for the same sapphire with reassemble. The reproducibility of the spherical-sapphire-based WGM resonator thermometer is mainly limited by the assemble status each time for the sapphires which have the same nominal specifications. Experiments also show that it is not sensitive to the cavity surface and size.

Uncertainty budget analysis results show that the measurement uncertainty mainly comes from the calibration components used for the experiments measurement. The combined uncertainty (95%) can be less than 10 mK.

In conclusion, the spherical-sapphire-based WGM resonator thermometer is accessible for the industrial thermometer based on the previous experiment results. However, for extensive application a much compact WGM resonator thermometer capsule whose size is similar to PRT is one of the main developing directions.

Chapter 4 Sapphire rod resonator thermometer experiments

4.1 Introduction

After the researches on sapphire ring resonator thermometer, sapphire rod was tested too to make the thermometer more and more compact. Because the diameter of the sapphire rod is small the WGM can be too high to be detected by network analyzer. Resonant modes were calculated by Mehl of which the modes that have most of the energy concentrated on the sapphire were studied. In the experiments two kinds of sapphire rods were studied, one is the 0° orientation ($\varepsilon_z = \varepsilon_{//}$) and the other one is 90° orientation ($\varepsilon_x = \varepsilon_{//}$). Some of the resonant modes for 0° orientation sapphire are double degenerate while for 90° orientation sapphire the degeneracy is highly lifted. An innovative thermometer was developed by using the birefringence of the sapphire. The ratios of these frequency pairs are sensitive to the temperature-dependent birefringence of the crystal and relatively insensitive to surface contamination and changes in the shape of the cavity. All the researches referred in this chapter are done at Fluid Metrology group in National Institute of Standards and Technology (NIST).

4.2 Sapphire rod supported by washers

For a better knowing of the theory of the resonator works, the preliminary experiments begin with a resonator which is simplified by using screws or washers that are not robust enough to support the sapphire rod and moreover the resonator may not be closed well. Even though it can't be a real thermometer, for the theory study it can be enough.

By simply supporting the sapphire rod inside of the cavity, a piece of washer is employed to clamp the sapphire rod in the center of the cavity. Three screw holes around the central equator of the cavity were drilled to hold the washer in place, see

Figure 4.1. The cavity is 42 mm in length and 18 mm in diameter (ID) while the sapphire is 30 mm long and 6 mm in diameter. The thickness of the Teflon washer is about 6 mm.

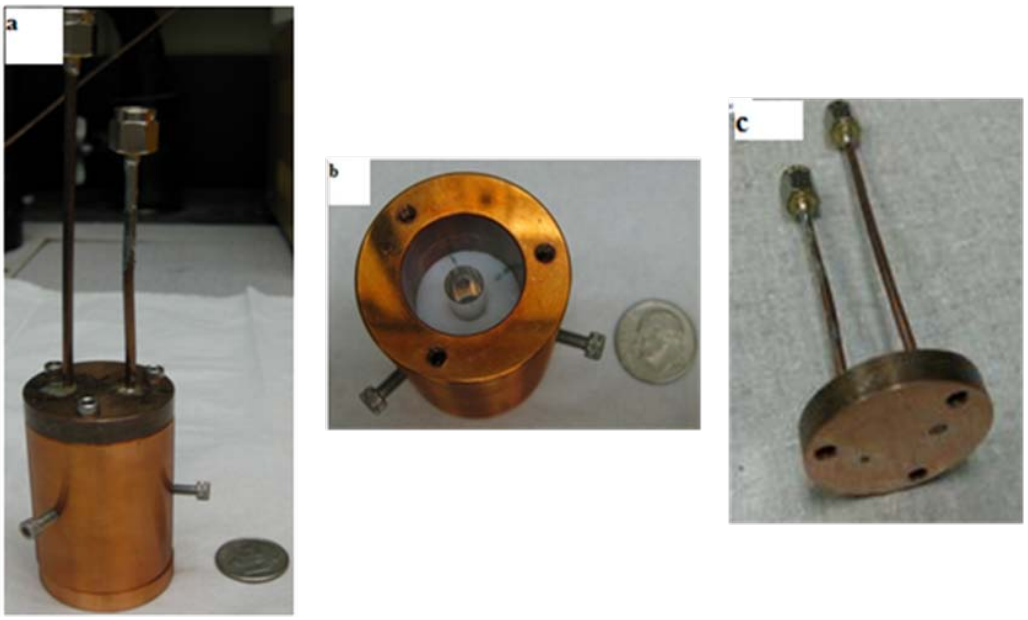

Figure 4.1 (a) Closed sapphire rod resonator, (b) open cavity with sapphire rod hold by washer and (c) flush probes soldered to the cap

4.2.1 Room ambient experiments

In order to match the calculation done by Mehl and my experiments results, experiments start from the empty cavity and then putting more and more perturbation inside and the last step is to put the sapphire inside.

4.2.1.1 Experiments of empty cavity

Experiments were done per the empty cavity with three steel screws around the central equator. Straight probes and loops were both tested. Table 4.1 gives the results based on straight probes and only TM modes can be coupled. While Table 4.2 shows both TM and TE modes can be coupled with loop probes. However, the reproducibility of the loop probes are not as good as straight probes, bigger perturbation of the loops, straight probes are the best coupling devices.

Table 4.1 Experimental data of empty cavity with straight probes

f_{exp}/GHz	Q_{exp}	Mode No.	f_{cal}/GHz	Q_{cal}	$\Delta f/f$	Q_{exp}/Q_{cal}	Mode type
12.702600	3265	5	12.737944	12678	-0.28%	0.258	TM
13.179500	1813	6	13.230133	10988	-0.38%	0.165	TM
14.548800	1447	9	14.607539	11530	-0.40%	0.126	TM

Table 4.2 Experimental data of empty cavity with loop probes

f_{exp}/GHz	Q_{exp}	Mode No.	f_{cal}/GHz	Q_{cal}	$\Delta f / f$	Q_{meas} / Q_{calc}	Mode type
10.374423	4396	1	10.387051	10340	-0.12%	0.425	TE
10.375647	1828	2	10.387054	10338	-0.11%	0.177	TE
12.079365	2308	3	12.092796	12367	-0.11%	0.187	TE
12.083284	3982	4	12.092798	12366	-0.08%	0.322	TE
12.783000	1022	5	12.737944	12678	0.35%	0.081	TM
13.366000	887	6	13.230133	10988	1.03%	0.081	TM
14.458007	1682	7	14.496379	14905	-0.26%	0.113	TE
14.486681	3934	8	14.496392	14905	-0.07%	0.264	TE
14.656000	729	9	14.607539	11530	0.33%	0.063	TM

As seen in these two tables the experimental Qs are too low compared to the calculation. Then the inside surfaces of the cavity and the cap surfaces are all polished to increase the conductivity of the conducting surfaces. Figure 4.2 shows significant improvements both in frequency and Q factor.

As shown in Figure 4.2, after polishing the Qs are improved a lot from only less than 30% of the calculated values to around 70% and the frequency differences between the experiment and calculation are decreased to around only half of the values before polishing, in other word, after polishing the frequency differences between the experiment and calculation for empty cavity is within 0.21% and the Qs are around 70% of the calculated values. The corresponding experimental data are enclosed in Appendix in Table A 13 and Table A 14.

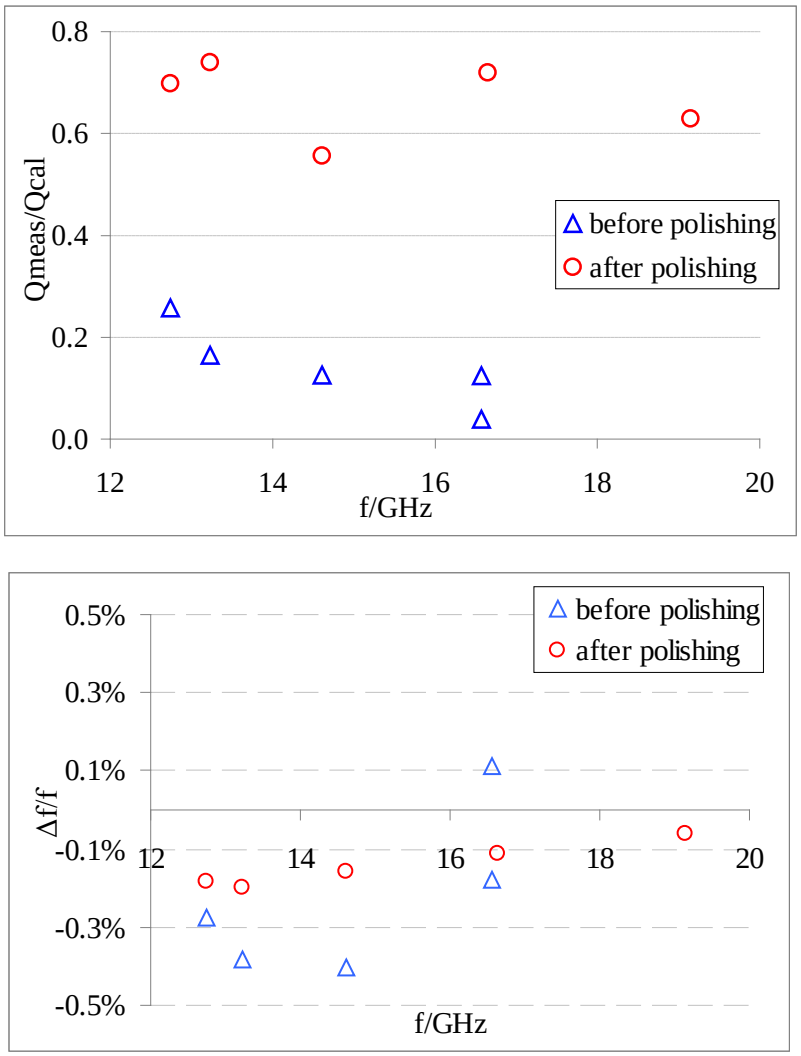

Figure 4.2 Comparisons of empty cavity before and after polishing for Q and f

4.2.1.2 Experiments of cavity with Teflon

After experiments on empty cavity match with the calculated values in certain accuracy, researches go to next step by putting a piece of washer inside of the empty cavity. Two kinds of washers were machined, one is nylon and the other one is Teflon. During the experiments, nylon has great perturbation to the microwave; most of the modes were absorbed by the nylon washer but not by Teflon.

Experiments were done per empty cavity with Teflon washer inside, good matches were also gotten, see Table 4.3. The frequency difference is within 0.7% and the Q is around 50% of the calculated values. Surely, the Q ratio between the experiment and calculation is smaller compared to the empty cavity; this is due to the losses come from both copper cavity and Teflon washer.

Table 4.3 Comparisons between experiment and calculation for cavity with Teflon

f_{exp}/GHz	Q_{exp}	Mode No.	f_{cal}/GHz	Q_{cal}	$\Delta f / f$	Q_{meas} / Q_{calc}
12.113800	7410	5	12.112070	13090	0.01%	0.57
13.082640	7869	6	13.081658	11397	0.01%	0.69
13.965050	6303	11	13.962855	10431	0.02%	0.60
15.979550	7246	12	15.880240	11941	0.63%	0.61
18.084100	6107	21	17.960034	16456	0.69%	0.37
18.361000	6856	22	18.237511	12723	0.68%	0.54

4.2.1.3 Experiments of cavity with Teflon and sapphire

The last step is to put the sapphire rod inside the cavity. Two orientations of sapphires were at hand: 0° orientation sapphire ($\varepsilon_x = \varepsilon_y = \varepsilon_\perp, \varepsilon_z = \varepsilon_{//}$) and 90° orientation sapphire ($\varepsilon_y = \varepsilon_z = \varepsilon_\perp, \varepsilon_x = \varepsilon_{//}$). Plenty of experiments have been done on 0° orientation sapphire, so the main attention was paid to 90° orientation sapphire in this part.

In accordance to theory, for 90° orientation sapphire some doublet modes should exist. Accordingly, for coupling more modes, it is better that the antennas are 45° to c-axis of the sapphire.

Before starting the comparisons between theory and calculation, it is better to know well all possible significant perturbations, like the screws for supporting the washers, the holes for the screws around the cavity, the washer and so on; so series of experiments for these were done first of all. Moreover, the relations between the frequencies and axial displacement are also very interesting and significative to the resonator.

4.2.1.3.1 Screws and comparisons

Of course, the screws that may matter are not the screws that are used to close the cavity but the screws around the central equators of the cavity to support the Teflon washer and sapphire in the center of the cavity. Firstly, different materials of screws in hand were compared, steel, nylon, aluminium and brass. The frequencies and Q were both compared in Figure 4.3. The corresponding data are enclosed in Appendix in Table A 15~Table A 18.

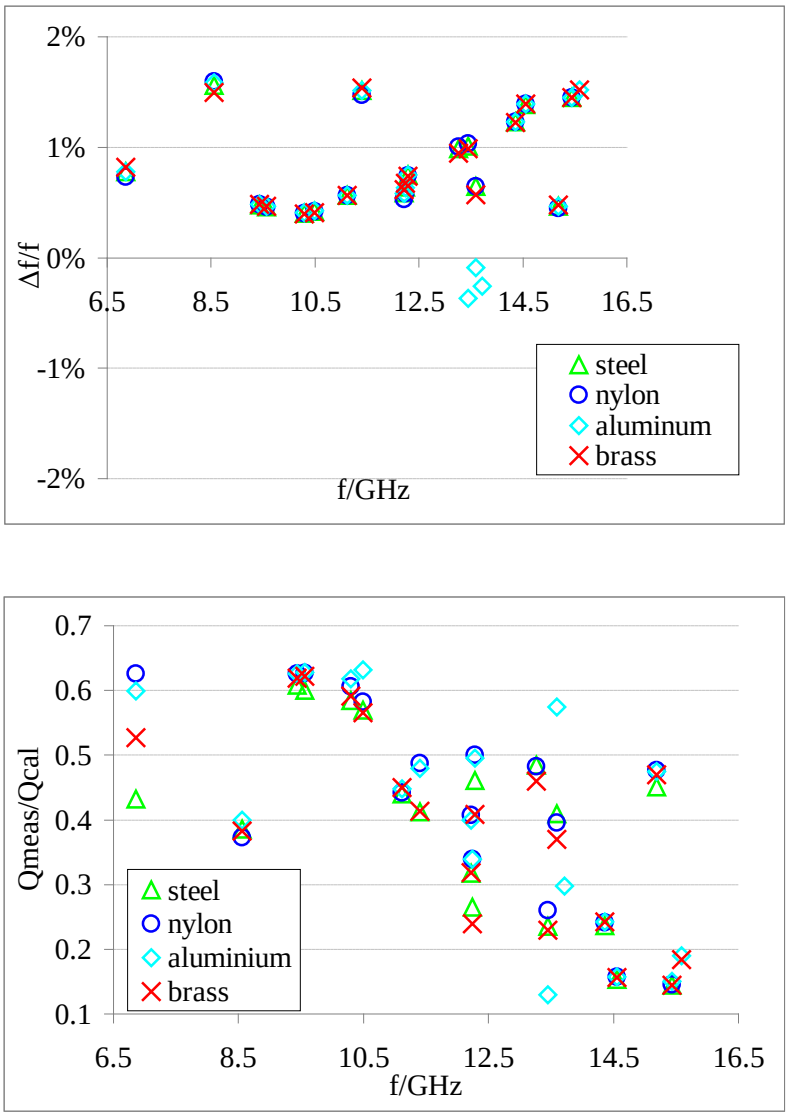

Figure 4.3 Frequencies and Qs comparisons between different materials of screws

Based on Figure 4.3 there is no significant differences between different screws, aluminium can be the best choice of all to render higher Q nonetheless. Afterwards, if there is no specific explanation all three screws used around the cavity are made of aluminium.

4.2.1.3.2 Comparisons between with and without and different orientation holes around the cavity

As seen in Figure 4.1 there are three screws holes around the cavity to support the Teflon washer which may or may not bring significant to resonant modes. Another new cavity which has the same dimensions as the old one was made but without holes around. This cavity is made only for comparison with the old one to explore the

affects of the existence and the orientation of the holes. Of course, no holes around the cavity mean that the washer can't be fixed but since the washer surface is not that smooth and it was made just fit the cavity snugly, for experiments phase it is acceptable.

Figure 4.4 presents the Qs and frequencies comparisons for the resonant modes that are both observed in two resonators between the cavity with and without holes around. For most modes the Qs are a little higher and frequencies differences are a bit smaller when there are no holes but obviously it is not significant at all. The experiments data for this figure will be given in Appendix in Table A 19 and Table A 20.

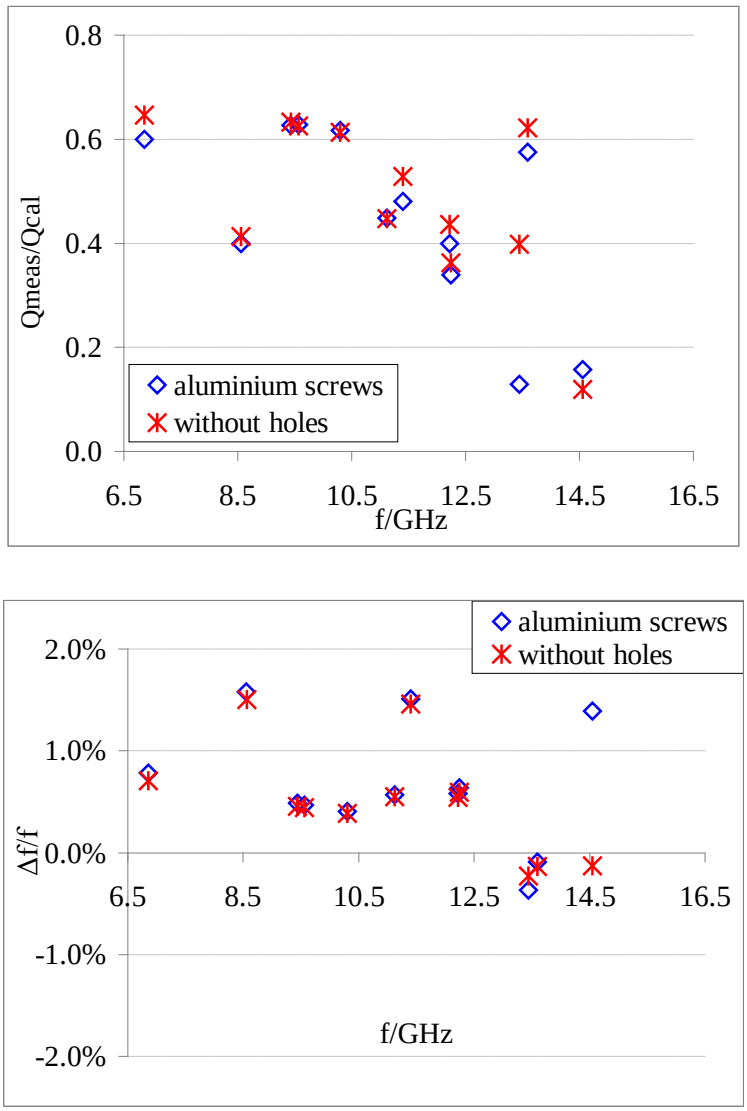

Figure 4.4 Frequencies and Qs comparisons between resonators with and without holes

Then by drilling the cavity with three holes that one of them are aligned with two antennas. In this way these three holes are turned about 30° to the former cavity. Qs and frequencies for the modes observed in both conditions were also compared, see Figure 4.5. No significant differences between different orientations can be seen. Table A 21 and Table A 22 present the experimental data.

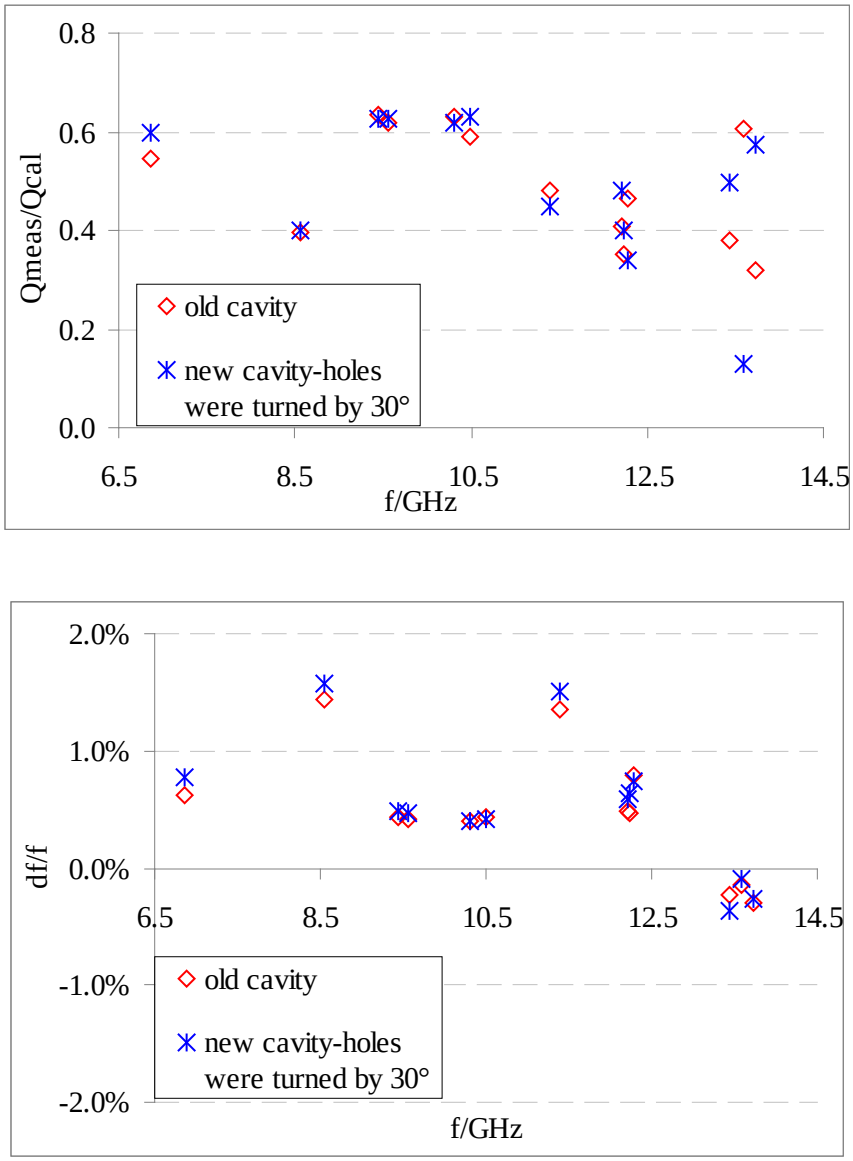

Figure 4.5 Frequencies and Qs comparisons between resonators with different orientations of holes

4.2.1.3.3 Comparisons between Teflon with and without holes

The Teflon washer is another concern of the perturbation. Whether or not the amounts of the Teflon matter significantly needs to be discovered. Three holes were drilled randomly on the washer through the upper surface to the bottom of the ring.

The comparisons for Qs and frequencies are as follows, see Figure 4. 6 and the corresponding experimental data are presented in Table A 23 and Table A 24.

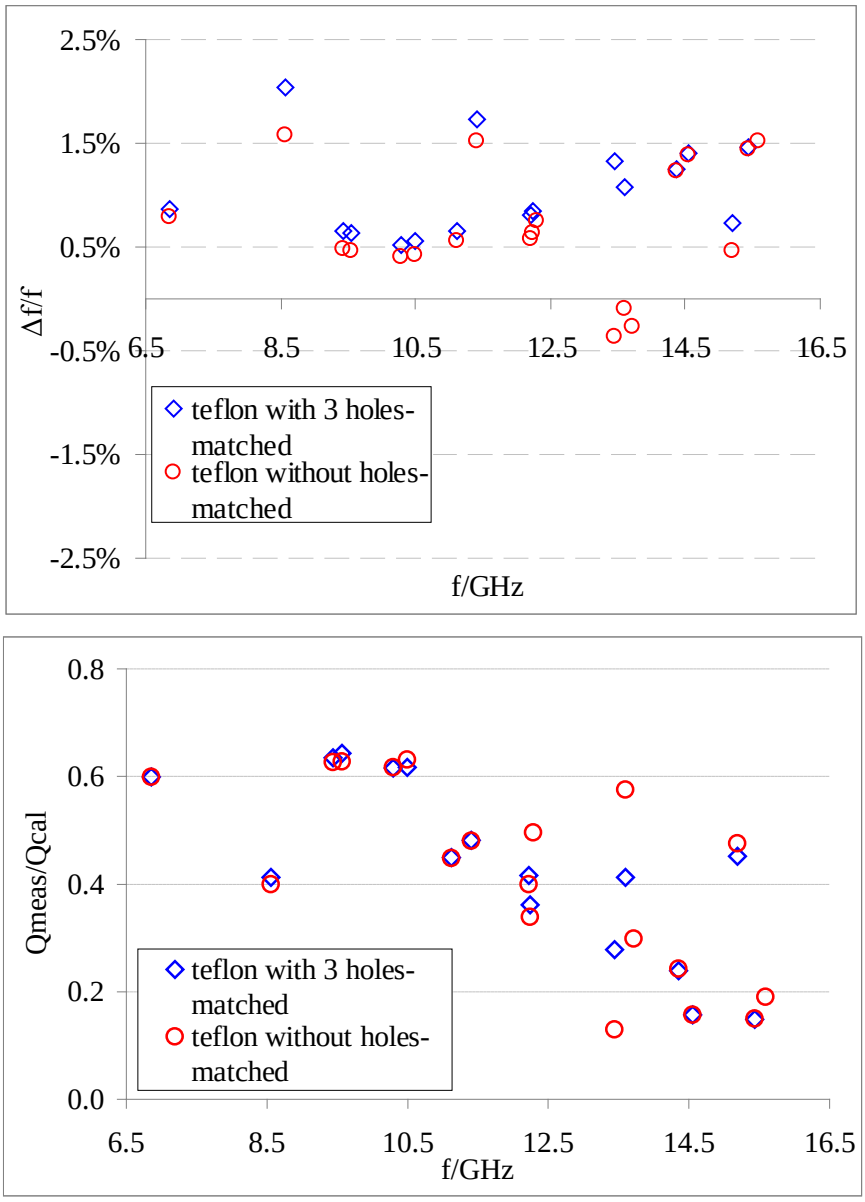

Figure 4.6 Frequencies and Qs comparisons between resonators with Teflon with and without holes

As seen in Figure 4.6, the Teflon without holes has insignificantly smaller frequencies differences compared to calculations for most of the modes which is normal because the calculated values are given based on the Teflon without holes, while the Qs are almost the same for both conditions. Therefore, the amounts of Teflon washers under the same thickness are insignificant too.

4.2.1.3.4 Relations between resonant frequencies and axial displacement

All the former experiments in this Chapter were done by putting the sapphire in the center, however, the displacement of the sapphire to the antennas not only change the coupling strength but also the resonant frequencies. Some tests were done to find out their relations.

For the sake of finding more modes to analyze sapphire was pushed closer and closer to the antennas from 5.9055 mm, then to 5.3975 mm, 4.2418 mm, 3.5433 mm, 2.7178 mm, and 1.9812 mm at last. The experimental results at each position are enclosed respectively in Appendix from Table A 25 to Table A 30. The relations between frequencies and axial displacement were analyzed for each mode respectively and it turns out that frequencies are as quadratic function of axial displacement. Take mode 6 and mode 7 as examples; see Figure 4.7, where the displacement 0 means it was in the center.

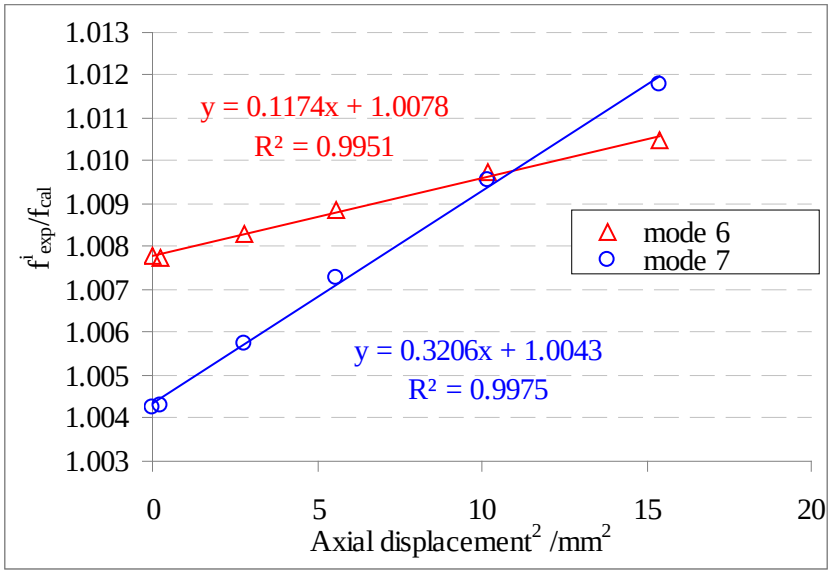

Figure 4.7 Linear fit for frequencies and square of axial displacements

4.2.1.3.5 Comparisons between experiments and calculations for sapphire rod resonator

After all the possible perturbations were considered and on account of that they are all insignificant, experiments based on 90° orientation sapphire supported in the center of the cavity by a whole piece of Teflon washer ring which is fixed by

aluminum screws were implemented by putting the c-axis of the sapphire 45° to the antennas. Comparisons between experiments and calculations were given in Table 4.4.

Table 4.4 Mode match between experiments and calculations

f_{exp} /GHz	Q_{exp}	mode No.	f_{cal} /GHz	Q_{cal}	$\Delta f / f$	Q_{meas} / Q_{calc}
6.908522	13565	1	6.854953	22634	0.78%	0.60
8.691660	9693	4	8.556413	24242	1.58%	0.40
9.481220	13481	5	9.435375	21525	0.49%	0.63
9.606620	12980	6	9.562123	20683	0.47%	0.63
10.340380	18574	7	10.298477	30082	0.41%	0.62
10.535680	18247	8	10.491155	28893	0.42%	0.63
11.184080	29057	9	11.121059	64821	0.57%	0.45
11.572500	9973	11	11.400001	20777	1.51%	0.48
12.290370	16307	15	12.219093	40827	0.58%	0.40
12.318000	15463	16	12.240126	45611	0.64%	0.34
12.378740	38658	17	12.286837	78051	0.75%	0.50
13.395650	8126	24	13.444917	62793	-0.37%	0.13
13.582700	17784	25	13.594677	30937	-0.09%	0.57
13.683060	13242	27	13.718765	44434	-0.26%	0.30
14.533620	39588	28	14.357122	163049	1.23%	0.24
14.755930	50198	29	14.553659	319388	1.39%	0.16
15.259100	7749	31	15.187942	16316	0.47%	0.47
15.661990	40841	32	15.438337	272301	1.45%	0.15
15.829640	47790	33	15.592459	251709	1.52%	0.19

As in Table 4.4, the experimental frequencies match with calculation within 2% while the experimental Qs are too low compared to the calculation which is acceptable because the calculated values are given without taking into account any losses from cavity, Teflon washer, sapphire and so on.

Besides, the highlighted two modes, mode 29 and 32, are a pair of doublets according to the calculation which will be paid lots of attentions because of the birefringence of the 90° sapphire. In the calculation, mode 29 and 32 have around 90% of the electric energy concentrated on the sapphire rod and only less than 2% of the electric energy are on Teflon washer which makes it available for a sapphire

resonator thermometer. Figure 4.8 shows the waveform distribution of electric energy density. The x-axis stands for the coordinate of the sapphire rod in z direction (unit: m) while y-axis means the electric energy density on the following position of the sapphire. It is very clear that there is no electric energy density in axial center of the sapphire thereby Teflon washer has less perturbation to this pair of modes.

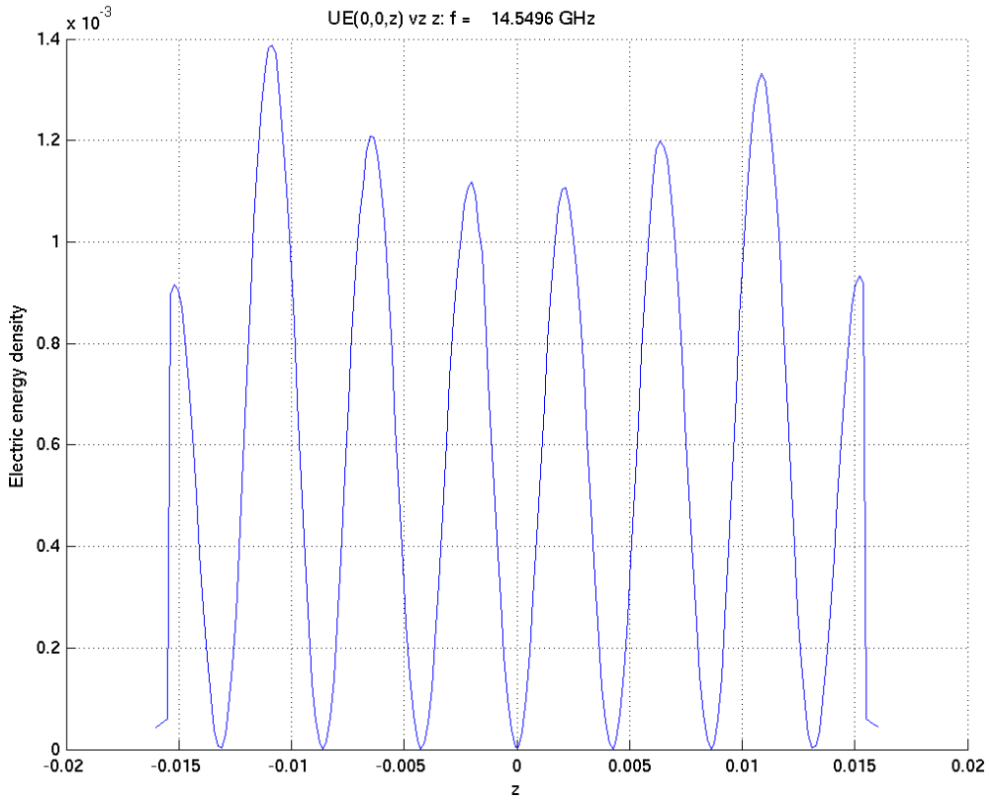

Figure 4.8 Waveform distribution of electric energy density

Figure 4.9 and Figure 4.10 give pictures of electric energy density distribution on sapphire body and upper surface separately. The modes types are the same for both modes and only the phase differs by 90°. The red color in Figure 4.9 means maximum electric energy density while blue color is for zero electric energy density which is different in Figure 4.10 that both blue and red mean electric energy peak but they are reversed in phase and green stands for zero nonetheless. Moreover, Figure 4.10 gives good explanation why putting the c-axis of the sapphire 45° to the antennas could couple with more modes.

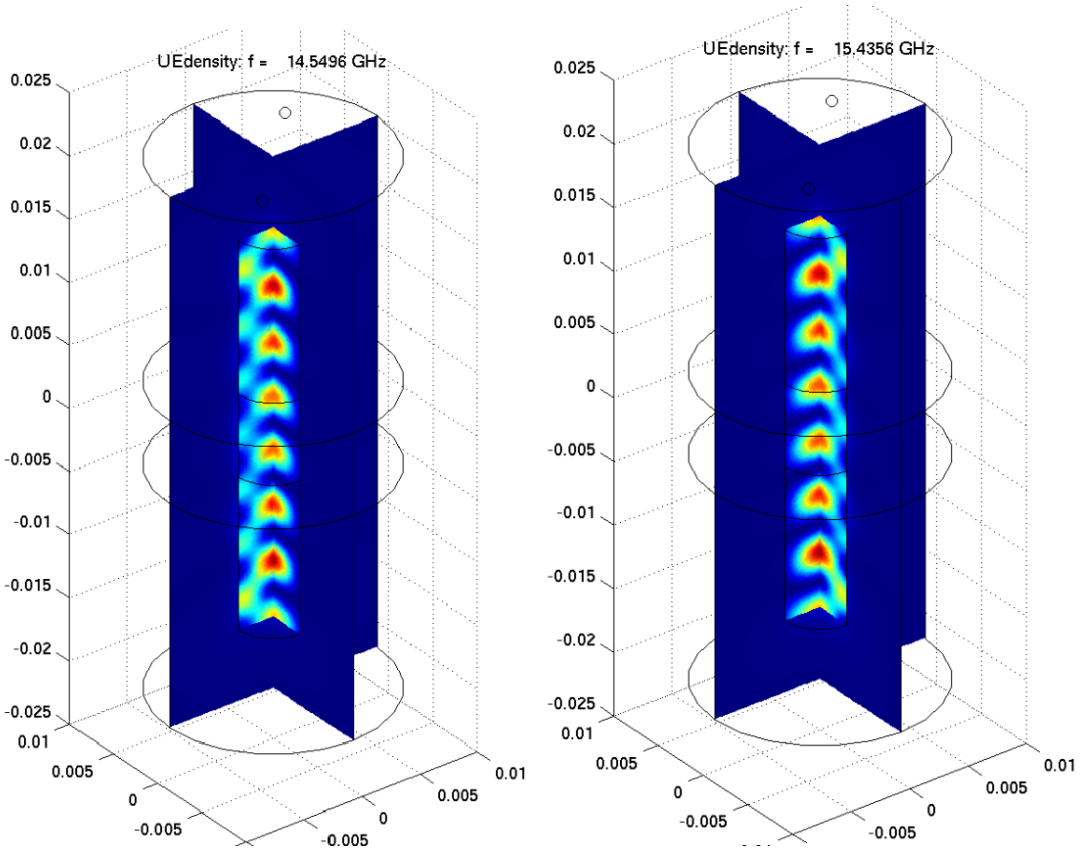

Figure 4.9 Waveform distribution of electric energy density for doublets

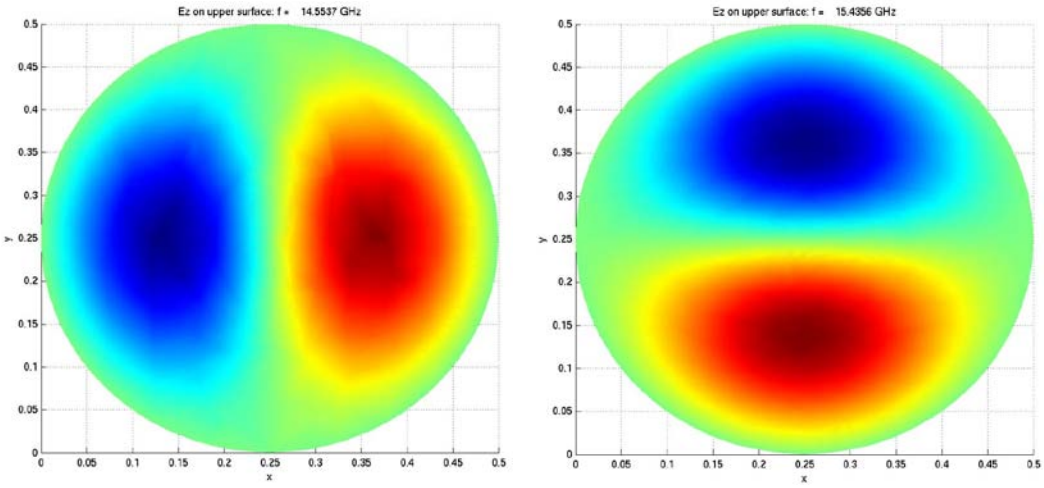

Figure 4.10 Waveform distribution of electric energy density for doublets

4.2.2 Dimension optimization

Based on the sapphire rod in hand dimension optimization for the cavity is implemented by Mehl. Firstly, the shield cylinder dimensions were varied so that the radial and end gaps were approximately equal. That is, using nominal dimensions of the sapphire (3 mm radius, 30 mm length), the shield cylinder dimensions were

chosen so tha $R_{cyl} = R_s + g$; $L_{cyl} = L_s + 2g$; g = gap : (1) The corresponding pairs (R_{cyl};L_{cyl}) are (4, 32), (4.5, 33), … (9, 42). Tefon supports at the center were 6.53 mm thick and filled the radial region between the sapphire and shield. The modes are identified as “A” and “B”, corresponding to modes 29 and 32 of the experimental resonator.

The relations between Q and cavity radius from 4 mm to 11 mm are given in Figure 4.11 where “NO-T” means no Teflon and “T” means with Teflon washer. The Teflon will decrease the Q certainly but the dependencies for both with and without Teflon are the same. The Q will not increase infinitely when the cavity becomes bigger but decreases after certain dimension. For the current calculations, when the radius of the cavity is within the range of 8 mm to 10 mm the Q is high.

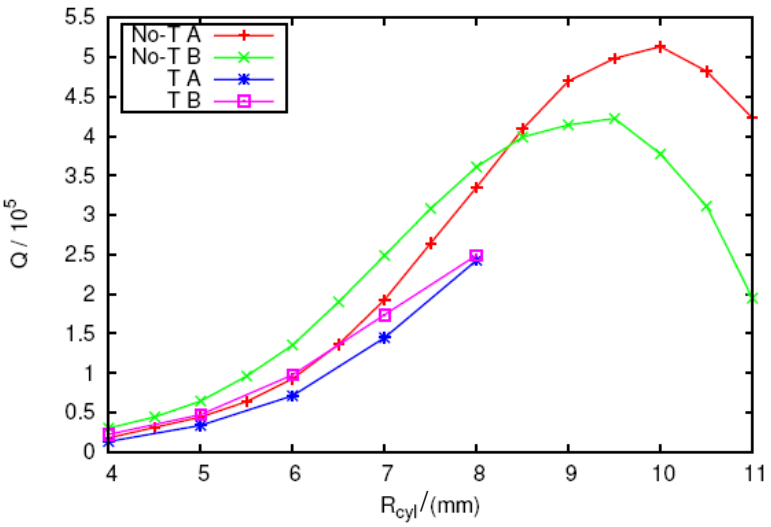

Figure 4.11 Q vs R_{cyl} for uniform-gap models with and without Teflon supports

The coupling strength is also an important factor to consider about because it is linked with whether or not this mode can be observed especially when the temperature goes higher. According to Figure 4.12 if both modes are to be studied it is better the radius of the cavity is no less than 8 mm.

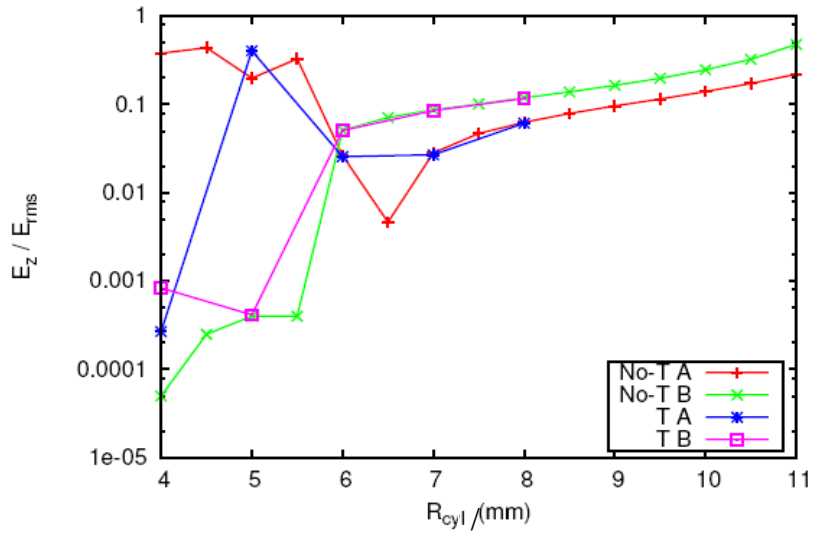

Figure 4.12 Probe coupling strength vs R_{cyl} for uniform-gap models with and without Teflon supports

As a good thermometer these two modes should have as much as possible energy on the sapphire. Figure 4.13 shows the calculation for fraction of energy in sapphire with different dimensions of the radius of the cavity. When the radius is in the range of 7 mm to 9 mm it has more than 88% of the electric energy on the sapphire.

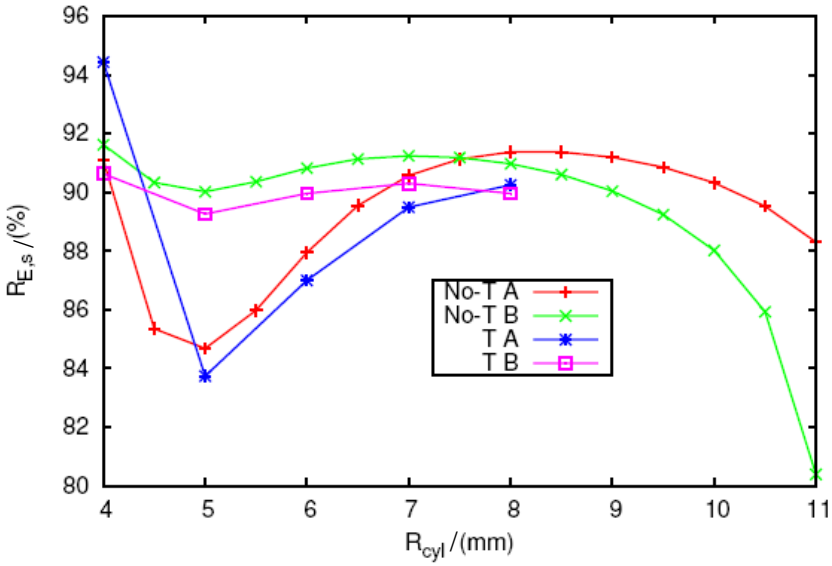

Figure 4.13 Fraction of electric energy in sapphire, $R_{E,s}$ vs R_{cyl} for uniform-gap models with and without Teflon supports

The frequencies also change with the radius as illustrated in Figure 4.14, it goes to lower frequencies when the radius becomes bigger.

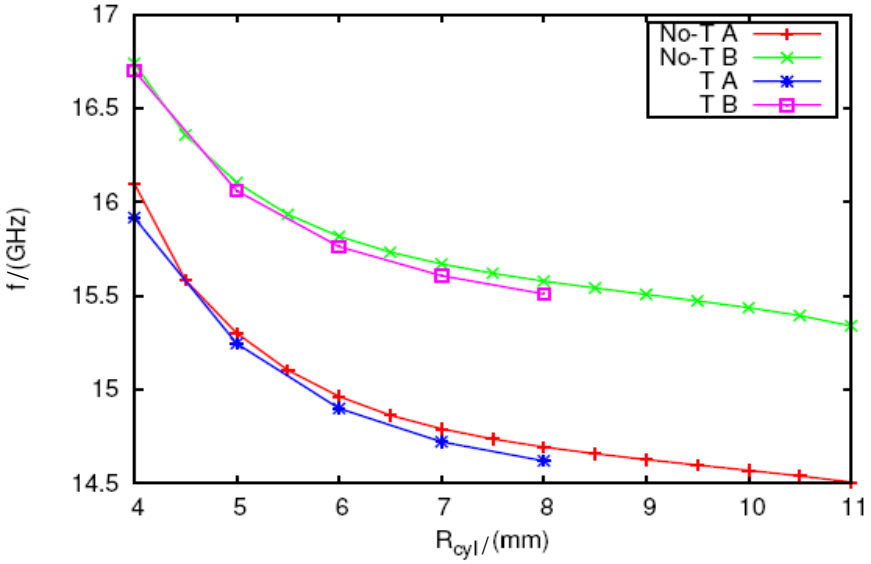

Figure 4.14 Eigenfrequencies vs R_{cyl} for uniform-gap models with and without Teflon supports

Summing up the forgoing four figures, resonators with the radius from 8 mm to 9 mm should render high Q, high electric energy percentage on dielectrics and high coupling strength based on the current 90° orientation sapphire rod which is 3 mm in radius and 30 mm in length with flush antennas. Since the cavity that has been using at the beginning of the chapter are 9 mm which conforms to the best dimension from the calculation by chance a serial of calculations for different lengths based on 9 mm radius were done too.

From Figure 4.15 when the length of the cavity is within the range of 42 mm to 44 mm it can gain higher Q and the Q is much more sensitive to the radial dimension than to the axial dimensions of the cavity compared to Figure 4.11. Figure 4.16 presents that the coupling becomes weaker and weaker when the cavity becomes longer and longer therefore with flush antenna the length of the cavity should be the shorter the better within the calculation range of 40 mm to 50 mm. As seen in Figure 4.17 the eigenfrequencies become smaller with the length of the cavity becomes longer too. By comparing Figure 4.14 and Figure 4.17 it is easy to observe that these two modes are more sensitive to the radial change than the axial change.

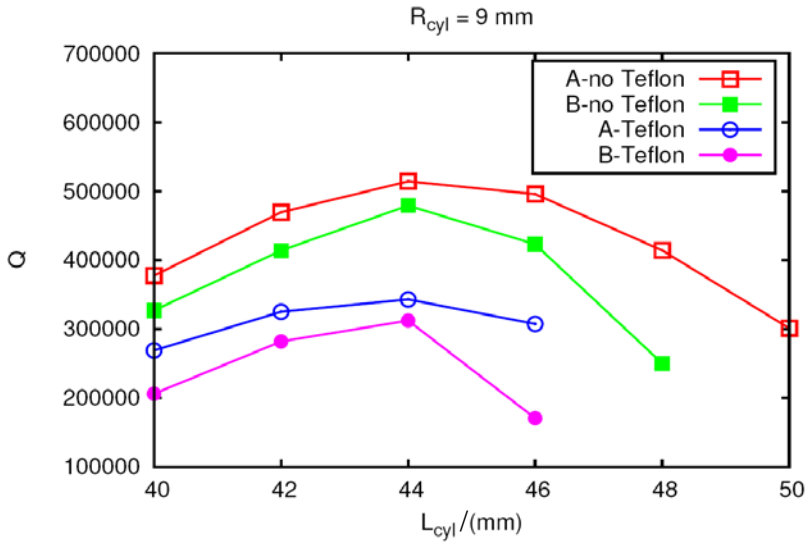

Figure 4.15 Q vs R_{cyl} for 9 mm-radius models with and without Teflon supports

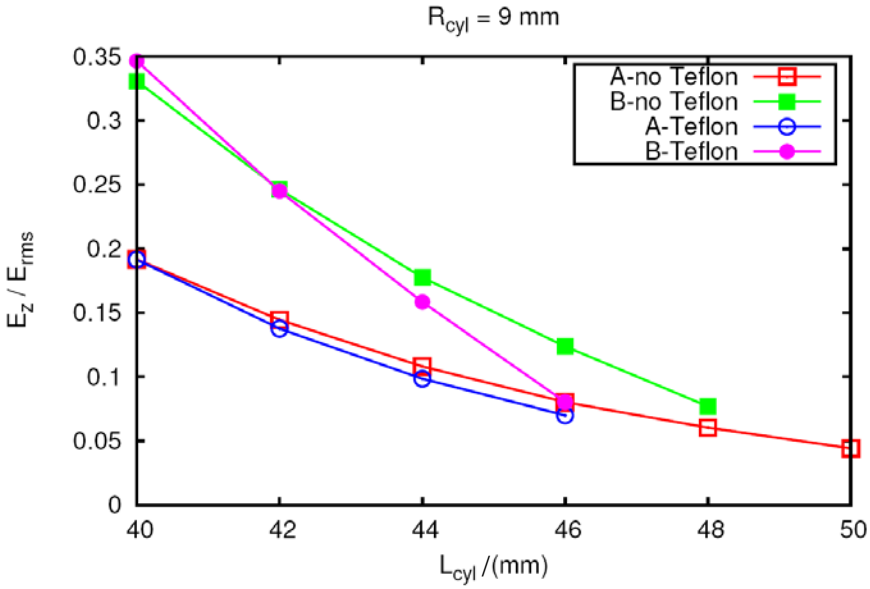

Figure 4.16 Probe coupling strength vs R_{cyl} for 9 mm-radius models with and without Teflon supports

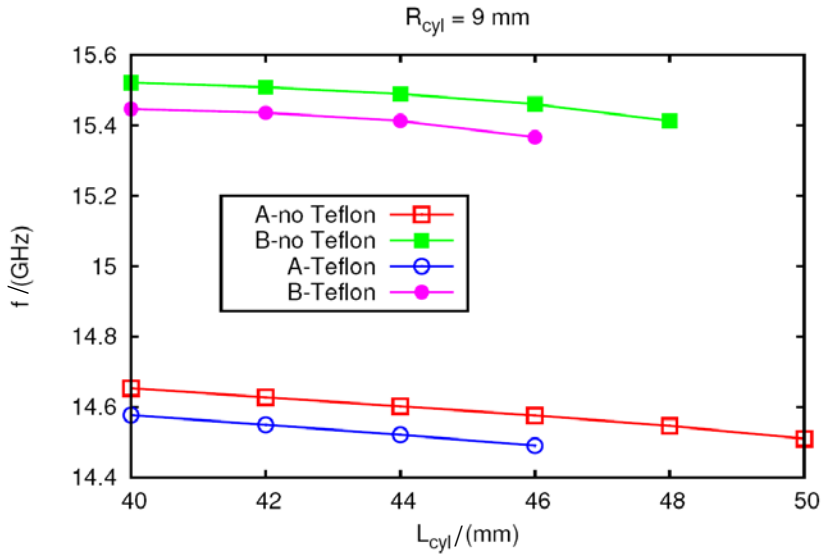

Figure 4.17 Eigenfrequencies vs R_{cyl} for 9 mm-radius models with and without Teflon supports

Now it is clear that when the length of the cavity is within 42 mm to 44 mm with 9 mm radius the resonator can offer high Q, high electric energy percentage on dielectrics and high coupling strength based on the current 90° orientation sapphire rod which is 3 mm in radius and 30 mm in length with flush antennas. The cavity in hand now is 9 mm in radius and 42 mm in length nominally which perfectly matches with the calculation results for dimension optimization.

4.2.3 Preliminary temperature experiments with air bath

After the dimension optimization some preliminary tests based on present sapphire rod resonator can be done and the former calculations for resonant modes and doublets are still available. Mode 29 and 32 are a pair of doublets which can be employed for exploring use of the birefringence of sapphire crystals as a thermometer. Before making a whole piece of sapphire supported inside the cavity but without any other perturbations like Teflon washer to limit its temperature range, a rough estimation of the thermometer based on the current resonator was implemented in an air bath with very low accuracy. In the experiments an ISOTECH HYPERION portable bath was used as an air bath and an Agilent N5230A network analyser works for logging data with Labview programme. No other calibrated PRT was employed considering that the aim of the experiments was only to investigate the possibility of

using the birefringence of the sapphire to make the thermometer and the underlying advantages and disadvantages. Figure 4.18 gives the system for roughly temperature measurements.

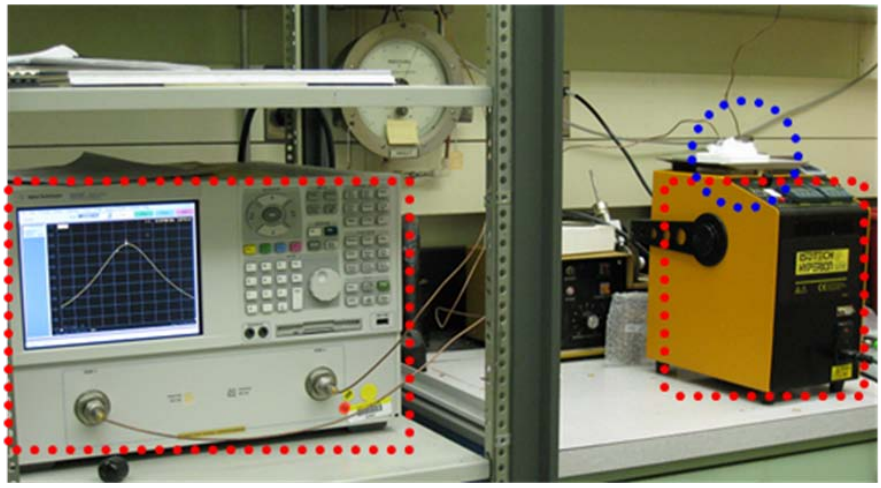

Figure 4.18 The system of the air bath temperature measurement for sapphire rod resonator

Comparisons for sapphire rod resonator thermometer between doublets frequency ratios and single frequencies are carried out. It is also obvious from Figure 4.19 that the ratios of the frequency pairs are sensitive to the temperature which makes it possible to make the sapphire resonator thermometer have an external shape that is close to the conventional platinum resistance thermometer and relatively insensitive to surface contamination and changes in the shape of the cavity. However, it has its disadvantage too. The frequency sensitivity $(\Delta f/\Delta T)/f$ of the frequency ratio (about 10 ppm/K) are much smaller than the frequency sensitivity of single frequency (about 50 ppm/K). The accuracies by using the frequency ratio are lower than using only single mode and the reason for this is uncertain but it may relate to that birefringence thermometer is more sensitive to some perturbations. More details will be given based on the real thermometer.

The accuracies for this thermometer are very low which is normal because of few reasons. One of the reasons is the Teflon washer has great losses and it will decrease the accuracy a lot. Secondly, no other thermometer is employed and the temperatures read out from the bath are the nominal values but not real temperatures. Moreover, the resonator is not closed well so the humidity will also affect the

accuracy of the thermometer. However, before starting to design a new available thermometer experiments based on these are reasonable.

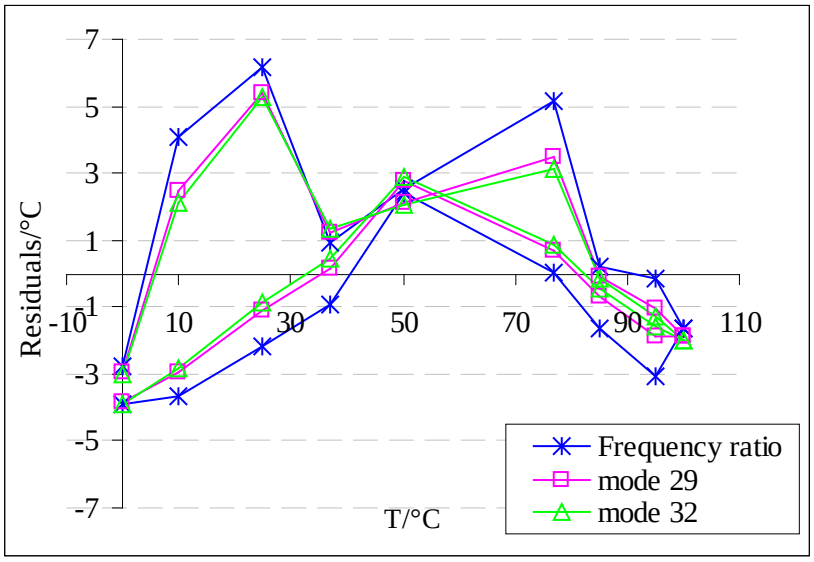

Figure 4.19 Rough temperature residuals comparisons between frequencies ratio and single mode of linear fit

4.3 Design of a real sapphire birefringence thermometer

Getting rid of the great perturbations of the Teflon washer, supporting screws *et al.* a new thermometer which based on the former experiments were designed.

One new whole piece of sapphire crystal that has similar shape as the Teflon washer supported old sapphire rod was designed, see Figure 4.20. The sapphire is composed of a rod with 3 mm in radius and 30 mm in length and a 3 mm thick sapphire ring with outer diameter of 9 mm. The c-axis of all the sapphire is still perpendicular to the geometric axis-z axis. The up and bottom surfaces of the ring part of the sapphire are chamfered for installation easy and tight.

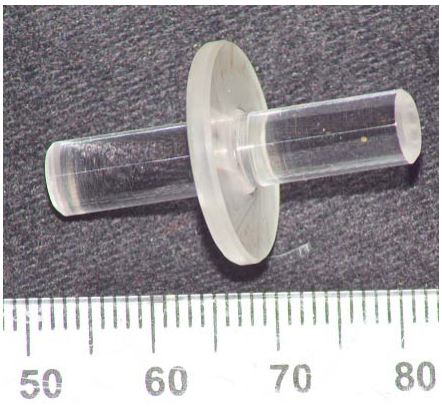

Figure 4.20 Picture for the new sapphire

The corresponding design for the cavity is also given in Figure 4.21, the cavity is made of stainless steel with gold plated. The gold plated feedthrough SMA connectors which can work within -80 °C to 450 °C are welded to the cavity. The schematic drawing for SMA connector are enclosed in Figure B 4. The hole around the feedthrough is for calibrated PRT to know the “real” temperature of the cavity block. A vacuum line on the body of the cavity is also needed. The schematic drawing for the full cavity are given in Figure B 5~Figure B 9.

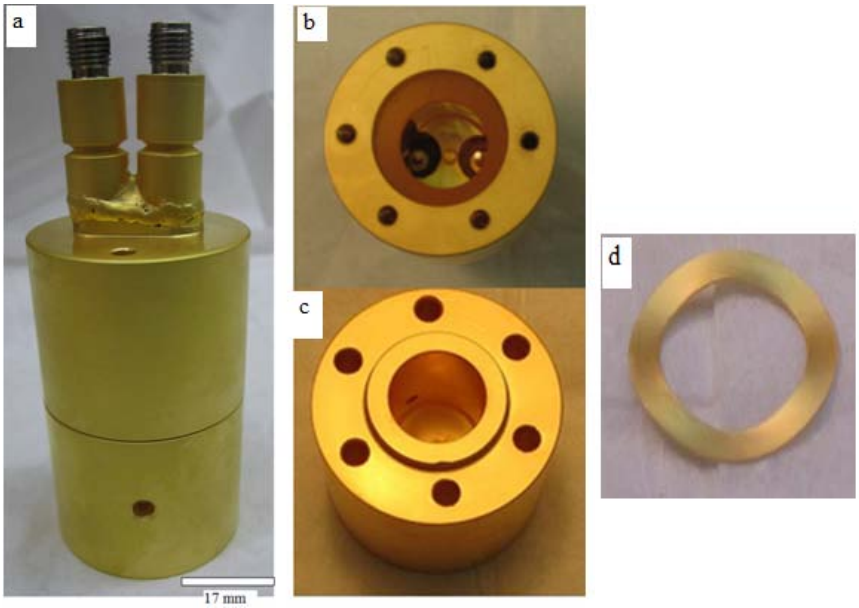

Figure 4.21 (a) closed cavity (b) upper part of the cavity (c) lower part of the cavity (d) gold plated Bellville washer

A gold plated Bellville washer is placed between the upper and lower part of the cavity to press the sapphire sit tightly on the slope of the upper body whose angle is

the same as the angle of the chamfered sapphire ring in order to fix and center the sapphire in the cavity. The dimension drawing for the washer is shown in Figure B 10.

The calculations were done based on the drawing of Figure 4.22 by ignoring the Bellville washer. All the calculation results are enclosed in Table A 31 of which two pairs of doublets are very attracting. One pair of them is near to 13.91 GHz and 14.69 GHz and another pairs are located around 14.82 GHz and 15.73 GHz. Table 4.5 presents these two pairs of doublets which have more than 88% of the electric energy concentrated on the sapphire rod but less than 10% of the electric energy density on the disk which only functions as support. The electric energy densities for these two pairs are given in Figure 4.23.

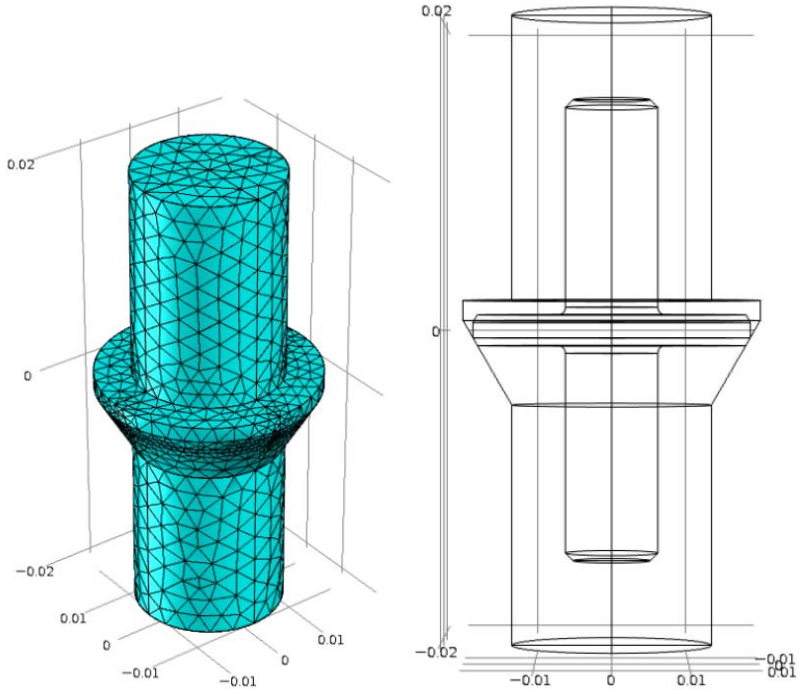

Figure 4.22 Drawings of the birefringence thermometer (no washer is drawn) for calculation

Table 4.5 Calculation results of energy proportion of two pairs of doublets

f/GHz	Q	$R_{E.s}$	$R_{H,s}$	$R_{E.sdisk}$	$R_{H,sdisk}$
13.914718	96704	89.07%	81.72%	8.83%	4.01%
14.693535	103847	90.37%	82.17%	9.75%	4.31%
14.821167	183307	92.10%	86.31%	4.35%	8.85%
15.725590	73268	88.39%	83.22%	5.03%	10.46%

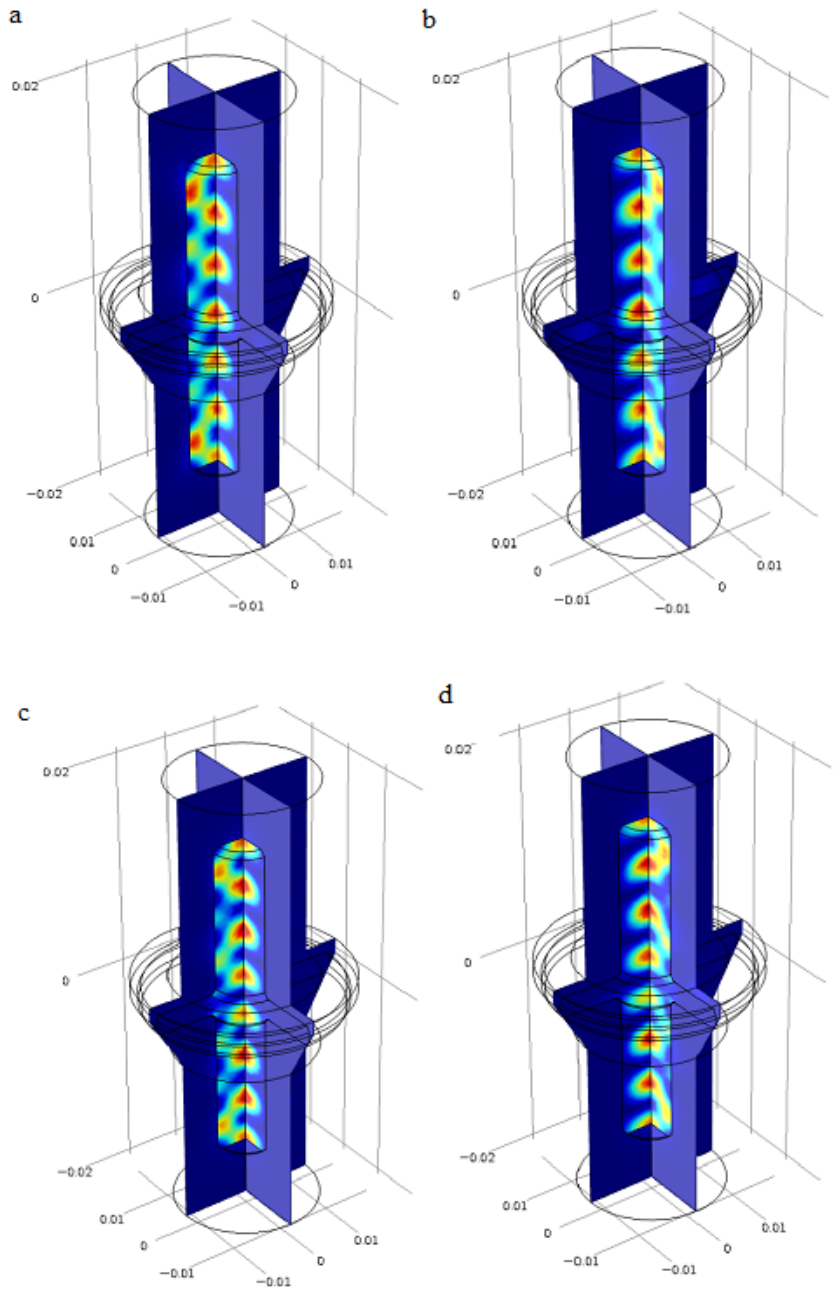

Figure 4.23 Electric energy density for the two doublets (a) and (b) are a pair that are around 13.91 GHz and 14.69 GHz and (c) and (d) are another pair that are close to 14.82 GHz and 15.73 GHz

Figure 4.24 presents the electric energy density on the top surface to indicate the coupling strength. The mode around 13.91 GHz is weaker than the other three modes by an order of magnitude.

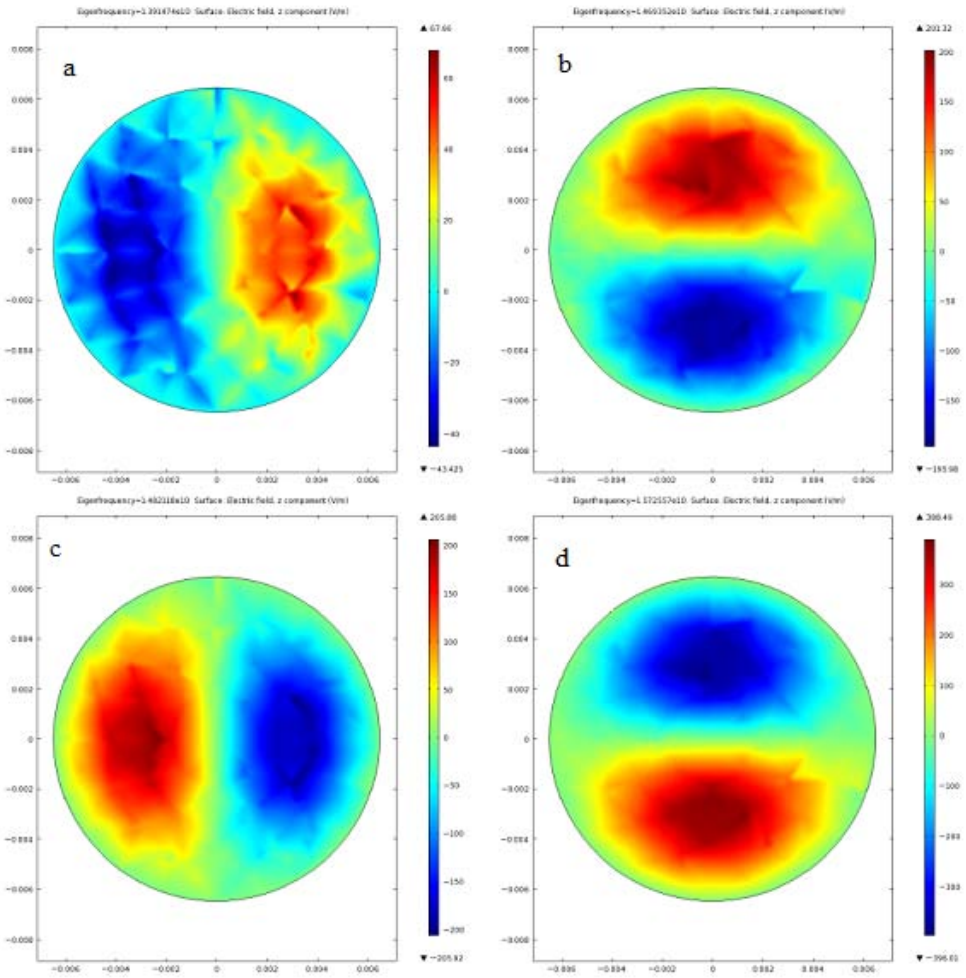

Figure 4.24 Normal electric field E_z on the top surface for the two doublets

However, underlying problems may exist. The nearest neighbours of these doublets are so close to them that they may couple to the doublets. The 13.89 GHz mode is 0.16% below 13.91 GHz, the 14.47 GHz mode is 0.21% below 14.69 GHz, the 14.87 GHz mode is 0.37% above the 14.82 GHz mode and the 15.77 GHz mode is 0.33% above the 15.72 GHz mode. What is worse is that these neighbours have high electric energy concentration on the sapphire disk, see Table 4.6, some of them even have stronger coupling to the antenna than the doublets.

Table 4.6 Calculation results of energy proportion and coupling strength of two pairs of doublets and their neighbours

f/GHz	Q	$R_{E.s}$	$R_{H,s}$	$R_{E.sdisk}$	$R_{H,sdisk}$	$\frac{E_{z,1}}{<E^2>^{1/2}}$
13.892002	16533	88.30%	59.95%	54.97%	28.19%	-0.0156
13.914718	96704	89.07%	81.72%	8.83%	4.01%	-0.0042
14.447995	27709	95.57%	69.08%	34.01%	18.34%	-0.0014
14.693535	103847	90.37%	82.17%	9.75%	4.31%	-0.0159
14.821167	183307	92.10%	86.31%	4.35%	8.85%	-0.0148
14.875606	10243	93.92%	58.45%	72.30%	38.96%	-0.0009
15.725590	73268	88.39%	83.22%	5.03%	10.46%	0.0315
15.777647	8824	74.20%	58.15%	65.07%	46.38%	0.0667

4.4 Conclusions

This chapter introduces my work done at NIST on birefringence resonator thermometer which has the possibility to make it shaped like a PRT. Lots of work was done for the preparation of the thermometer.

Different perturbations in the experiments were considered respectively, materials of supporting screws, amounts of the Teflon washer under the same thickness; whether or not there are holes around the cavity central equator *et al.* and they are all proved to be insignificant.

The resonant frequencies are sensitive to the axial displacement and from the experiments it can be concluded that the frequencies are quadratic function of axial displacement.

Calculations by Mehl [130] can match very well with experiments with the frequencies differences of less than 2% for observed modes of which one pair of doublets modes near 14.7 GHz and 15.6 GHz are most concerned. They have most of the energy concentrated on the sapphire and most importantly, they are doublets because of the birefringence.

Dimension optimization was implemented for the current sapphire rod in hand. According to the calculation by Mehl[130], the Q of the resonator has a peak at

certain dimension of the cavity and then becomes smaller by increasing or decreasing the cavity. Eigenfrequency lowers with the increase of the cavity dimension and it is more sensitive to the radial change than the axial change. It turns out that for 90° orientation sapphire rod that is 6 mm in diameter and 30 mm in length the best dimensions for the cavity are 8 mm~9 mm in radius and 42 mm~44 mm in length.

Some preliminary experiments based on a cavity that is 9 mm in radius and 42 mm in length were implemented in air bath with low accuracy. It proves the possibility to make the birefringence thermometer shaped like a conventional PRT but with lower frequency sensitivity and accuracy compared to the single mode sapphire rod resonator thermometer. Besides, the birefringence thermometer should be relatively insensitive to the surface contamination and changes in the shape.

A new piece of sapphire which has rod diameter of 6 mm and 30 mm in length with ring diameter of 18 mm and 3 mm in thickness and the corresponding new cavity were designed. Calculations for the new birefringence thermometer were also done by Mehl [130] and possible difficulty may face in the experiments were predicted too.

Work in this chapter is very meaningful for the great possibility to make the sapphire WGM resonator thermometer shaped like a conventional platinum resistance thermometer.

Reference

1. Strouse, G., *Sapphire Whispering Gallery Thermometer*. International Journal of Thermophysics, 2007. **28**(6): p. 1812-1821.
2. Collot, L., et al., *Very high-Q whispering-gallery mode resonances observed on fused-silica microspheres.* Europhysics Letters, 1993. **23**(5): p. 327-334.
3. Stratton, J., *Elliptic cylinder and spheroidal wave functions including tables of separation constants and coefficients*. 1941, Wiley,New York.
4. Laine, J.-P., *Design and Applications of Optical Microsphere Resonators.* 2003.
5. Jiao, X.H., P. Guillon, and L.A. Bermudez, *Resonant frequencies of whispering-gallery dielectric resonator modes.* Microwaves, Antennas and Propagation, IEE Proceedings H, 1987. **134**(6): p. 497-501.
6. Vedrenne, C. and J. Arnaud, *Whispering-gallery modes of dielectric resonators.* IEE PROC, 1982. **129**: p. 183-187.
7. Badnikar, S.L., N. Shanmugam, and V.R.K. Murthy, *Resonant frequencies of whispering gallery modes of dielectric resonator*. Defence Science Journal, 2001. **51**(2): p. 189-193.
8. Rayleigh, L., *The problem of the whispering gallery.* Scientific Papers (Cambridge University), 1912(**5**): p. 617-620.
9. Rayleigh, J.W.S. Baron, and R.B. Lindsay, *The Theory of Sound.* New York, Dover 1945.
10. Rayleigh, L., *Further applications of Bessel's functions of high order to the whispering gallery and allied problems.* Phil. Mag., 1914. **27**: p. 100-109.
11. Mie, G., *Beitrage zur optik truber medien, speziell kolloidaler metallosungen.* Annalen der Physik, 1908. **25**: p. 377-445.
12. Debye, P., *Der Lichtdruck auf Kugeln von beliebigem Material.* Ann. Phys., 1909. **30**: p. 57-136.
13. Garrett, C.G.B., W. Kaiser, and W.L. Bond, *Stimulated Emission into Optical Whispering Modes of Spheres.* Physical Review, 1961. **124**(6): p. 1807-1809.
14. Walsh, P. and G. Kemeny, *Laser Operation Without Spikes in a Ruby Ring* J. Appl. Phys., 1963. **34**: p. 956-957.
15. Ashkin, A. and J.M. Dziedzic, *Observation of Resonances in the Radiation Pressure on Dielectric Spheres.* Physical Review Letters, 1977. **38**(23): p. 1351-1354.
16. Chylek, P., J.T. Kiehl, and M.K.W. Ko, *Optical levitation and partial-wave resonances.* Physical Review A, 1978. **18**(5): p. 2229.
17. Benner, R.E., et al., *Observation of Structure Resonances in the Fluorescence Spectra from Microspheres.* Physical Review Letters, 1980. **44**(7): p. 475-478.
18. Hill, S.C., et al., *Structural resonances observed in the fluorescence emission from small spheres on substrates.* Appl. Opt., 1984. **23**(11): p. 1680-1683.
19. Hill, S.C., et al., *Sizing dielectric spheres and cylinders by aligning measured and computed resonance locations: algorithm for multiple orders.* Appl. Opt., 1985. **24**(15): p. 2380-2390.
20. Thurn, R. and W. Kiefer, *Raman-Microsampling Technique Applying Optical Levitation by Radiation Pressure.* Appl. Spectrosc., 1984. **38**(1): p. 78-83.

21. Qian, S.-X., J.B. Snow, and R.K. Chang, *Coherent Raman mixing and coherent anti-Stokes Raman scattering from individual micrometer-size droplets.* Opt. Lett., 1985. **10**(10): p. 499-501.
22. Snow, J.B., S.-X. Qian, and R.K. Chang, *Stimulated Raman scattering from individual water and ethanol droplets at morphology-dependent resonances.* Opt. Lett., 1985. **10**(1): p. 37-39.
23. Barton, J.P., D.R. Alexander, and S.A. Schaub, *Internal and near-surface electromagnetic fields for a spherical particle irradiated by a focused laser beam.* Journal of Applied Physics, 1988. **64**(4): p. 1632-1639.
24. Lock, J.A. and G. Gouesbet, *Rigorous justification of the localized approximation to the beam-shape coefficients in generalized Lorenz-Mie theory. I. On-axis beams.* J. Opt. Soc. Am. A, 1994. **11**(9): p. 2503-2515.
25. Khaled, E.E.M., et al., *Near-resonance excitation of dielectric spheres with plane waves and off-axis Gaussian beams.* Appl. Opt., 1992. **31**(9): p. 1166-1169.
26. Lock, J.A., *Excitation efficiency of a morphology-dependent resonance by a focused Gaussian beam.* J. Opt. Soc. Am. A, 1998. **15**(12): p. 2986-2994.
27. Serpengüzel, A., et al., *Enhanced coupling to microsphere resonances with optical fibers.* J. Opt. Soc. Am. B, 1997. **14**(4): p. 790-795.
28. Sarid, D., P.J. Cressman, and R.L. Holman, *High-efficiency prism coupler for optical waveguides.* Applied Physics Letters, 1978. **33**(6): p. 514-515.
29. Sarid, D., *High efficiency input-output prism waveguide coupler: an analysis.* Appl. Opt., 1979. **18**(17): p. 2921-2926.
30. Gorodetsky, M.L. and V.S. Ilchenko, *High-Q optical whispering-gallery microresonators: precession approach for spherical mode analysis and emission patterns with prism couplers.* Optics Communications, 1994. **113**: p. 133-143.
31. Gorodetsky, M.L. and V.S. Ilchenko, *Optical microsphere resonators: optimal coupling to high-Q whispering-gallery modes.* J. Opt. Soc. Am. B, 1999. **16**(1): p. 147-154.
32. Schiller, S. and R.L. Byer, *High-resolution spectroscopy of whispering gallery modes in large dielectric spheres.* Opt. Lett., 1991. **16**(15): p. 1138-1140.
33. Rowland, D.R. and J.D. Love, *Evanescent wave coupling of whispering gallery modes of a dielectric cylinder.* Optoelectronics, IEE Proceedings J, 1993. **140**(3): p. 177-188.
34. Treussart, F., et al., *Evidence for intrinsic Kerr bistability of high-Q microsphere resonators in superfluid helium.* The European Physical Journal D - Atomic, Molecular, Optical and Plasma Physics, 1998. **1**(3): p. 235-238.
35. Pan, Y.-L. and R.K. Chang, *Highly efficient prism coupling to whispering gallery modes of a square mu cavity.* Applied Physics Letters, 2003. **82**(4): p. 487-489.
36. Serpengüzel, A., S. Arnold, and G. Griffel, *Excitation of resonances of microspheres on an optical fiber.* Opt. Lett., 1995. **20**(7): p. 654-656.
37. Griffel, G., et al., *Morphology-dependent resonances of a microsphere-optical fiber system.* Opt. Lett., 1996. **21**(10): p. 695-697.
38. Dubreuil, N., et al., *Eroded monomode optical fiber for whispering-gallery mode excitation in fused-silica microspheres.* Opt. Lett., 1995. **20**(8): p. 813-815.
39. Knight, J.C., et al., *Phase-matched excitation of whispering-gallery-mode resonances by a fiber taper.* Opt. Lett., 1997. **22**(15): p. 1129-1131.

40. Chin, M.K. and S.T. Ho, *Design and modeling of waveguide-coupled single-mode microring resonators.* Lightwave Technology, Journal of, 1998. **16**(8): p. 1433-1446.
41. Little, B.E., J.P. Laine, and H.A. Haus, *Analytic theory of coupling from tapered fibers and half-blocks into microsphere resonators.* Lightwave Technology, Journal of, 1999. **17**(4): p. 704-715.
42. Cai, M., O. Painter, and K.J. Vahala, *Observation of Critical Coupling in a Fiber Taper to a Silica-Microsphere Whispering-Gallery Mode System.* Physical Review Letters, 2000. **85**.
43. Cai, M. and K. Vahala, *Highly efficient optical power transfer to whispering-gallery modes by use of a symmetrical dual-coupling configuration.* Opt. Lett., 2000. **25**(4): p. 260-262.
44. Spillane, S.M., et al., *Ideality in a fiber-taper-coupled microresonator system for application to cavity quantum electrodynamics.* Phys. Rev. Lett., 2003. **91**.
45. Barclay, P.E., K. Srinivasan, and O. Painter, *Design of photonic crystal waveguides for evanescent coupling to optical fiber tapers and integration with high-Q cavities.* J. Opt. Soc. Am. B, 2003. **20**(11): p. 2274-2284.
46. Srinivasan, K., et al., *Optical-fiber-based measurement of an ultrasmall volume high-Q photonic crystal microcavity.* Physical Review B, 2004. **70**(8): p. 081306.
47. Nurenberg, A. and G. Schweiger, *Excitation and recording of morphology-dependent resonances in spherical microresonators by hollow light guiding fibers.* Applied Physics Letters, 2004. **84**(12): p. 2043-2045.
48. Ilchenko, V.S., X.S. Yao, and L. Maleki, *Pigtailing the high-Q microsphere cavity: a simple fiber coupler for optical whispering-gallery modes.* Opt. Lett., 1999. **24**(11): p. 723-725.
49. Ilchenko, V.S., et al., *Microsphere Integration in Active and Passive Photonics Devices* SPIE Proc., 2000. **3930**: p. 154-162.
50. Vassiliev, V.V., et al., *Narrow-line-width diode laser with a high-Q microsphere resonator.* Opt. Commun., 1998. **158**: p. 305-312.
51. Vassiliev, V.V., S.M. Il'ina, and V.L. Velichansky, *Diode laser coupled to a high-Q microcavity via a GRIN lens.* Applied Physics B: Lasers and Optics, 2003. **76**(5): p. 521-523.
52. Rafizadeh, D., et al., *Waveguide-coupled AlGaAs/GaAs microcavity ring and disk resonators with high finesse and 21.6-nm free spectral range.* Opt. Lett., 1997. **22**: p. 1244-1246.
53. Blom, F.C., et al., *Experimental study of integrated-optics microcavity resonators: Toward an all-optical switching device.* Applied Physics Letters, 1997. **71**(6): p. 747-749.
54. Little, B.E., et al., *Pedestal antiresonant reflecting waveguides for robust coupling to microsphere resonators and for microphotonic circuits.* Opt. Lett., 2000. **25**(1): p. 73-75.
55. Laine, J.P., et al., *Microsphere resonator mode characterization by pedestal anti-resonant reflecting waveguide coupler.* Photonics Technology Letters, IEEE, 2000. **12**(8): p. 1004-1006.
56. Garaei, M.A., M. Sabaeian, and H. Nadgaran. *Design and modeling of low-temperature fiber sensor based on microdisk whispering gallery modes*. in *Photonics Global Conference (PGC), 2010*.

57. Chylek, P., et al., *Simultaneous determination of refractive index and size of spherical dielectric particles from light scattering data.* Appl. Opt., 1983. **22**(15): p. 2302-2307.
58. Ashkin, A. and J.M. Dziedzic, *Observation of optical resonances of dielectric spheres by light scattering.* Applied optics, 1981. **20**(10): p. 1803-14.
59. Owen, J.F., et al., *Determination of optical-fiber diameter from resonances in the elastic scattering spectrum.* Optics letters, 1981. **6**(6): p. 272-4.
60. Savchenkov, A.A., et al., *Second-order filter response with series-coupled silica microresonators.* Ieee Photonics Technology Letters, 2003. **15**(4): p. 543-544.
61. Chu, S.T., et al., *Wavelength trimming of a microring resonator filter by means of a UV sensitive polymer overlay.* Ieee Photonics Technology Letters, 1999. **11**(6): p. 688-690.
62. Savchenkov, A.A., et al., *Ultraviolet-assisted frequency trimming of optical microsphere resonators.* Optics letters, 2003. **28**(8): p. 649-650.
63. Ilchenko, V.S., et al., *Tunability and synthetic lineshapes in high-Q optical whispering gallery modes.* Proc. SPIE Int. Soc. Opt. Eng., 2003. **4969**: p. 195-206.
64. Ilchenko, V.S., et al., *Nonlinear optics and crystalline whispering gallery mode cavities.* Physical Review Letters, 2004. **92**(4): p. 4.
65. Savchenkov, A.A., et al., *Tunable filter based on whispering gallery modes.* Electronics Letters, 2003. **39**(4): p. 389-391.
66. Schwelb, O. and I. Frigyes, *All-optical tunable filters built with discontinuity-assisted ring resonators.* Lightwave Technology, Journal of, 2001. **19**(3): p. 380-386.
67. Ilchenko, V.S., X.S. Yao, and L. Maleki, *Microsphere integration in active and passive photonics devices.* Proc. SPIE Int. Soc. Opt. Eng., 2000. **3930**: p. 154-162.
68. Ilchenko, V.S. and L. Maleki, *Novel whispering-gallery resonators for lasers, modulators, and sensors* Proc. SPIE Int. Soc. Opt. Eng., 2001. **4270**: p. 120-130.
69. Nadeau, J.L., et al., *High-Q whispering-gallery mode sensor in liquids.* Proc. SPIE Int. Soc. Opt. Eng., 2002. **4629**: p. 172-180.
70. Lukosz, W., *Integrated optical chemical and direct biochemical sensors.* Sensors and Actuators B-Chemical, 1995. **29**(1-3): p. 37-50.
71. Schult, K., et al., *Disposable optical sensor chip for medical diagnostics: New ways in bioanalysis.* Analytical Chemistry, 1999. **71**(23): p. 5430-5435.
72. Foster, M.W., D.J. Ferrell, and R.A. Lieberman, *Surface plasmon resonance biosensor miniaturization* Proc. SPIE Int. Soc. Opt. Eng., 1995. **2293**: p. 122-131.
73. Weisser, M., et al., *Specific bio-recognition reactions observed with an integrated Mach-Zehnder interferometer.* Biosensors & Bioelectronics, 1999. **14**(4): p. 405-411.
74. Vollmer, F., et al., *Multiplexed DNA quanti. cation by spectroscopic shift of two microsphere cavities.* Biophysical Journal, 2003. **85**(3): p. 1974-1979.
75. Arnold, S., et al., *MicroParticle photophysics illuminates viral bio-sensing.* Faraday Discussions, 2008. **137**: p. 65-83.
76. Boyd, R.W. and J.E. Heebner, *Sensitive Disk Resonator Photonic Biosensor.* Appl. Opt., 2001. **40**(31): p. 5742-5747.

77. Laine, J.P., et al., *Acceleration sensor based on high-Q optical microsphere resonator and pedestal antiresonant reflecting waveguide coupler.* Sensors and Actuators a-Physical, 2001. **93**(1): p. 1-7.
78. Armenise, M.N., et al., *Modeling and design of a novel miniaturized integrated optical sensor for gyroscope systems.* Journal of Lightwave Technology, 2001. **19**(10): p. 1476-1494.
79. Matsko, A.B., et al., *Optical gyroscope with whispering gallery mode optical cavities.* Opt. Commun., 2004. **233**: p. 107-112.
80. Huston, A.L. and J.D. Eversole, *Strain-sensitive elastic scattering from cylinders.* Optics letters, 1993. **18**(13): p. 1104-1106.
81. Ilchenko, V.S., M.L. Gorodetsky, and S.P. Vyatchanin, *Coupling and tunability of optical whispering gallery modes—a basis for coordinate meter.* Optics Communications, 1994. **107**(1-2): p. 41-48.
82. Braginsky, V.B., M.L. Gorodetsky, and V.S. Ilchenko, *Quality-factor and nonlinear properties of optical whispering-gallery modes.* Physics Letters A, 1989. **137**(7-8): p. 393-397.
83. Eschmann, A. and C.W. Gardiner, *STABILITY AND SWITCHING IN WHISPERING-GALLERY-MODE MICRODISK LASERS.* Physical Review A, 1994. **49**(4): p. 2907-2913.
84. Heebner, J.E., et al., *Distributed and localized feedback in microresonator sequences for linear and nonlinear optics.* Journal of the Optical Society of America B-Optical Physics, 2004. **21**(10): p. 1818-1832.
85. Ilchenko, V.S. and A.B. Matsko, *Optical resonators with whispering-gallery modes-part II: applications.* Selected Topics in Quantum Electronics, IEEE Journal of, 2006. **12**(1): p. 15-32.
86. Braginsky, V.B., V.P.Mitrafanov, and V.I.Panov, *Systems with Small Dissipation.* Univ. of Chicago, 1985.
87. Dobromyslov, V.S. and V.F. Vzyatyshev, Trans. Moscow Eng. Inst., 1973. **16**: p. 78.
88. Tsarapkin, D.P. and E.N. Ivanov, Moscow Power Engineering Institute, not published.
89. Benmessai, K., et al., *Frequency instability measurement system of cryogenic maser oscillator.* Electronics Letters, 2007. **43**(25): p. 1436-1437.
90. Daniel L. Creedon, K. Benmessaï, and M.E. Tobar, *High-Power Solid-State Sapphire Whispering Gallery Mode Maser.* IEEE Transactions on Ultrasonics Ferroelectrics and Frequency Control, Ferroelectrics, and Frequency Control, , March 2010. **57**(3).
91. Bourgeois, P.Y., et al., *Maser oscillation in a whispering-gallery-mode microwave resonator.* Applied Physics Letters, 2005. **87**(22): p. 224104-3.
92. Chang, S., A.G. Mann, and A.N. Luiten. *Cryogenic sapphire oscillator with improved frequency stability*. in *Frequency Control Symposium and Exhibition, 2000. Proceedings of the 2000 IEEE/EIA International*. 2000.
93. Hartnett, J.G., et al., *Cryogenic sapphire oscillator with exceptionally high long-term frequency stability.* Applied Physics Letters, Nov. 2006. **89**.
94. Taber, R.C. and C.A. Flory, *Microwave oscillators incorporating cryogenic sapphire dielectric resonators.* Ultrasonics, Ferroelectrics and Frequency Control, IEEE Transactions on, 1995. **42**(1): p. 111-119.
95. Zychowicz, T., J. Krupka, and M.E. Tobar, *Whispering gallery modes in hollow spherical dielectric resonators.* Journal of the European Ceramic Society, 2006. **26**(10-11): p. 2193-2194.

96. Lajoie, I., et al., *High Q microwave resonators using quartz monocrystal.* Electronics Letters, 2000. **36**(2): p. 150-152.
97. Monaco, O.D. and Y. Kersale, *Resonance degeneration and spurious mode suppression in a cryogenic Whispering Gallery Mode sapphire resonator.* Microwave and Guided Wave Letters, 2000. **10**: p. 368--346.
98. Locke, C.R., et al., *Invited Article: Design techniques and noise properties of ultrastable cryogenically cooled sapphire-dielectric resonator oscillators.* Review of Scientific Instruments, 2008. **79**(5): p. 051301-12.
99. Dick, G.J. and J. Saunders, *Measurement and analysis of a microwave oscillator stabilized by a sapphire dielectric ring resonator for ultra-low noise.* Ieee Transactions on Ultrasonics Ferroelectrics and Frequency Control, 1990. **37**(5): p. 339-346.
100. Zaki, K.A. and X.P. Liang. *Higher order modes, high Q dielectric resonators for oscillator applications*. in *Frequency Control Symposium, 1992. 46th., Proceedings of the 1992 IEEE*. 1992.
101. Tobar, M.E., et al. *Low noise microwave oscillators based on high-Q temperature stabilized sapphire resonators*. in *Frequency Control Symposium, 1994. 48th., Proceedings of the 1994 IEEE International*. 1994.
102. Tobar, M.E., et al. *High-Q TE stabilized sapphire microwave resonators for low noise applications*. in *Frequency Control Symposium, 1993. 47th., Proceedings of the 1993 IEEE International*. 1993.
103. A.J.Giles, A.G.Mann, and S.K.Jones, *A very high stability sapphire loaded superconducting cavity oscillator*. physica B, 1990: p. 165-166.
104. Mann, A.G., et al. *Ultrastable cryogenic sapphire dielectric microwave resonators*. in *Frequency Control Symposium, 1992. 46th., Proceedings of the 1992 IEEE*. 1992.
105. Krupka, J., K. Derzakowski, and M. Tobar, *Complex permittivity of some ultralow loss dielectric crystals at cryogenic temperatures.* Meas. Sci. Technol, 1999. **10**: p. 387-392.
106. Krupka, J. and K. Derzakowski, *Use of Whispering-gallery Modes for Complex Permittivity Determinations of Ultra-Low-Loss Dielectric Materials.* Transactions on Microwave Theory and Techniques, 1999. **47**: p. 752-759.
107. Giordano, **V.**, et al., *High - Q $Si0_2$ Whispering Gallery Mode Resonator*. 1999 Joint Meeting EFTF-IEEE IFCS, 1999.
108. Krupka, J., *Precise measurements of the complex permittivity of dielectric materials at microwave frequencies.* Materials Chemistry and Physics, 2003. **79**(2-3): p. 195-198.
109. Krupka, J., et al., *A dielectric resonator for measurements of complex permittivity of low loss dielectric materials as a function of temperature Meas. Sci. Technol.*, 1998. **9**: p. 1751-1756.
110. Hartnett, J.G., M.E. Tobar, and J. Krupka, *Dependence of the dielectric permittivity of single-crystal quartz on thermal deformation at cryogenic temperatures.* Journal of Applied Physics, 2007. **102**(7): p. 5.
111. Krupka, J., *Frequency domain complex permittivity measurements at microwave frequencies.* Measurement Science & Technology, 2006. **17**(6): p. R55-R70.
112. Nakayama, A. and H. Yoshikawa, *Permittivity measurements at millimeter wave frequencies using dielectric rod resonator excited by NRD-guide.* Journal of the European Ceramic Society, 2006. **26**(10-11): p. 1853-1856.

113. Hartnett, J.G., M.E. Tobar, and J. Krupka, *The dependence of the permittivity of sapphire on the thermal deformation at cryogenic temperatures.* Meas. Sci. Technol, 2004. **15**: p. 203-210.
114. Hartnett, J.G., et al., *Room temperature measurement of the anisotropic loss tangent of sapphire using the whispering gallery mode technique.* Ieee Transactions on Ultrasonics Ferroelectrics and Frequency Control, 2006. **53**(1): p. 34-38.
115. Annino, G., et al., *Dielectric properties of materials using whispering gallery dielectric resonators: Experiments and perspectives of ultra-wideband characterization.* Journal of Chemical Physics, 2000. **112**(5): p. 2308-2314.
116. Moldover, M.R., D. Ripple, and G. Strouse, *Dielectric Resonator Thermometer and a Method of Using the same*. 2008: United States.
117. McNeilage, C., et al. *A review of sapphire whispering gallery-mode oscillators including technical progress and future potential of the technology*. in *Frequency Control Symposium and Exposition, 2004. Proceedings of the 2004 IEEE International*. 2004.
118. Jackson, J.D., ed. *Classical Electrodynamics*. 3 ed. 1998: California.
119. Pozar, D.M., ed. *Microwave Engineering*. 3 ed. 2003. 700.
120. M E Tobary, J.K., E N Ivanovy and R A Woodey, *Dielectric frequency–temperature-compensated microwave whispering-gallery-mode resonators.* J. Phys. D: Appl. Phys., 1997. **30**: p. 2770-2775.
121. Tobar, M.E., et al., *The dual-mode frequency-locked technique for the characterization of the temperature coefficient of permittivity of anisotropic materials.* Measurement Science & Technology, 2004. **15**(1): p. 29-34.
122. Shelby, R., J. Fontanella, and C. Andeen, *The low temperature electrical properties of some anisotropic crystals.* Journal of Physics and Chemistry of Solids, 1980. **41**(1): p. 69-74.
123. Dick, G.J., D.G. Santiago, and R.T. Wang. *Temperature compensated sapphire resonator for ultra-stable oscillator capability at temperatures above 77 kelvin*. in *Frequency Control Symposium, 1994. 48th., Proceedings of the 1994 IEEE International*. 1994.
124. Krupka, J., et al., *Extremely high-Q factor dielectric resonators for millimeter-wave applications.* Ieee Transactions on Microwave Theory and Techniques, 2005. **53**(2): p. 702-712.
125. Krupka, J., et al., *Study of whispering gallery modes in anisotropic single-crystal dielectric resonators.* Microwave Theory and Techniques, IEEE Transactions on, 1994. **42**(1): p. 56-61.
126. Blair, D.G. and I.N. Evans, *High Q microwave properties of a sapphire ring resonator.* J. Phys. D: Appl. Phys., 1982. **15**: p. 1651-1656.
127. Ratheesh, R., et al., *Whispering Gallery mode microwave characterization of $Ba(Mg_{1/3},Ta_{2/3})O_3$ dielectric resonators.* Journal of Physics D-Applied Physics, 1999. **32**(21): p. 2821-2826.
128. Tobar, M., et al., *Compact, High-Q, Zero Temperature Coe cient, TE011 sapphire-rutile microwave distributed Bragg reflector resonators.* 2000 IEEE/EIA International Frequency Control Symposium and Exhibition.
129. Tobar, M.E., et al. *Analysis of the rutile-ring method of frequency-temperature compensation of a high-Q whispering gallery sapphire resonator*. in *Frequency Control Symposium and Exhibition, 2000. Proceedings of the 2000 IEEE/EIA International*. 2000.
130. Mehl, J., Cooperator, 2010-2011.

131. le Floch, J.-M., et al., *Whispering modes in anisotropic and isotropic dielectric spherical resonators.* Physics Letters A, 2006. **359**(1): p. 1-7.
132. Kishimoto, I., et al., *Development of a Stable Transfer Standard Thermometer. I Evaluation of Vibration Damage on Standard Platinum Resistance Thermometers.* SICE, 2002: p. 1047-1048.
133. Hartnett, J.G., et al. *Exceptionally-enhanced Q-factor sapphire-loaded-cavity TE mode resonators*. in *Frequency Control Symposium and PDA Exhibition, 2002. IEEE International*. 2002.
134. Tobar, M.E., et al., *Distributed Bragg reflector resonators with cylindrical symmetry and extremely high Q-factors.* Ultrasonics, Ferroelectrics and Frequency Control, IEEE Transactions on, 2005. **52**(1): p. 17-26.
135. Flory, C.A. and R.C. Taber. *High performance distributed Bragg reflector microwave resonator*. in *Frequency Control Symposium, 1996. 50th., Proceedings of the 1996 IEEE International*. 1996.
136. Tobar, M.E., et al., *High-Q thermoelectric-stabilized sapphire microwave resonators for low-noise applications.* Ieee Transactions on Ultrasonics Ferroelectrics and Frequency Control, 1994. **41**(3): p. 391-396.

Appendix A

Table A 1 Thermal cycle experiment results of the cylindrical sapphire WGMRT based on sapphire 1

T_{nom} / °C	T_{real} /°C	Std Dev	WGM31 /GHz	Q31	WGM41 /GHz	Q41	WGM51 /GHz	Q51
-40	-39.884	0.001	12.457791	99809	15.246195	141783	18.004292	168837
-30	-29.889	0.001	12.450424	94812	15.236962	129102	17.993218	152236
-20	-19.901	0.001	12.442907	90385	15.227544	116813	17.981923	138364
-10	-9.904	0.001	12.435246	86022	15.217942	107125	17.970413	125284
0	0.0012	0.001	12.427525	78508	15.208271	100869	17.958826	114624
5	5.089	0.001	12.423524	78841	15.203253	99215	17.952805	109764
15	15.093	0.001	12.415570	74365	15.193283	94745	17.940854	100409
25	25.091	0.001	12.407529	68858	15.183198	90798	17.928763	92173
50	50.097	0.002	12.386968	56773	15.157503	78889	17.897963	77689
75	75.117	0.001	12.366037	52602	15.131234	68720	17.866480	66826
85	85.129	0.001	12.357569	47724	15.120585	64868	17.853718	62523
75	75.112	0.001	12.366030	51844	15.131237	68350	17.866485	66314
50	50.092	0.001	12.386972	55709	15.157509	78474	17.897972	77959
25	25.078	0.001	12.407539	65059	15.183210	90257	17.928779	91876
15	15.094	0.001	12.415569	74630	15.193284	93879	17.940854	100542
5	5.082	0.001	12.423529	75791	15.203259	99561	17.952816	109508
0	0.0013	0.001	12.427525	78501	15.208271	100934	17.958825	114622
-10	-9.904	0.001	12.435245	85817	15.217942	108031	17.970412	125907
-20	-19.904	0.001	12.442908	90593	15.227545	115691	17.981925	137757
-30	-29.891	0.001	12.450425	94819	15.236964	128736	17.993219	152470
-40	-39.885	0.001	12.457791	99357	15.246195	142748	18.004292	168827

Table A 2 Thermal cycle experiment results of the cylindrical sapphire WGMRT based on sapphire 2

T_{nom} /°C	T_{real} /°C	Std Dev /°C	WGM32 /GHz	Q32	WGM42 /GHz	Q42	WGM52 /GHz	Q52
-40	-39.954	0.001	12.460047	97236	15.248160	142889	18.006388	172902
-30	-29.993	0.000	12.452709	92313	15.238963	130954	17.995356	155766
-20	-20.041	0.001	12.445220	87382	15.229580	120867	17.984104	141092
-10	-10.067	0.001	12.437577	83158	15.220002	117653	17.972623	127907
0	-0.0009	0.001	12.429738	81304	15.210182	117598	17.960848	116980
5	4.907	0.001	12.425878	82168	15.205340	108738	17.955039	111504
15	14.867	0.001	12.417955	79293	15.195413	102232	17.943141	102109
25	24.834	0.001	12.409930	75071	15.185359	95266	17.931090	93728
50	49.766	0.001	12.389481	65645	15.159747	81062	17.900392	78467
75	74.695	0.002	12.368592	58090	15.133575	67756	17.869028	66777
85	84.648	0.005	12.360137	54807	15.122988	63989	17.856345	62830
75	74.701	0.002	12.368577	57179	15.133568	68687	17.869021	66897
50	49.776	0.001	12.389464	63506	15.159737	84185	17.900383	78780
25	24.849	0.001	12.409912	72319	15.185345	100385	17.931078	93988
15	14.876	0.001	12.417944	76122	15.195406	107600	17.943136	102239
5	4.905	0.001	12.425875	78789	15.205341	113877	17.955044	111606
0	-0.0003	0.001	12.429738	81331	15.210181	117704	17.960847	117006
-10	-10.045	0.001	12.437559	83318	15.219980	117331	17.972598	128092
-20	-20.025	0.001	12.445207	87864	15.229564	120076	17.984087	141250
-30	-29.985	0.001	12.452701	92548	15.238955	130696	17.995346	155909
-40	-39.955	0.001	12.460048	96781	15.248161	143395	18.006390	173025

Table A 3 Thermal cycle experiment results of the cylindrical sapphire WGMRT based on sapphire 2’ (reassembled sapphire 2)

T_{nom} /°C	T_{real} /°C	Std Dev /°C	WGM32’ /GHz	Q32’	WGM42’ /GHz	Q42’	WGM52’ /GHz	Q52’
-30	-29.889	0.001	12.450175	93738	15.238178	78841	/	/
-20	-19.900	0.001	12.442662	87726	15.228766	77852	17.983706	128922
-10	-9.904	0.001	12.435004	81354	15.219167	75716	17.972201	120210
0	-0.008	0.001	12.427296	70514	15.209514	74983	17.960625	110808
5	5.081	0.001	12.423283	70491	15.204486	69348	17.954605	105564
15	15.085	0.001	12.415323	67906	15.194521	67542	17.942655	79758
25	25.084	0.001	12.407271	67542	15.184436	64723	17.930564	89528
50	50.092	0.002	12.386763	61891	15.158745	60385	17.899763	75111
75	75.115	0.001	12.365797	55066	15.132471	55531	17.868271	64758
85	85.129	0.001	12.357304	52464	15.121823	53815	17.855509	61042
75	75.112	0.001	12.365802	55022	15.132475	55833	17.868275	64790
50	50.086	0.001	12.386772	59502	15.158755	61790	17.899772	75690
25	25.077	0.001	12.407278	64987	15.184449	69396	17.930572	90605
15	15.081	0.001	12.415326	65694	15.194531	71529	17.942661	98328
5	5.081	0.001	12.423284	66554	15.204497	78071	17.954607	107091
0	-0.0045	0.001	12.427297	70415	15.209514	75036	17.960625	110380
-10	-9.912	0.001	12.435005	77628	15.219174	77463	17.972211	120865
-20	-19.907	0.001	12.442661	84354	15.228770	80069	17.983712	130412
-30	-29.892	0.001	12.450173	90232	15.238180	81361	/	/
-40	-39.883	0.001	12.457534	97123	15.247408	89880	18.006099	165921

Table A 4 Ice melting point repeatability experiment results based on sapphire 1 of the cylindrical sapphire WGMRT

Number	T /°C	WGM3 /GHz	dT_3 /mK	WGM4 /GHz	dT_4 /mK	WGM5 /GHz	dT_5 /mK
1	0.0012	12.427525	-0.18	15.208271	-0.32	17.958826	-0.37
2	0.0013	12.427525	-0.01	15.208271	-0.26	17.958825	-0.19
3	0.0014	12.427525	0.04	15.208271	-0.21	17.958825	-0.13
4	0.0012	12.427525	0.15	15.208271	-0.10	17.958825	-0.07
5	0.0013	12.427524	0.17	15.208271	-0.11	17.958825	-0.19
6	0.0013	12.427525	-0.01	15.208270	0.03	17.958825	0.01
7	0.0013	12.427525	0.09	15.208270	0.07	17.958825	0.07
8	0.0013	12.427525	0.08	15.208270	0.00	17.958825	0.08
9	0.0014	12.427525	0.08	15.208270	0.02	17.958825	-0.05
10	0.0013	12.427525	0.08	15.208270	0.05	17.958825	0.13
11	0.0017	12.427525	-0.07	15.208270	0.26	17.958825	0.18
12	0.0017	12.427525	-0.08	15.208270	0.18	17.958825	0.18
13	0.0014	12.427525	-0.11	15.208270	0.19	17.958825	0.05
14	0.0016	12.427525	-0.01	15.208270	0.10	17.958825	0.23
15	0.0016	12.427525	-0.03	15.208270	0.10	17.958825	0.08
Std Dev / mK	0.16						

Table A 5 Ice melting point repeatability experiment results based on sapphire 2 of the cylindrical sapphire WGMRT

No.	T /°C	WGM3 /GHz	dT_3 /mK	WGM4 /GHz	dT_4 /mK	WGM5 /GHz	dT_5 /mK
1	-0.0085	12.429743	-4.59	15.210188	-4.37	17.960855	-4.49
2	-0.0076	12.429742	-3.20	15.210187	-3.09	17.960854	-3.07
3	-0.0058	12.429741	-1.73	15.210185	-1.96	17.960852	-1.67
4	-0.0026	12.429740	-0.11	15.210184	-0.92	17.960850	-0.38
5	-0.0019	12.429739	0.61	15.210183	-0.07	17.960849	0.51
6	-0.0009	12.429738	1.59	15.210182	0.92	17.960848	1.45
7	-0.0004	12.429738	2.27	15.210178	5.13	17.960847	2.40
8	-0.0002	12.429738	2.58	15.210181	2.27	17.960847	2.70
9	-0.0004	12.429738	2.58	15.210181	2.08	17.960847	2.55
Std Dev / mK	3.27						

Table A 6 Thermal cycling experiment results of spherical-sapphire-based WGMRT (sapphire 1')

Nominal T/ °C	Real T/°C	Std Dev/°C	$WGM_{1'}$/GHz	$Q_{1'}$
85	85.12807	0.00120	13.536962	52685
75	75.11183	0.00113	13.545950	56295
50	50.08668	0.00184	13.568108	65639
25	25.07822	0.00105	13.589755	76298
15	15.08169	0.00124	13.598243	80872
5	5.08246	0.00104	13.606628	85279
-10	-9.90653	0.00116	13.618950	93118
-20	-19.9014	0.00111	13.627014	98674
-30	-29.88723	0.00075	13.634921	105359
-40	-39.87934	0.00073	13.642666	112168
-30	-29.8846	0.00089	13.634919	105228
-20	-19.8978	0.00107	13.627011	98547
-10	-9.9008	0.00116	13.618944	92357
0	0.09828	0.00158	13.610739	86776
5	5.08969	0.00132	13.606600	84110
15	15.09401	0.00100	13.598211	79105
25	25.09162	0.00108	13.589723	74387
50	50.09684	0.00227	13.568084	63845
75	75.11586	0.00115	13.545940	55555

Table A 7 Thermal cycling experiment results of spherical-sapphire-based WGMRT (sapphire 2)

Nominal T/ °C	Real T/°C	Std Dev/°C	WGM_2/GHz	Q_2
85	85.1294	0.00114	13.536945	56559
75	75.1123	0.00117	13.545933	59149
50	50.0567	0.00187	13.568082	66492
25	25.0788	0.00105	13.589720	75859
15	15.0823	0.00124	13.598205	79580
5	5.0825	0.00117	13.606582	82971
0	0.0861	0.00152	13.610725	83044
-10	-9.9116	0.00110	13.618922	87693
-20	-19.9060	0.00112	13.626978	93380
-30	-29.8912	0.00102	13.634875	99183
-40	-39.8825	0.00114	13.642613	105680
-30	-29.8873	0.00082	13.634867	99487
-20	-19.9000	0.00087	13.626959	93382
-10	-9.9028	0.00130	13.618893	87531
0	0.09546	0.00138	13.610691	82320
5	5.0828	0.00116	13.606590	80295
15	15.0866	0.00098	13.598202	74984
25	25.0852	0.00100	13.589712	73242
50	50.0949	0.00303	13.568069	66645

Table A 8 Thermal cycling experiment results of spherical-sapphire-based WGMRT (sapphire 3)

Nominal T/ °C	Real T/°C	Std Dev/°C	WGM_3/GHz	Q_3
75	75.11314	0.00108	13.546465	55343
50	50.08940	0.00153	13.568619	64065
25	25.08018	0.00105	13.590256	74508
15	15.08310	0.00111	13.598740	79498
5	5.08221	0.00123	13.607121	83867
0	0.09622	0.00128	13.611255	83733
-10	-9.90580	0.00125	13.619455	88873
-20	-19.90281	0.00114	13.627516	93703
-30	-29.88964	0.00110	13.635418	99270
-40	-39.88243	0.00096	13.643158	105404
-30	-29.88695	0.00069	13.635415	99411
-20	-19.89976	0.00100	13.627510	94190
-10	-9.90290	0.00152	13.619447	88768
0	0.09762	0.00172	13.611247	83620
5	5.08770	0.00123	13.607106	82365
15	15.09171	0.00102	13.598724	77983
25	25.08956	0.00100	13.590241	71668
50	50.09625	0.00269	13.568606	61727
75	75.11655	0.00116	13.546463	55149

Table A 9 Thermal cycling experiment results of spherical-sapphire-based WGMRT (sapphire 4)

Nominal T/ °C	Real T/°C	Std Dev/°C	WGM_4/GHz	Q_4
85	85.1282	0.00130	13.538023	52922
75	75.1123	0.00112	13.547014	55746
50	50.08666	0.00218	13.569174	63813
25	25.07912	0.00103	13.590817	73325
15	15.08298	0.00103	13.599304	77278
5	5.08247	0.00124	13.607688	81034
0	0.08593	0.00216	13.611830	80000
-10	-9.91189	0.00113	13.620033	84145
-20	-19.90704	0.00125	13.628095	89009
-30	-29.89177	0.00052	13.636000	93911
-40	-39.8837	0.00065	13.643742	99252
-30	-29.88811	0.00070	13.635995	93767
-20	-19.89980	0.00079	13.628087	88552
-10	-9.90322	0.00104	13.620016	83424
0	0.09620	0.00130	13.611819	79473
5	5.08272	0.00107	13.607671	79396
15	15.08642	0.00101	13.599281	67483
25	25.0843	0.00102	13.590800	72316
50	50.09304	0.00294	13.569159	62691

Table A 10 Fractional frequency temperature sensitivity for spherical-sapphire-based WGM resonator thermometer

Real T/℃	((Δf/ΔT)/f)/ (ppm/K)
-39.88386	-56
-29.88818	-57
-19.89965	-59
-9.90244	-60
0.00154	-61
5.09074	-61
15.09538	-62
25.09465	-63
50.10045	-65
75.11768	-66
85.12865	-67
75.11186	-66
50.08646	-65
25.08480	-63
15.08684	-62
5.08554	-61
0.00190	-61
-9.91082	-60
-19.90646	-59
-29.89110	-57
-39.88496	-56

Table A 11 Ice melting point repeatability experiment data for spherical-sapphire-based WGM resonator thermometer in three days (sapphire 1)

Time	Real T/℃	Std Dev/℃	f_{exp}/GHz	Q_{exp}	dT/mK
24/10/2011 11.15	0.00190	0.00098	13.6118452	82073	0.09
24/10/2011 13.24	0.00148	0.00102	13.6118453	82298	-0.09
24/10/2011 15.23	0.00134	0.00089	13.6118456	82560	-0.42
24/10/2011 17.10	0.00141	0.00099	13.6118456	82546	-0.38
25/10/2011 10.25	0.00154	0.00091	13.6118453	82481	-0.08
25/10/2011 11.42	0.00145	0.00093	13.6118453	82482	-0.09
25/10/2011 15.27	0.00151	0.00097	13.6118454	82498	-0.12
25/10/2011 17.10	0.00146	0.00094	13.6118453	82461	-0.08
25/10/2011 18.30	0.00142	0.00096	13.6118453	82422	-0.02
26/10/2011 10.22	0.00151	0.00095	13.6118451	82498	0.14
26/10/2011 12.30	0.00141	0.00097	13.6118450	82466	0.29
26/10/2011 14.53	0.00149	0.00095	13.6118451	82449	0.19
26/10/2011 16.32	0.00155	0.00091	13.6118450	82456	0.29
26/10/2011 17.53	0.00150	0.00099	13.6118450	82443	0.28

Table A 12 Ice melting point repeatability experiment data for spherical-sapphire-based WGM resonator thermometer in three days (sapphire 4)

Time	Real T/℃	Std Dev/℃	f_{exp}/GHz	Q_{exp}	dT/mK
18/01/2012 12.32	-0.00524	0.00100	13.611904	80002	-2.64
18/01/2012 14.18	-0.00345	0.00091	13.611904	80010	-2.35
18/01/2012 15.50	-0.00299	0.00099	13.611903	79996	-2.04
18/01/2012 17.22	-0.00333	0.00109	13.611903	80007	-1.95
18/01/2012 18.18	-0.00379	0.00091	13.611903	80016	-2.05
19/01/2012 11.42	-0.00106	0.00096	13.611902	79995	-0.15
19/01/2012 13.37	-0.00177	0.00098	13.611902	80009	0.26
19/01/2012 15.04	-0.00174	0.00095	13.611902	80023	0.26
19/01/2012 16.13	-0.00175	0.00089	13.611901	80008	0.31
19/01/2012 17.33	-0.00170	0.00101	13.611902	80011	0.24
19/01/2012 18.16	-0.00176	0.00093	13.611902	79995	0.20
20/01/2012 11.32	0.00083	0.00098	13.611901	79995	0.96
20/01/2012 13.56	0.00053	0.00094	13.611900	79993	1.62
20/01/2012 15.19	0.00028	0.00100	13.611900	79988	1.79
20/01/2012 16.13	0.00005	0.00106	13.611900	80047	1.80
20/01/2012 17.12	-0.00001	0.00092	13.611900	79952	1.83
20/01/2012 18.06	-0.00012	0.00090	13.611900	79967	1.92

Table A 13 Experiment data of unpolished empty cavity

$f_{exp\text{-}no\ polishing}$/GHz	$Q_{exp\text{-}no\ polishing}$	Mode	f_{cal}/GHz	Q_{cal}	Δf/f	Q_{exp}/Q_{cal}
12.702600	3265	5	12.737944	12678	-0.28%	0.258
13.179500	1813	6	13.230133	10988	-0.38%	0.165
14.548800	1447	9	14.607539	11530	-0.40%	0.126
16.538350	397	10	16.568093	10135	-0.18%	0.039
16.587196	1260	11	16.568317	10140	0.11%	0.124

Table A 14 Experiment data of polished empty cavity

$f_{exp\text{-}polished}$/GH	$Q_{exp\text{-}\ polished}$	Mode	f_{cal}/GHz	Q_{cal}	Δf/f	Q_{exp}/Q_{cal}
12.714360	8856	5	12.737944	12678	-0.19%	0.699
13.203740	8128	6	13.230133	10988	-0.20%	0.740
14.584530	6420	9	14.607539	11530	-0.16%	0.557
16.633415	8831	12	16.568093	10135	-0.11%	0.719
19.139600	8253	17	16.568317	10140	-0.06%	0.629

Table A 15 Comparisons of calculation with experiments of cavity with steel screws

new cavity-flush-90 sapphire-45 plane-steel						
f_{exp}/GHz	Q_{exp}	Mode	f_{cal}/GHz	Q_{cal}	Δf / f	Q_{exp} / Q_{cal}
6.908515	9777	1	6.854953	22634	0.78%	0.432
8.689940	9351	4	8.556413	24242	1.56%	0.386
9.480650	13097	5	9.435375	21525	0.48%	0.608
9.606250	12409	6	9.562123	20683	0.46%	0.600
10.339615	17573	7	10.298477	30082	0.40%	0.584
10.535300	16455	8	10.491155	28893	0.42%	0.570
11.183830	28501	9	11.121059	64821	0.56%	0.440
11.572705	8577	11	11.400001	20777	1.51%	0.413
12.290940	12974	15	12.219093	40827	0.59%	0.318
12.318210	12102	16	12.240126	45611	0.64%	0.265
12.378790	35936	17	12.286837	78051	0.75%	0.460
13.394430	7949	22	13.263249	16412	0.99%	0.484
13.580810	14779	24	13.444917	62793	1.01%	0.235
13.682060	12659	25	13.594677	30937	0.64%	0.409
14.533460	38612	28	14.357122	163049	1.23%	0.237
14.755750	48977	29	14.553659	319388	1.39%	0.153
15.258700	7361	31	15.187942	16316	0.47%	0.451
15.661940	39249	32	15.438337	272301	1.45%	0.144

Table A 16 Comparisons of calculation with experiments of cavity with nylon screws

new cavity-flush-90 sapphire-45 plane-nylon						
f_{exp}/GHz	Q_{exp}	Mode	f_{cal}/GHz	Q_{cal}	$\Delta f / f$	Q_{exp} / Q_{cal}
6.905210	14176	1	6.854953	22634	0.73%	0.626
8.692760	9038	4	8.556413	24242	1.59%	0.373
9.480720	13464	5	9.435375	21525	0.48%	0.626
9.606160	12971	6	9.562123	20683	0.46%	0.627
10.340020	18221	7	10.298477	30082	0.40%	0.606
10.535120	16830	8	10.491155	28893	0.42%	0.583
11.183840	28636	9	11.121059	64821	0.56%	0.442
11.567660	10132	11	11.400001	20777	1.47%	0.488
12.283940	16622	15	12.219093	40827	0.53%	0.407
12.311530	15490	16	12.240126	45611	0.58%	0.340
12.378480	39027	17	12.286837	78051	0.75%	0.500
13.396200	7919	22	13.263249	16412	1.00%	0.483
13.583850	16307	24	13.444917	62793	1.03%	0.260
13.682630	12237	25	13.594677	30937	0.65%	0.396
14.533520	39338	28	14.357122	163049	1.23%	0.241
14.755870	50299	29	14.553659	319388	1.39%	0.157
15.256200	7776	31	15.187942	16316	0.45%	0.477
15.661760	39620	32	15.438337	272301	1.45%	0.146

Table A 17 Comparisons of calculation with experiments of cavity with aluminum screws

new cavity-flush-90 sapphire-45 plane-aluminum						
f_{exp}/GHz	Q_{exp}	Mode	f_{cal}/GHz	Q_{cal}	$\Delta f / f$	Q_{exp} / Q_{cal}
6.908522	13565	1	6.854953	22634	0.78%	0.599
8.691660	9693	4	8.556413	24242	1.58%	0.400
9.481220	13481	5	9.435375	21525	0.49%	0.626
9.606620	12980	6	9.562123	20683	0.47%	0.628
10.340380	18574	7	10.298477	30082	0.41%	0.617
10.535680	18247	8	10.491155	28893	0.42%	0.632
11.184080	29057	9	11.121059	64821	0.57%	0.448
11.572500	9973	11	11.400001	20777	1.51%	0.480
12.290370	16307	15	12.219093	40827	0.58%	0.399
12.318000	15463	16	12.240126	45611	0.64%	0.339
12.378740	38658	17	12.286837	78051	0.75%	0.495
13.395650	8126	24	13.263249	16412	-0.37%	0.129
13.582700	17784	25	13.444917	62793	-0.09%	0.575
13.683060	13242	27	13.594677	30937	-0.26%	0.298
14.533620	39588	28	14.357122	163049	1.23%	0.243
14.755930	50198	29	14.553659	319388	1.39%	0.157
15.259100	7749	31	15.187942	16316	0.47%	0.475
15.661990	40841	32	15.438337	272301	1.45%	0.150
15.829640	47790	33	15.592459	251709	1.52%	0.190

Table A 18 Comparisons of calculation with experiments of cavity with brass screws

new cavity-flush-90 sapphire-45 plane-brass						
f_{exp}/GHz	Q_{exp}	Mode	f_{cal}/GHz	Q_{cal}	$\Delta f / f$	Q_{exp} / Q_{cal}
6.910920	11936	1	6.854953	22634	0.82%	0.527
8.684400	9285	4	8.556413	24242	1.50%	0.383
9.481200	13332	5	9.435375	21525	0.49%	0.619
9.606440	12863	6	9.562123	20683	0.46%	0.622
10.339555	17775	7	10.298477	30082	0.40%	0.591
10.533970	16329	8	10.491155	28893	0.41%	0.565
11.184000	29191	9	11.121059	64821	0.57%	0.450
11.575420	8587	11	11.400001	20777	1.54%	0.413
12.294150	12998	15	12.219093	40827	0.61%	0.318
12.322600	10921	16	12.240126	45611	0.67%	0.239
12.377720	31838	17	12.286837	78051	0.74%	0.408
13.388600	7551	22	13.263249	16412	0.95%	0.460
13.577600	14400	24	13.444917	62793	0.99%	0.229
13.672550	11430	25	13.594677	30937	0.57%	0.369
14.532990	39488	28	14.357122	163049	1.22%	0.242
14.756030	50003	29	14.553659	319388	1.39%	0.157
15.260100	7669	31	15.187942	16316	0.48%	0.470
15.662110	39286	32	15.438337	272301	1.45%	0.144
15.829600	46444	33	15.592459	251709	1.52%	0.185

Table A 19 Comparisons between calculation and experiments of cavity with holes

new cavity-flush-90 sapphire-45 plane-with holes						
f_{exp}/GHz	Q_{exp}	Mode	f_{cal}/GHz	Q_{cal}	$\Delta f / f$	Q_{exp} / Q_{cal}
6.908522	13565	1	6.854953	22634	0.78%	0.60
8.691660	9693	4	8.556413	24242	1.58%	0.40
9.481220	13481	5	9.435375	21525	0.49%	0.63
9.606620	12980	6	9.562123	20683	0.47%	0.63
10.340380	18574	7	10.298477	30082	0.41%	0.62
11.184080	29057	9	11.121059	64821	0.57%	0.45
11.572500	9973	11	11.400001	20777	1.51%	0.48
12.290370	16307	15	12.219093	40827	0.58%	0.40
12.318000	15463	16	12.240126	45611	0.64%	0.34
13.395650	8126	24	13.444917	62793	-0.37%	0.13
13.582700	17784	25	13.594677	30937	-0.09%	0.57
14.755930	50198	29	14.553659	319388	1.39%	0.16

Table A 20 Comparisons between calculation and experiments of cavity without holes

new cavity-flush-90 sapphire-45 plane-without holes						
f_{exp}/GHz	Q_{exp}	Mode	f_{cal}/GHz	Q_{cal}	$\Delta f / f$	Q_{exp} / Q_{cal}
6.904280	14644	1	6.855774	22640	0.71%	0.65
8.686770	10014	4	8.558162	24250	1.50%	0.41
9.479260	13636	5	9.436183	21544	0.46%	0.63
9.605200	12950	6	9.563010	20703	0.44%	0.63
10.338860	18440	7	10.299313	30088	0.38%	0.61
11.182510	28976	9	11.121551	64789	0.55%	0.45
11.568860	11011	11	11.402191	20822	1.46%	0.53
12.284880	17911	15	12.218625	41103	0.54%	0.44
12.312430	16660	16	12.239870	45947	0.59%	0.36
13.413280	25261	24	13.444415	63513	-0.23%	0.40
13.576900	19337	25	13.595455	31092	-0.14%	0.62
14.532380	38442	29	14.550967	321303	-0.13%	0.12

Table A 21 Experimental data per old cylinder cavity

Old cavity-flush-90 sapphire-45 plane-aluminum-three holes drilled						
f_{exp}/GHz	Q_{exp}	Mode	f_{cal}/GHz	Q_{cal}	$\Delta f / f$	Q_{exp} / Q_{cal}
6.897981	12310	1	6.854953	22634	0.63%	0.54
8.679680	9617	4	8.556413	24242	1.44%	0.40
9.475710	13673	5	9.435375	21525	0.43%	0.64
9.602150	12802	6	9.562123	20683	0.42%	0.62
10.339390	18952	7	10.298477	30082	0.40%	0.63
10.536420	17096	8	10.491155	28893	0.43%	0.59
11.555130	9975	11	11.400001	20777	1.36%	0.48
12.277840	16614	15	12.219093	40827	0.48%	0.41
12.296890	16015	16	12.240126	45611	0.46%	0.35
12.383090	36351	17	12.286837	78051	0.78%	0.47
13.390410	9284	22	13.263249	16412	0.96%	0.57
13.414010	23728	24	13.444917	62793	-0.23%	0.38
13.574690	18770	25	13.594677	30937	-0.15%	0.61
13.678800	14258	27	13.718765	44434	-0.29%	0.32

Table A 22 Experimental data per new cylinder cavity whose holes are drilled by turning 30°

New cavity-flush-90 sapphire-45 plane-aluminum-holes were turned by 30°						
f_{exp}/GHz	Q_{exp}	Mode	f_{cal}/GHz	Q_{cal}	$\Delta f / f$	Q_{exp} / Q_{cal}
6.908522	13565	1	6.854953	22634	0.78%	0.60
8.691660	9693	4	8.556413	24242	1.58%	0.40
9.481220	13481	5	9.435375	21525	0.49%	0.63
9.606620	12980	6	9.562123	20683	0.47%	0.63
10.340380	18574	7	10.298477	30082	0.41%	0.62
10.535680	18247	8	10.491155	28893	0.42%	0.63
11.184080	29057	9	11.121059	64821	0.57%	0.45
11.572500	9973	11	11.400001	20777	1.51%	0.48
12.290370	16307	15	12.219093	40827	0.58%	0.40
12.318000	15463	16	12.240126	45611	0.64%	0.34
12.378740	38658	17	12.286837	78051	0.75%	0.50
13.395650	8126	24	13.444917	62793	-0.37%	0.13
13.582700	17784	25	13.594677	30937	-0.09%	0.57
13.683060	13242	27	13.718765	44434	-0.26%	0.30
14.533620	39588	28	14.357122	163049	1.23%	0.24
14.755930	50198	29	14.553659	319388	1.39%	0.16
15.259100	7749	31	15.187942	16316	0.47%	0.47
15.661990	40841	32	15.438337	272301	1.45%	0.15
15.829640	47790	33	15.592459	251709	1.52%	0.19

Table A 23 Comparisons between calculation and experiment when the Teflon has holes

New cavity-flush-90 sapphire-45 plane-aluminum-teflon with 3 holes						
f_{exp}/GHz	Q_{exp}	Mode	f_{cal}/GHz	Q_{cal}	$\Delta f / f$	Q_{exp} / Q_{cal}
6.913980	13547	1	6.854953	22634	0.86%	0.60
8.731490	9993	4	8.556413	24242	2.05%	0.41
9.497260	13674	5	9.435375	21525	0.66%	0.64
9.622140	13305	6	9.562123	20683	0.63%	0.64
10.351720	18534	7	10.298477	30082	0.52%	0.62
10.549440	17842	8	10.491155	28893	0.56%	0.62
11.193530	29134	9	11.121059	64821	0.65%	0.45
11.598200	9997	11	11.400001	20777	1.74%	0.48
12.317160	16979	15	12.219093	40827	0.80%	0.42
12.343140	16465	16	12.240126	45611	0.84%	0.36
13.623200	17464	24	13.444917	62793	1.33%	0.28
13.740300	12775	25	13.594677	30937	1.07%	0.41
14.537860	38993	28	14.357122	163049	1.26%	0.24
14.757730	50014	29	14.553659	319388	1.40%	0.16
15.299000	7377	31	15.187942	16316	0.73%	0.45
15.663760	40591	32	15.438337	272301	1.46%	0.15

Table A 24 Comparisons between calculation and experiment when the Teflon hasn't holes

New cavity-flush-90 sapphire-45 plane-aluminum-teflon without holes						
f_{exp}/GHz	Q_{exp}	Mode	f_{cal}/GHz	Q_{cal}	$\Delta f / f$	Q_{exp} / Q_{cal}
6.908522	13565	1	6.854953	22634	0.78%	0.60
8.691660	9693	4	8.556413	24242	1.58%	0.40
9.481220	13481	5	9.435375	21525	0.49%	0.63
9.606620	12980	6	9.562123	20683	0.47%	0.63
10.340380	18574	7	10.298477	30082	0.41%	0.62
10.535680	18247	8	10.491155	28893	0.42%	0.63
11.184080	29057	9	11.121059	64821	0.57%	0.45
11.572500	9973	11	11.400001	20777	1.51%	0.48
12.290370	16307	15	12.219093	40827	0.58%	0.40
12.318000	15463	16	12.240126	45611	0.64%	0.34
13.395650	8126	24	13.444917	62793	-0.37%	0.13
13.582700	17784	25	13.594677	30937	-0.09%	0.57
14.533620	39588	28	14.357122	163049	1.23%	0.24
14.755930	50198	29	14.553659	319388	1.39%	0.16
15.259100	7749	31	15.187942	16316	0.47%	0.47
15.661990	40841	32	15.438337	272301	1.45%	0.15

Table A 25 Experimental results when the displacement between antenna to sapphire is 5.9055 mm

Experiments-45° plane-14-metal-5.9055 mm								
f_{exp}/GHz	Q_{exp}	Mode	f_{cal}/GHz	Q_{cal}	Q_{exp} / Q_{cal}	f_1/f_{cal}	ds1/mm	$ds1^2/mm^2$
6.912350	9007	1	6.854953	22634	0.40	1.008373	0	0
8.738680	8541	4	8.556413	24242	0.35	1.021302	0	0
9.489150	12387	5	9.435375	21525	0.58	1.005699	0	0
9.636820	12291	6	9.562123	20683	0.59	1.007812	0	0
10.342360	15048	7	10.298477	30082	0.50	1.004261	0	0
11.187890	22145	9	11.121059	64821	0.34	1.006009	0	0
11.520470	21753	11	11.400001	20777	1.05	1.010567	0	0
11.600500	5151	12	11.428924	65426	0.08	1.015012	0	0
12.301038	11927	16	12.240126	45611	0.26	1.004976	0	0

Table A 26 Experimental results when the displacement between antenna to sapphire is 5.3975 mm

Experiments-45° plane-14-metal-5.3975 mm							
f_{exp}/GHz	Q_{exp}	f_{cal}/GHz	Q_{cal}	Q_{exp} /	f_1/f_{cal}	ds1/mm	$ds1^2/mm^2$
6.911660	9473	6.854953	22634	0.42	1.008272	-0.02	0.0004
8.736450	8445	8.556413	24242	0.35	1.021041	-0.02	0.0004
9.489030	12448	9.435375	21525	0.58	1.005687	-0.02	0.0004
9.636100	12072	9.562123	20683	0.58	1.007736	-0.02	0.0004
10.343000	15277	10.298477	30082	0.51	1.004323	-0.02	0.0004
11.188650	22449	11.121059	64821	0.35	1.006078	-0.02	0.0004
11.520040	20297	11.400001	20777	0.98	1.010530	-0.02	0.0004
11.593090	5010	11.428924	65426	0.08	1.014364	-0.02	0.0004
12.304440	12707	12.219093	40827	0.31	1.006985	-0.02	0.0004
12.346450	15801	12.240126	45611	0.35	1.008687	-0.02	0.0004

Table A 27 Experimental results when the displacement between antenna to sapphire is 4.2418 mm

Experiments-45° plane-14-metal-4.2418mm							
f_{exp}/GHz	Q_{exp}	f_{cal}/GHz	Q_{cal}	Q_{exp} / Q_{cal}	f1/f_{cal}	ds1/mm	$ds1^2/mm^2$
6.894740	9057	6.854953	22634	0.40	1.005804	-0.0655	0.0043
8.743560	8179	8.556413	24242	0.34	1.021872	-0.0655	0.0043
9.493310	12427	9.435375	21525	0.58	1.006140	-0.0655	0.0043
9.641360	12247	9.562123	20683	0.59	1.008287	-0.0655	0.0043
10.357670	15478	10.298477	30082	0.51	1.005748	-0.0655	0.0043
11.208680	22971	11.121059	64821	0.35	1.007879	-0.0655	0.0043
11.506760	6046	11.400001	20777	0.29	1.009365	-0.0655	0.0043
11.547820	14509	11.428924	65426	0.22	1.010403	-0.0655	0.0043
11.944910	29112	11.864948	151667	0.19	1.006739	-0.0655	0.0043
12.287800	16995	12.219093	40827	0.42	1.005623	-0.0655	0.0043
12.336280	13433	12.240126	45611	0.29	1.007856	-0.0655	0.0043
12.486400	18891	12.286837	78051	0.24	1.016242	-0.0655	0.0043

Table A 28 Experimental results when the displacement between antenna to sapphire is 3.5433 mm

Experiments-45° plane-14-metal-3.5433mm							
f_{exp}/GHz	Q_{exp}	f_{cal}/GHz	Q_{cal}	Q_{exp} / Q_{cal}	f1/f_{cal}	ds1/mm	$ds1^2/mm^2$
6.874580	9507	6.854953	22634	0.42	1.002863	-0.0930	0.0086
8.750520	8039	8.556413	24242	0.33	1.022686	-0.0930	0.0086
9.497660	12606	9.435375	21525	0.59	1.006601	-0.0930	0.0086
9.646780	12104	9.562123	20683	0.59	1.008853	-0.0930	0.0086
10.373300	15671	10.298477	30082	0.52	1.007265	-0.0930	0.0086
10.596500	14386	10.491155	28893	0.50	1.010041	-0.0930	0.0086
11.230950	22654	11.121059	64821	0.35	1.009881	-0.0930	0.0086
11.425900	11629	11.400001	20777	0.56	1.002272	-0.0930	0.0086
11.429980	5700	11.428924	65426	0.09	1.000092	-0.0930	0.0086
11.941380	25204	11.864948	151667	0.17	1.006442	-0.0930	0.0086
12.259820	17069	12.219093	40827	0.42	1.003333	-0.0930	0.0086
12.365240	13728	12.240126	45611	0.30	1.010222	-0.0930	0.0086
12.874000	20346	12.828263	10679	1.91	1.003565	-0.0930	0.0086

Table A 29 Experimental results when the displacement between antenna to sapphire is 2.7178 mm

Experiments-45° plane-14-metal-2.7178mm							
f_{exp}/GHz	Q_{exp}	f_{cal}/GHz	Q_{cal}	Q_{exp} / Q_{cal}	f_1/f_{cal}	ds1/mm	$ds1^2/mm^2$
6.835880	8956	6.854953	22634	0.40	0.997218	-0.1255	0.0158
8.755340	7647	8.556413	24242	0.32	1.023249	-0.1255	0.0158
9.503960	12761	9.435375	21525	0.59	1.007269	-0.1255	0.0158
9.655220	12205	9.562123	20683	0.59	1.009736	-0.1255	0.0158
10.396880	16207	10.298477	30082	0.54	1.009555	-0.1255	0.0158
10.626220	14224	10.491155	28893	0.49	1.012874	-0.1255	0.0158
11.266150	23121	11.121059	64821	0.36	1.013047	-0.1255	0.0158
11.313050	5183	11.400001	20777	0.25	0.992373	-0.1255	0.0158
11.945930	23014	11.864948	151667	0.15	1.006825	-0.1255	0.0158
12.236300	16042	12.219093	40827	0.39	1.001408	-0.1255	0.0158
12.401520	13729	12.240126	45611	0.30	1.013186	-0.1255	0.0158
12.890540	23530	12.828263	10679	2.20	1.004855	-0.1255	0.0158
12.858611	37851	12.842157	11407	3.32	1.001281	-0.1255	0.0158

Table A 30 Experimental results when the displacement between antenna to sapphire is 1.9812 mm

Experiments-45° plane-14-metal-1.9812mm							
f_{exp} /GHz	Q_{exp}	f_{cal} /GHz	Q_{cal}	Q_{exp} / Q_{cal}	f_1/f_{cal}	ds1 /mm	ds12 $/mm^2$
6.781960	8766	6.854953	22634	0.39	0.989352	-0.1545	0.0239
7.530400	3524	7.440836	11358	0.31	1.012037	-0.1545	0.0239
8.747400	6956	8.556413	24242	0.29	1.022321	-0.1545	0.0239
9.509440	12549	9.435375	21525	0.58	1.007850	-0.1545	0.0239
9.662560	11983	9.562123	20683	0.58	1.010504	-0.1545	0.0239
10.420000	15883	10.298477	30082	0.53	1.011800	-0.1545	0.0239
10.655780	14169	10.491155	28893	0.49	1.015692	-0.1545	0.0239
11.194850	4435	11.121059	64821	0.07	1.006635	-0.1545	0.0239
11.304480	21553	11.400001	20777	1.04	0.991621	-0.1545	0.0239
11.960800	19312	11.864948	151667	0.13	1.008079	-0.1545	0.0239
12.222940	15799	12.219093	40827	0.39	1.000315	-0.1545	0.0239
12.431620	14957	12.240126	45611	0.33	1.015645	-0.1545	0.0239
12.890500	30101	12.828263	10679	2.82	1.004852	-0.1545	0.0239

Table A 31 Calculation results for birefringence thermometer

f /GHz	Q	$R_{E.s}$	$R_{H,s}$	$R_{E.sdisk}$	$R_{H,sdisk}$
6.935025	8297	77.68%	33.00%	66.17%	17.86%
7.387147	8779	75.58%	32.78%	62.09%	17.51%
7.444222	12028	70.49%	36.03%	8.77%	17.66%
9.106225	16027	73.25%	27.78%	18.21%	2.51%
10.249506	11383	91.92%	53.45%	77.61%	32.16%
10.466183	17766	52.08%	51.41%	9.34%	15.29%
10.694466	16716	51.07%	48.56%	7.94%	13.27%
10.703770	8047	86.89%	34.52%	83.64%	30.35%
11.010445	11089	90.82%	51.67%	74.47%	30.69%
11.044570	15713	42.15%	43.26%	2.74%	0.71%
11.294872	15448	43.24%	41.68%	3.13%	0.74%
11.625620	31054	66.89%	61.70%	4.25%	7.97%
11.981635	33022	70.39%	62.18%	3.83%	7.67%
12.127791	44870	80.61%	68.22%	5.72%	2.03%
12.243104	12370	33.48%	39.52%	6.51%	16.30%
12.476704	13979	73.15%	62.12%	26.21%	28.38%
12.540225	35982	81.51%	67.20%	7.11%	3.82%
12.646774	14547	64.94%	58.25%	14.80%	23.89%
12.763745	12230	91.66%	56.74%	68.27%	34.62%
12.925643	50996	93.57%	83.92%	0.42%	1.52%
12.975412	7710	91.29%	42.80%	88.57%	39.89%
13.100502	50278	93.86%	80.70%	4.55%	1.80%
13.130088	14238	79.94%	60.28%	30.73%	18.50%
13.372641	13051	83.60%	54.40%	52.99%	26.95%
13.635946	29342	86.20%	71.82%	19.10%	14.61%
13.861349	17327	41.57%	34.61%	13.24%	4.38%
13.892002	16533	88.30%	59.95%	54.97%	28.19%
13.914718	96704	89.07%	81.72%	8.83%	4.01%
14.207971	91337	94.35%	81.48%	2.24%	4.93%
14.353004	23845	76.09%	48.22%	16.86%	6.89%
14.416930	22299	73.21%	45.57%	16.22%	6.51%
14.447995	27709	95.57%	69.08%	34.01%	18.34%
14.693535	103847	90.37%	82.17%	9.75%	4.31%
14.821167	183307	92.10%	86.31%	4.35%	8.85%
14.875606	10243	93.92%	58.45%	72.30%	38.96%
14.953252	7456	92.72%	49.40%	91.67%	48.03%
15.231151	11345	94.44%	60.77%	69.74%	38.67%
15.610490	7688	56.57%	58.20%	43.26%	41.83%
15.725590	73268	88.39%	83.22%	5.03%	10.46%
15.777647	8824	74.20%	58.15%	65.07%	46.38%
15.933792	13722	91.51%	64.61%	61.90%	39.56%
15.998268	56622	88.83%	82.94%	10.20%	5.84%
16.048083	75392	95.28%	78.35%	11.44%	11.17%
16.261001	9868	49.77%	50.49%	16.61%	22.60%
16.406485	9153	45.87%	46.61%	14.52%	21.95%
16.797935	7847	93.63%	56.15%	91.50%	53.75%
16.826385	7400	93.69%	54.65%	92.92%	53.80%
16.958808	62804	92.45%	78.38%	18.61%	16.29%

Appendix B

Unit: mm

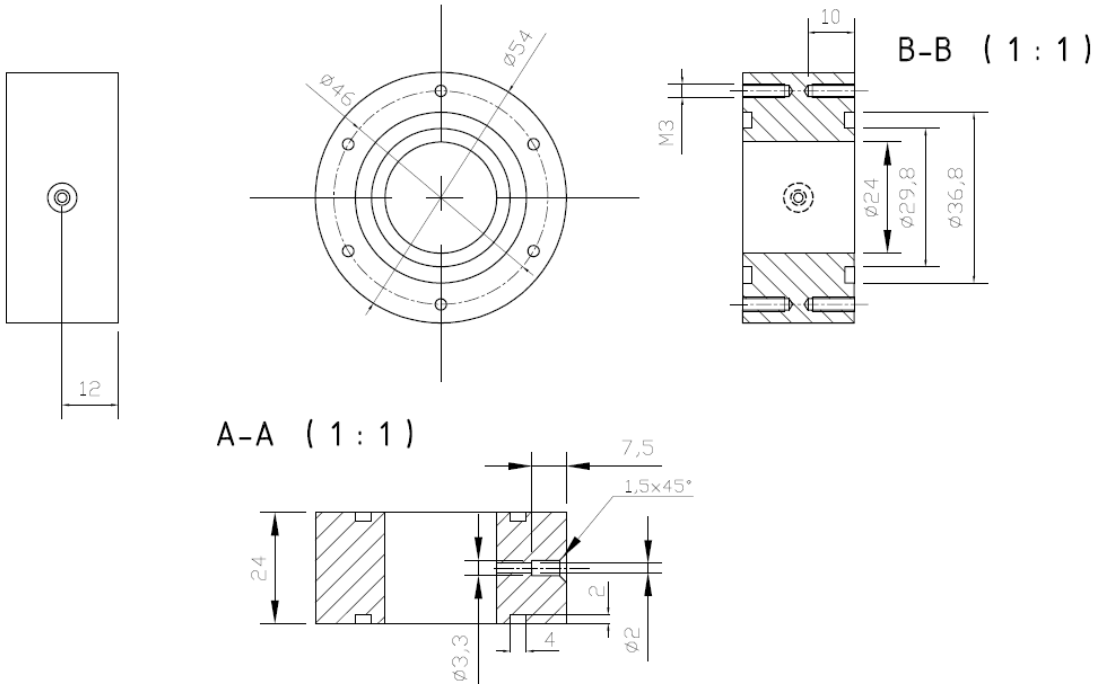

Figure B 1 Cavity body

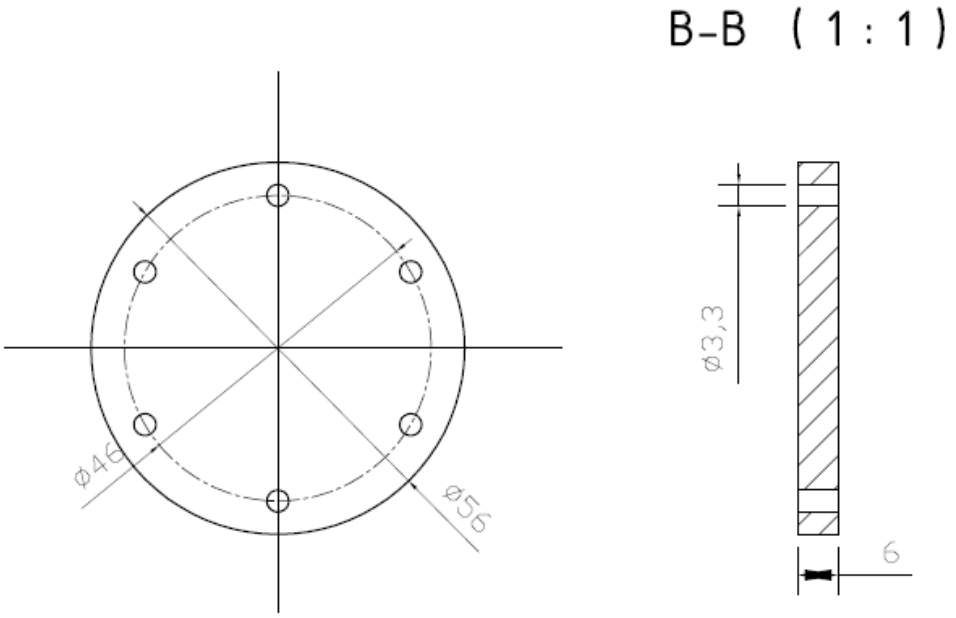

Figure B 2 Lower cap

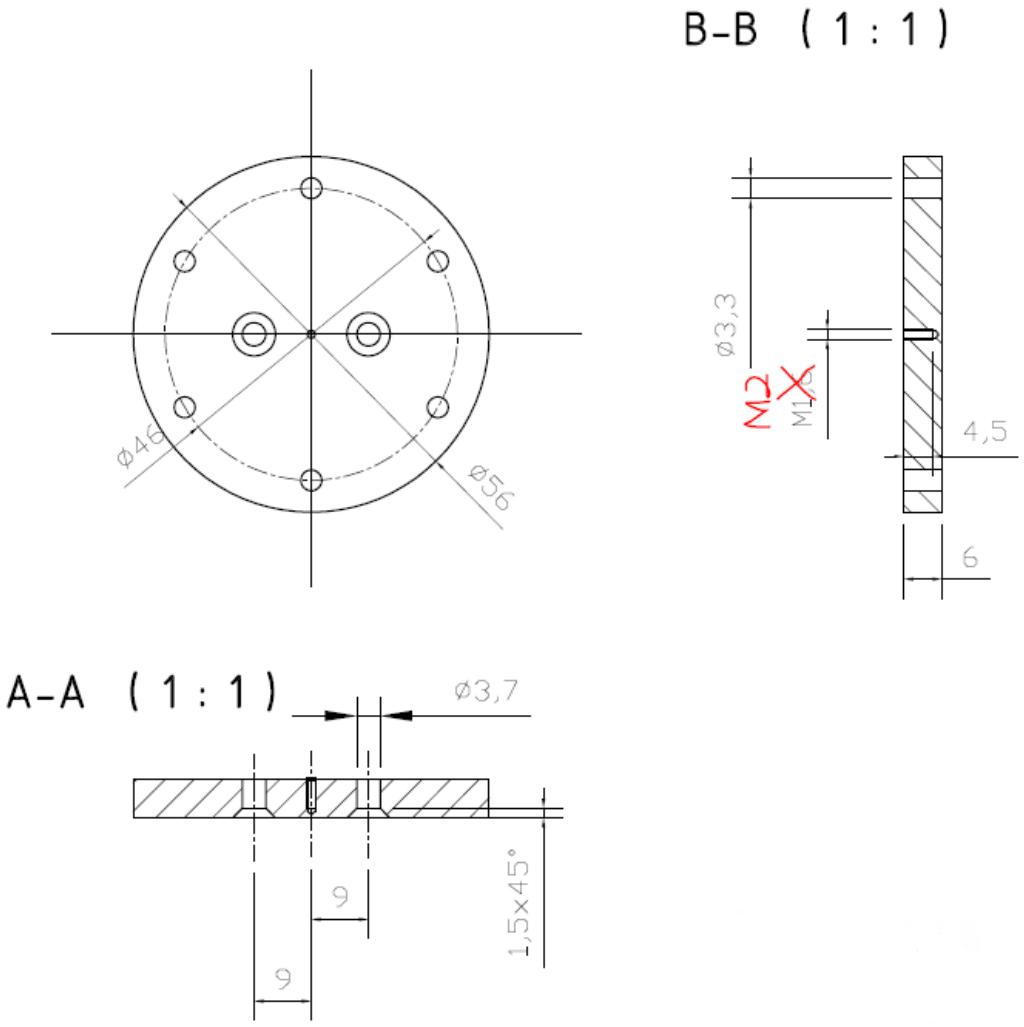

Figure B 3 Top cap

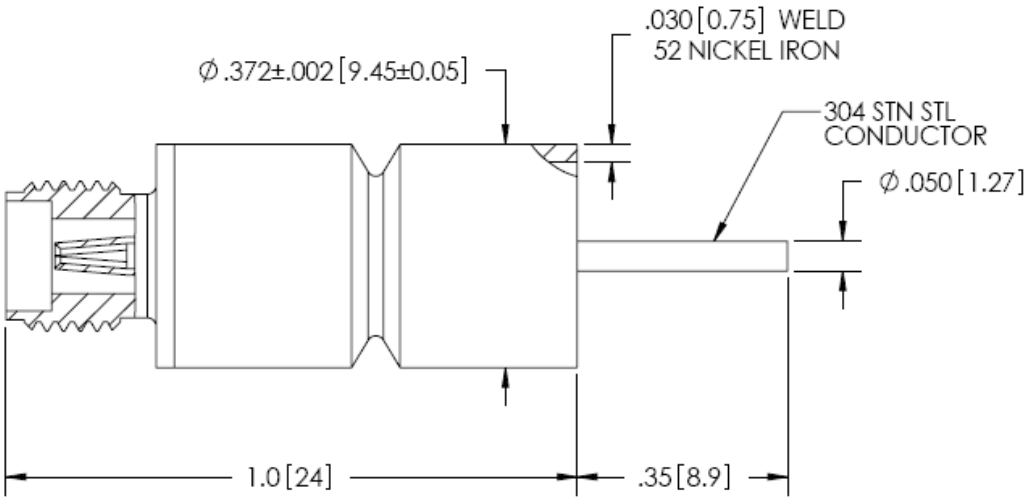

Figure B 4 SMA connector drawing view (Unit: inch)

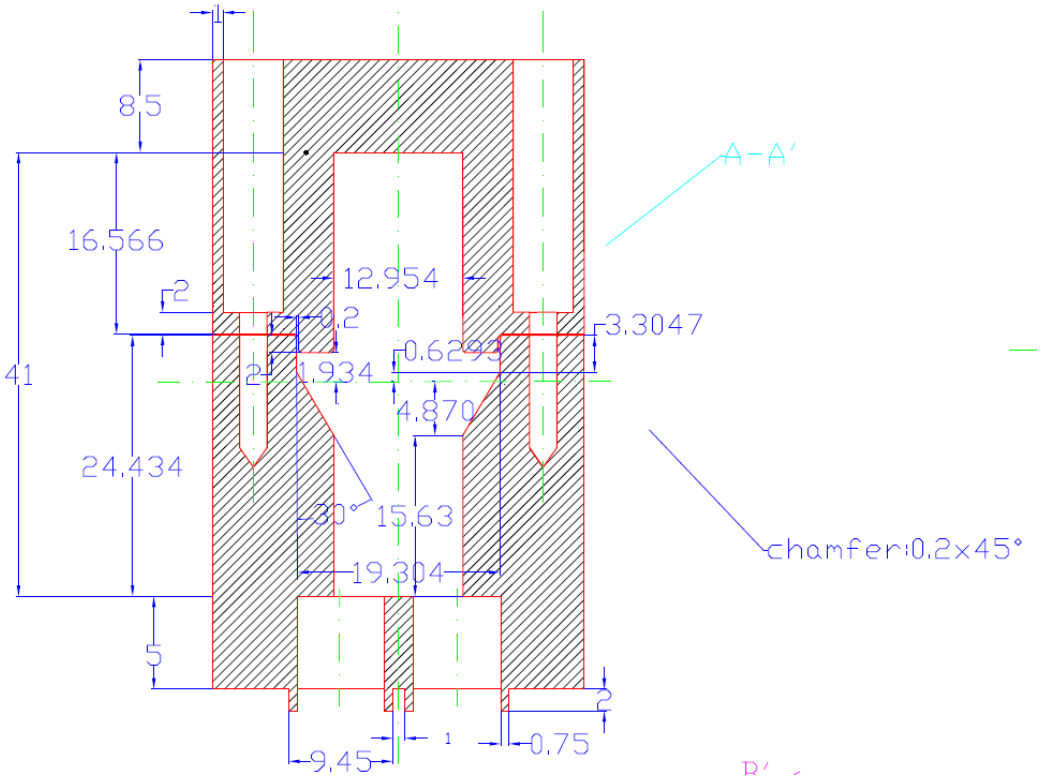

Figure B 5 Cut plane 1 of the cavity body front view

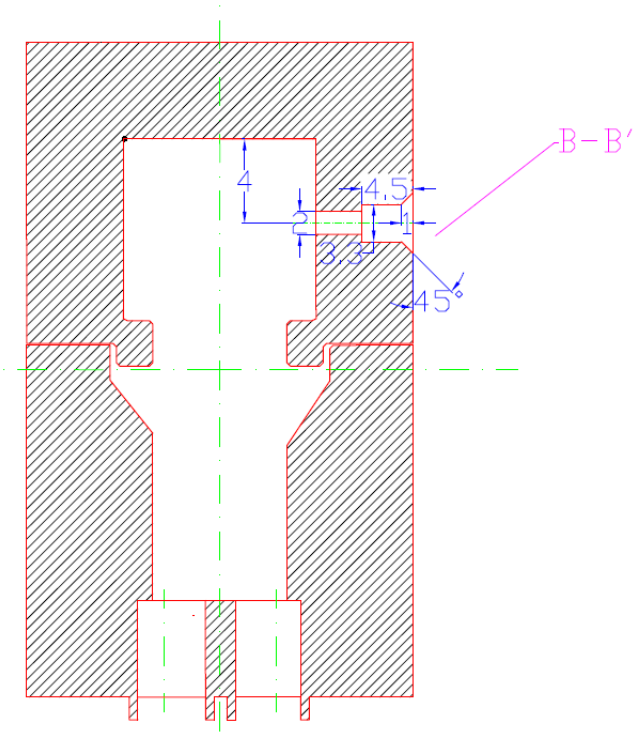

Figure B 6 Cut plane 2 of the cavity body front view (cut from the vacuum line)

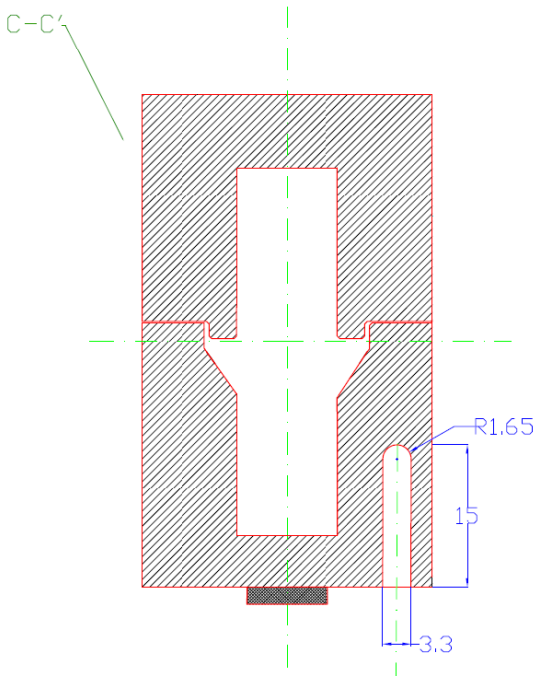

Figure B 7 Cut plane 3 of the cavity body front view (perpendicular to Figure B 5)

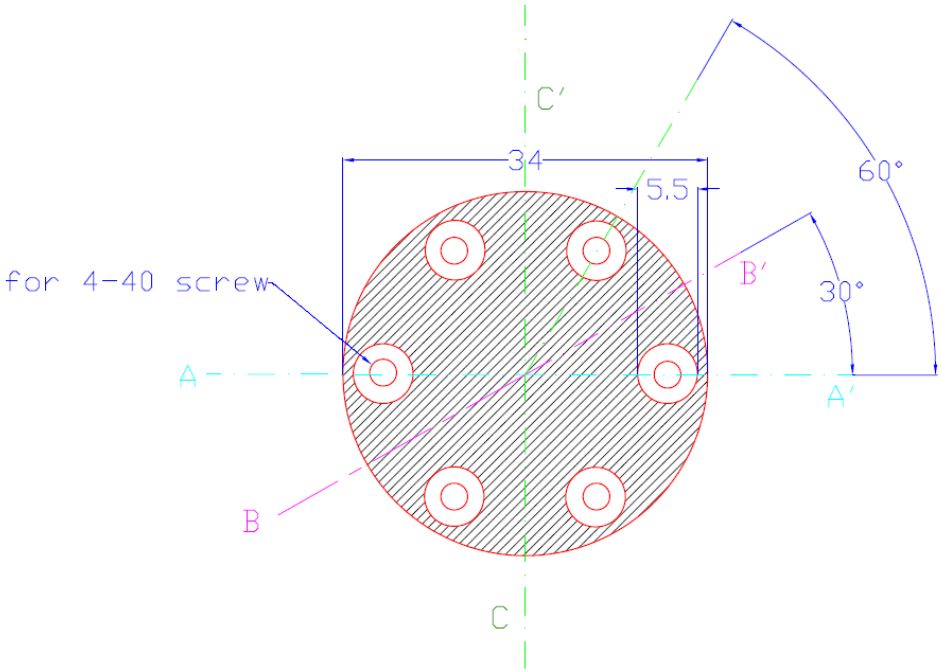

Figure B 8 Cavity bottom view

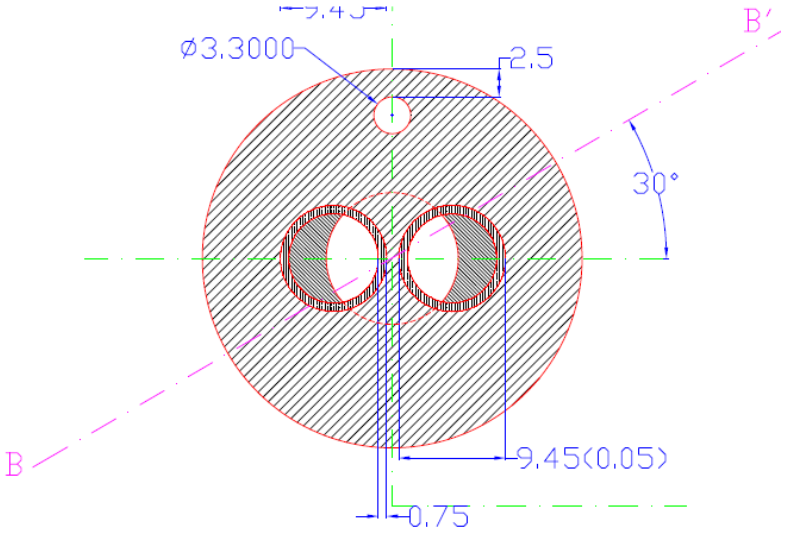

Figure B 9 Cavity top view

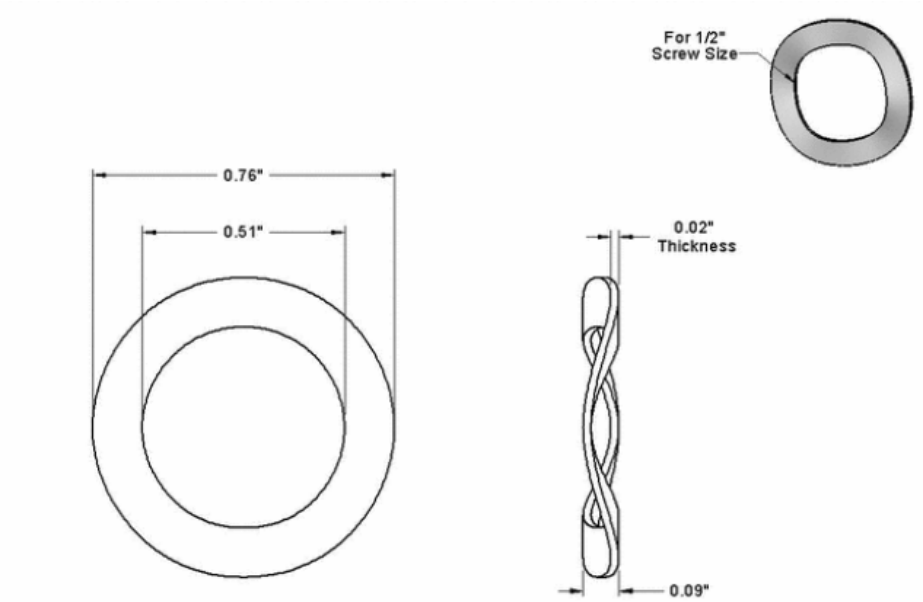

Figure B 10 Steel triple-wave washer